学位申請論文

^{3}He Nuclear Spin Relaxation in Solid ^{3}He with ^{4}He Impurities

前川覚

主論文

THESIS

^{3}He Nuclear Spin Relaxation in Solid ^{3}He with ^{4}He Impurities

Satoru Maegawa

Department of Physics
Faculty of Science
Kyoto University

(January 1979)

CONTENTS

ABSTRACT

Nuclear spin lattice relaxation behaviors in solid ^{3}He have been studied systematically, varying the impurity concentration x of ^{4}He with wide range, $2.0 \times 10^{-5} \leq x \leq 1.47 \times 10^{-2}$. For hcp samples at the temperature below about 1.2 K, three kinds of relaxation times were observed. We measured the temperature and concentration dependence of all the relaxation times. In order to analyze the data, a phenomenological four bath model is proposed, four baths being the Zeeman bath, the phonon bath, the X bath and the Y bath. The concentration dependence of the energy constants of all the baths have been also measured. The X bath consists of the exchange (^{3}He - ^{3}He exchange and ^{3}He - ^{4}He exchange) bath and some part of the ^{4}He - ^{4}He strain field interaction bath. The Y bath is thought to be the main part of the strain field interaction bath.

The relaxation behavior corresponding to the process between the X bath and the Y bath can not be expressed by a simple exponential function of time and the relaxation rate strongly depends on the ^{4}He concentration, as x^{-n} with $n = 3 \sim 4$. This process may be related to the internal thermal equilibrium process in the strain field interaction bath.

The theory for the ^{4}He impurity dependent relaxation

time between the exchange bath and the phonon bath gives the temperature dependence of T^{-9}. For hcp solid ^3He, however, the relaxation time has a temperature dependence of T^{-7} and can not be explained by the existing theories. We propose a new mechanism to explain the experimental results in hcp phase.

CHAPTER I

INTRODUCTION

The most striking and interesting feature of solid Helium is that the zero point energy is large compared with the Van der Waals binding energy due to a light mass of a He atom, so that the atoms undergo large zero point vibrations whose amplitudes are about a third of the interatomic distance. This leads to a large overlap of the atomic wave functions between the neighboring atoms and there is a large probability that atoms can exchange their positions with each other by quantum tunneling effect. The solid Helium is so called a quantum solid. The magnetic and thermal properties of solid ^{3}He at low temperature are influenced to a large extent by this exchange interaction.

As a ^{3}He has a spin I = $\frac{1}{2}$, the nuclear magnetic relaxation method is one of the most powerful techniques to observe the atomic motions. Fortunetly solid ^{3}He has no quadrupole interaction complicating the results.

As well as ^{3}He atoms, the vacancies and ^{4}He atoms in solid ^{3}He exchange their positions with the neighboring ^{3}He atoms. At low temperature these motions give rise to the fluctuation of the local field in the ^{3}He spin systems,

so that the measurement of the nuclear magnetic relaxation times gives us the informations about the motions and the interactions between them.

The spin lattice relaxation time in solid ^{3}He has an interesting temperature variation because the different kinds of motions or interactions are dominant in various temperature ranges. Above about 1K the spin lattice relaxation times in solid ^{3}He has been interpreted on the basis of the three bath model[1)-3)], the three baths being the Zeeman, the exchange, and the phonon. In this temperature range the dominant motions which fluctuate the spin system are the ^{3}He - ^{3}He exchange and the vacancy motions. But below about 1K the spin lattice relaxation times can not be explained by the simple three bath model. In this temperature range a small amount of ^{4}He isotope (even ppm order) gives efficient influence on the spin lattice relaxation times, and in addition the large specific heat which depends on the ^{4}He concentrations appears. For bcc samples the nonexponential recovery of magnetigation whose relaxation rate was strongly affected by ^{4}He impurities has been observed.

The ^{4}He impurity effects have been studied comparably well for bcc solid ^{3}He[4)-11)]. While for hcp solid ^{3}He there have been no systematic data about the effects of ^{4}He impurities. Some data of the relaxation times in hcp

phase[6),8),10),12),13)] seem to be inconsistent with each other and to be different from those in bcc phase.

To explain the ^{4}He impurity effects on the spin lattice relaxation times, some model have been proposed [14),15),16)]. For bcc solid ^{3}He with a small amount of ^{4}He impurities, these theories are now usually accepted, but the experimental data are not necessarily definitive. Also the difference of the relaxation times between two phases has not been explained sufficiently because of the lack of data in hcp phase.

On this point of view we have measured the spin lattice relaxation times mainly in hcp solid ^{3}He to understand the ^{4}He effects on the relaxation mechanisms in solid ^{3}He systematically and compared the results in bcc and hcp phases. This study will make it possible to understand the interactions of atoms and excitations in quantum crystals.

Recently it has been possible to decrease the temperature down to about 1 mK by the technical developments of the refregirators such as the dilution refregirator, the Pomeranchuk cooling refregirator and the nuclear adiabatic demagnetization refregirator. In solid ^{3}He the nuclear spin ordering is expected to take place at ultra low temperature (about 1 mK). In order to study the behavior of spins in solid ^{3}He at ultra low temperature,

it is very important to know the relaxation mechanisms between the spin system and the lattice system and the effects of ^{4}He impurity which is inevitably contained in the sample.

The plan of this thesis is as follows. In chapter II, we give the background to understand the nuclear spin relaxation in solid ^{3}He. The excitation systems in solid He and their interactions are mentioned. The bath model and the relations between the observed values and the intrinsic values are discussed. The development of the investigations in our temperature range is found in chapter II, § 4. The theories of the relaxation mechanisms between the exchange bath and the phonon bath are shown in § 5. In chapter III, the constructions of the cryostat and the pulsed NMR apparatus are described. Experimental procedures are also mentioned in the chapter. In chapter IV the experimental results are shown, and a phenomenological new bath model is proposed. Following this bath model, our data are analyzed in the chapter. The relaxation mechanisms between these baths are discussed in chapter V. We manifest the impurity effects and compare the experimental results in two phases. In the last chapter we summarize the results.

CHAPTER II

THEORETICAL AND EXPERIMENTAL BACKGROUND

§ 1 Phase Diagrams of ^{3}He and ^{4}He

The phase diagrams of ^{3}He and ^{4}He are shown in Fig. 1 and Fig. 2 respectively[17]. One of the unusual features in helium is that the solid helium can only exist at the pressure not less than about 30 kg/cm^2 due to a large zero point motion.

The solid ^{3}He crystallizes in a bcc lattice between about 30 and 110 kg/cm^2. Above this pressure a hcp lattice is the stable phase and a fcc lattice can be obtained at the high pressure above about 1600 kg/cm^2. For ^{4}He there exist also hcp, bcc and fcc solid phases.

When ^{3}He and ^{4}He are mixed, there appear several mixed phases near the phase boundary curves according to the Gibb's phase rule and the phase diagrams become very complicated. But in solid ^{3}He with the ^{4}He impurity of the ppm order which we used for our experiments, the change of the PVT relations on the melting curve is negligebly small.

Fig.1

Phase Diagram of ^3He

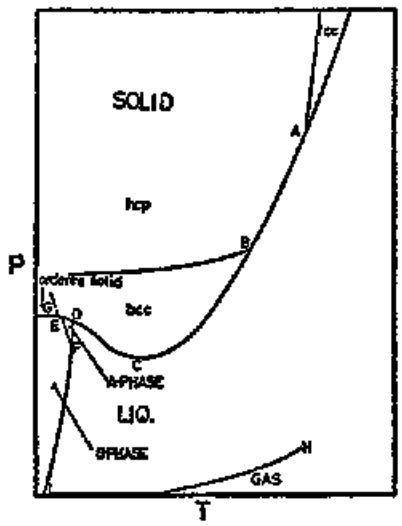

	P (atm)	T (K)
A :	1608	17.78
B :	135.44	3.138
C :	28.92	0.32
D :	34.7	2.6×10^{-3}
E :	34.7	2.1×10^{-3}
F :	21.8	2.4×10^{-3}
G :	34.7	1.2×10^{-3}
H :	1.1487	3.324
I :	0	0.93×10^{-3}

Fig.2

Phase Diagram of ^4He

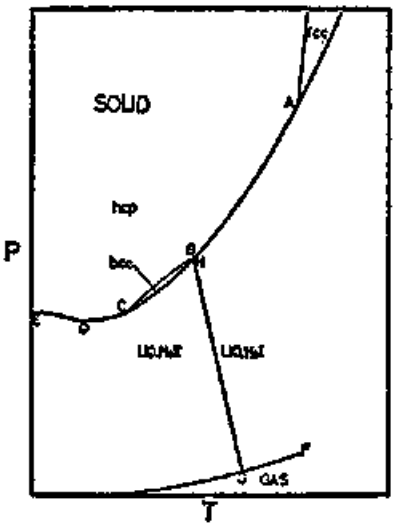

	P (atm)	T (K)
A :	1050	14.91
B :	29.67	1.773
C :	25.93	1.437
D :	24.96	0.775
E :	P_{min}+0.0075	0
F :	2.259	5.199
G :	0.0497	2.172
H :	29.74	1.763

§ 2 Excitations in Solid ^{3}He

2-1 Introduction

In order to understand the results of the NMR experiments on solid ^{3}He, it is significant to know the excitations in solid ^{3}He and the interactions between them. In quantum crystal there are several kinds of interesting excitations. Each of the excitation systems can be considered to be a heat bath to analyze the experimental results of the nuclear spin relaxation behavior, if the system can attain its therrnal equilibrium within itself in a time sufficiently short compared with the relaxation times which characterize the coupling with the other excitation systems. If the condition is satisfied, the temperature of the bath can be defined.

The energy E_i of an excitation system i is calculated from the Hamiltonian $\mathcal{H}_i$ of the system;

$$E_i = \langle \mathcal{H}_i \rangle = \mathrm{tr}\, \mathcal{H}_i\, e^{-\beta_i \mathcal{H}_i} \quad , \qquad (2\text{-}1)$$

where $\beta_i = 1/k_B T_i$ and T_i is the temperature of the system. The specific heat is then given by

$$C_i = \frac{dE_i}{dT_i} \qquad (2\text{-}2)$$

and the energy constant which is often met in the calculations of the relaxation times is defined as

$$k_i = \frac{dE_i}{d\beta_i} \quad . \tag{2-3}$$

2-2 Zeeman Bath

When a sample containing nuclear spins is placed in the magnetic field H_o, each of the spins precesses about the magnetic field with the Larmor frequeny;

$$\omega_o = \gamma H_o \quad , \tag{2-4}$$

where $\gamma = 2.038 \times 10^4$ rad G^{-1} sec^{-1} for ^3He. When the spins have come to thermal equilibrium, the population of the two spin states for spin 1/2 is

$$\frac{P_-}{P_+} = \exp\left(-\frac{\gamma \hbar H_o}{k_B T}\right) \quad . \tag{2-5}$$

If the energy is dumped into the spin system by the rf pulse, the spin system is driven away from equilibrium. If the spins return to equilibrium among themselves in a time short compared with the time required for excess energy in the spin system to decay away, the spin system can be described by a spin temperature. The spin system is thus regarded as a heat bath and is called the Zeeman

bath. The Zeeman bath is described by the Zeeman Hamiltonian given by

$$\mathcal{H}_z = -\mathbb{H}_0 \cdot \sum_{i=1}^{N} \mathcal{M}_i \quad . \tag{2-6}$$

At $k_B T \gg \hbar\omega_0$, that is the high temperature approximation, the energy of the Zeeman bath is

$$E_z = -\frac{N}{4}\frac{(\hbar\omega_0)^2}{k_B T} \quad . \tag{2-7}$$

The specific heat and the energy constant of the Zeeman bath are obtained from eq.(2-2), (2-3) and (2-7) as

$$C_z = \frac{Nk_B}{4}\left(\frac{\hbar\omega_0}{k_B T}\right)^2 \tag{2-8}$$

$$k_z = -\frac{N}{4}(\hbar\omega_0)^2 \quad . \tag{2-9}$$

The Zeeman bath is the first bath from which the energy flows to the other heat bath.

Next we mention the excitation systems in quantum crystals. There are three kinds of excitations in pure solid ^{3}He. These are phonons, vacancy motions and exchange excitations. In the case of the solid ^{3}He with a small amount of ^{4}He impurities, in addition to these three excitations in the pure solid ^{3}He, there exist the excitations associated with the motions of the ^{4}He atoms in the ^{3}He medium.

2-3 Phonon

Because the atoms take place very large zero point vibrations in solid He, it may become necessary to consider the effects of the unharmonic term of vibrations. It may require to build up a new phonon theory about the unharmonic crystals[18),19)]. However in the NMR experiments the results have been successfully understood by the usual Debye solid model and the unharmonicity of the atomic vibrations has been unnecessary to take into account.

The phonons play a very significant role in transferring energy from a certain excitation system to the other system, and the phonon system is a heat reservoir which has an infinite heat capacity in our experimental temperature range.

The Hamiltonian of the phonon bath is

$$\mathcal{H}_p = \sum_q \hbar\omega(q) \left(n(q) + \frac{3}{2} \right) \quad , \qquad (2\text{-}10)$$

where $\omega(q)$ is the phonon frequency and $n(q)$ is the number of phonons with the wave vector q. The energy, the specific heat and the energy constant of the phonon bath are given, following the Debye model, by

$$E_p = \frac{3\pi^4}{5} N k_B T \left(\frac{T}{\theta}\right)^3 \qquad (2\text{-}11)$$

$$C_p = \frac{12\pi^4}{5} N k_B \left(\frac{T}{\theta}\right)^3 \qquad (2\text{-}12)$$

$$k_p = -\frac{12\pi^4}{5} N (k_B T)^2 \left(\frac{T}{\theta}\right)^3 , \qquad (2\text{-}13)$$

where θ is taken to be the experimentally observed Debye temperature.

2-4 Exchange

The exchange in solid ^{3}He is the direct exchange of ^{3}He atoms by tunneling caused by the overlap between the wave functions of the adjacent atoms. This is different from the simple process associated with antisymmetrizing wave functions for fermions. The Hamiltonian of the exchange excitation is described by

$$\mathcal{H}_T = \hbar \sum_{ij} J_{ij} \mathbf{I}_i \cdot \mathbf{I}_j \qquad (2\text{-}14)$$

If the exchange interaction is assumed to be only between

the nearest neighboring ^{3}He atoms and $J_{ij} = J$, the energy of the ^{3}He - ^{3}He exchange bath is at $k_B T \gg \hbar J$

$$E_T = - \frac{3}{8} Nz \frac{(\hbar J)^2}{k_B T} \quad , \tag{2-15}$$

The specific heat and the energy constant are

$$C_T = \frac{3}{8} Nz \, k_B \frac{(\hbar J)^2}{(k_B T)^2} \tag{2-16}$$

and

$$k_T = - \frac{3}{8} Nz \, (\hbar J)^2 \quad , \tag{2-17}$$

where z is the number of the nearest neighbors.

2-5 Vacancy

The vacancy motion is the drastic phenomena which reflects the nature of quantum solid. In the case of the usual classical solid, an atom must get over the high potential barrier to move into a vacancy site in its neighborhood, and the probability is proportional to $\exp(-\Delta\varepsilon / k_B T)$, which decreases rapidly in the low temperature. $\Delta\varepsilon$ is the activation energy. Thus the vacancies can not move in the classical solid at low

$$V(r) = -30\pi d b^2 \Gamma \frac{1}{r^3} \quad , \qquad (2\text{-}20)$$

where

$$d = C_{11} - C_{12} - 2C_{44}$$

and C_{11}, C_{12}, C_{44} are the elastic constant.

$$\Gamma = l^4 + m^4 + n^4 - \frac{3}{5}$$

where (l,m,n) are the direction cosines between the two impurities. The constant b is the strength of the defect which is related with the difference between the atomic volume of ^{3}He and that of ^{4}He in the solid.

Nakajima et al.[16] and Guyer [30] have introduced the ^{4}He - ^{4}He strain field interaction bath in order to explain the ^{4}He impurity effects on the nuclear spin lattice relaxation in solid ^{3}He. The Hamiltonian of this bath is given by

$$\mathcal{H}_{44} = \sum_{i \neq j} \hbar V_0 \left(\frac{\Delta}{r_{ij}} \right)^3 n(r_i)\, n(r_j) \qquad (2\text{-}21)$$

where n(r) is the number of ^{4}He atom at r and Δ is the nearest neighbor distance. V_0 is the magnitude of the strain field interaction, negrecting the anisotropy.

$$V(r) = -30\pi d b^2 \Gamma \frac{1}{r^3} \quad , \qquad (2\text{-}20)$$

where

$$d = C_{11} - C_{12} - 2C_{44}$$

and C_{11}, C_{12}, C_{44} are the elastic constant.

$$\Gamma = l^4 + m^4 + n^4 - \frac{3}{5}$$

where (l,m,n) are the direction cosines between the two impurities. The constant b is the strength of the defect which is related with the difference between the atomic volume of ^{3}He and that of ^{4}He in the solid.

Nakajima et al.[16] and Guyer [30] have introduced the ^{4}He - ^{4}He strain field interaction bath in order to explain the ^{4}He impurity effects on the nuclear spin lattice relaxation in solid ^{3}He. The Hamiltonian of this bath is given by

$$\mathcal{H}_{44} = \sum_{i \neq j} \hbar V_0 \left(\frac{\Delta}{r_{ij}} \right)^3 n(r_i) n(r_j) \qquad (2\text{-}21)$$

where n(r) is the number of ^{4}He atom at r and Δ is the nearest neighbor distance. V_0 is the magnitude of the strain field interaction, neglecting the anisotropy.

The energy constant k_{44} of this bath is calculated as

$$k_{44} = -\frac{Nx^2}{2}\,(\hbar V_0)^2 \sum_{i(\neq 0)} \left(\frac{\Delta}{r_i}\right)^6 \quad . \qquad (2\text{-}23)$$

Because $\sum_{i(\neq 0)} r_i^{-6}$ is evaluated as $12.25\ \Delta^{-6}$ for bcc crystal and $14.45\ \Delta^{-6}$ for hcp crystal, we have

$$k_{44} = \begin{cases} -\,6.13\ Nx^2\,(\hbar V_0)^2 & (\text{bcc}) \\ -\,7.22\ Nx^2\,(\hbar V_0)^2 & (\text{hcp}) \end{cases} \qquad (2\text{-}24)$$

§ 3 Rate Equation

The spin lattice relaxation time T_1 is the time constant of which the energy delivered to the spin system (Zeeman bath) by rf pulse flows to the lattice (phonon). In solid ^{3}He there are some kinds of heat baths between the Zeeman bath and the lattice phonon bath, so the energy flow experiences some bottlenecks to reach the reservoir. On nuclear magnetic relaxation experiment we measure the time evolution of magnetization which is inversely proportional to the temperature of the Zeeman bath. But we can not observe the time evolutions of the temperature in the other heat baths directly.

When there are some heat baths between the Zeeman bath and the lattice phonon bath, the recovery of magnetization which is observed on the NMR measurement is the sum of exponential functions of time on proper conditions. Accordingly we can get some relaxation times corresponding to the number of bottlenecks between the Zeeman bath and the phonon bath. But the observed relaxation time is not the same value as the intrinsic relaxation time between the two baths. The observed relaxation time is a function of the intrinsic relaxation time and the energy constants of the heat baths.

For instance we show here the relations between the

observed values and the intrinsic values in the case that three baths connect in series as shown in Fig.3-a. The first bath is corresponding to the Zeeman bath and the third bath corresponding to the lattice phonon bath. The energy constants of each bath are k_1,k_2 and k_3. Here the value of k_3 is assumed to be infinite because the phonon bath is considered to be an infinite heat reservoir in our temperature range. The intrinsic relaxation times between each bath are defined by T_{12} and T_{23}. On this bath model the rate equations can be written as

$$\begin{cases} \dfrac{d\beta_1}{dt} = \dfrac{1}{T_{12}} (\beta_2 - \beta_1) \\ \dfrac{d\beta_2}{dt} = \dfrac{1}{T_{21}} (\beta_1 - \beta_2) + \dfrac{1}{T_{23}} (\beta_3 - \beta_2) \\ \dfrac{d\beta_3}{dt} = 0 \end{cases} , \qquad (2\text{-}25)$$

where $\beta_i = 1/k_B T_i$. T_i is the temperature of each bath and k_B is the Boltzman constant. As the third bath is a infinite heat reservoir, the temperature of this bath does not change at all times.

We now consider the relation between T_{12} and T_{21}.

If T_{23} is infinite, the relaxation will occur between the 1-bath and 2-bath, and the energy conservation between these baths requires

$$k_1 \dot{\beta}_1 + k_2 \dot{\beta}_2 = 0 \quad , \tag{2-26}$$

where dot denotes the time derivative. From (2-25) and (2-26) we get

$$\frac{k_1}{T_{12}} = \frac{k_2}{T_{21}} \quad . \tag{2-27}$$

If we define the constants as

$$\eta_{12} = 1/T_{12}$$

$$\eta_{23} = 1/T_{23}$$

$$\rho = \frac{k_1}{k_2} \quad , \tag{2-28}$$

we can rewrite (2-25) as

$$\begin{cases} \dot{\beta}_1 = \eta_{12} (\beta_2 - \beta_1) \\ \dot{\beta}_2 = \rho \eta_{12} (\beta_1 - \beta_2) + \eta_{23} (\beta_3 - \beta_2) \\ \dot{\beta}_3 = 0 \end{cases} . \qquad (2\text{-}29)$$

The initial conditions corresponding to our experimental conditions (90° pulse method) are at $t = 0$

$$\begin{cases} \beta_{1(0)} = 0 \\ \beta_{2(0)} = \beta_3 \\ \beta_{3(0)} = \beta_3 \end{cases} . \qquad (2\text{-}30)$$

The system of the linear ordinary differential equations (2.29) has the solutions as

$$\begin{cases} \beta_1(t) = \beta_3 \left(1 - \frac{\lambda_2 - \eta_{12}}{\lambda_2 - \lambda_1} e^{-\lambda_1 t} + \frac{\lambda_1 - \eta_{12}}{\lambda_2 - \lambda_1} e^{-\lambda_2 t} \right) \\ \beta_2(t) = \beta_3 \left(1 - \frac{\lambda_2 - \eta_{12}}{\lambda_2 - \lambda_1} \frac{\eta_{12} - \lambda_1}{\eta_{12}} e^{-\lambda_1 t} + \frac{\lambda_1 - \eta_{12}}{\lambda_2 - \lambda_1} \frac{\eta_{12} - \lambda_2}{\eta_{12}} e^{-\lambda_2 t} \right) \\ \beta_3(t) = \beta_3 \end{cases} . \qquad (2\text{-}31)$$

where

$$\lambda_{\frac{1}{2}} = \frac{1}{2}\left[(1+\rho)\eta_{12} + \eta_{23} \pm \sqrt{\{(1+\rho)\eta_{12} + \eta_{23}\}^2 - 4\eta_{12}\eta_{23}} \right] . \tag{2-32}$$

Let's consider the following cases.

$$\text{(A)} \quad \rho\eta_{12} \ll \eta_{23} \qquad \left(\frac{k_2}{k_1} T_{12} \gg T_{23} \right)$$

This condition leads (2-31) and (2-32) to

$$\begin{cases} \beta_{1(t)} = \beta_3 \left\{ 1 - \exp(-t/T_{12}) \right\} \\ \beta_{2(t)} = \beta_3 \end{cases} . \tag{2-33}$$

As the 1-bath corresponds to Zeeman bath and the magnetization M is proportional to β_1, the magnetization recovery which is observed by NMR experiment is expressed as

$$\frac{M(\infty) - M(t)}{M(\infty)} = \exp\left(-\frac{t}{T_{12}}\right) . \tag{2-34}$$

The graph of this magnetization recovery is pictured in Fig. 3-b for comparison with the next case.

In this case the observed relaxation time is equal to the intrinsic relaxation time T_{12} and any of the energy constant can not be measured. This case means that the 2-bath is tightly coupled with the 3-bath and hence we can not observe the relaxation time T_{23}.

$$(B) \quad \rho\eta_{12} \gg \eta_{23} \qquad \left(\frac{k_2}{k_1} T_{12} \ll T_{23} \right)$$

This condition means that the 2-bath is coupled with the 1-bath more tightly than with the 3-bath. In this case we get from (2-31) and (2-32)

$$\begin{cases} \beta_{1(t)} = \beta_3 \left\{ 1 - \frac{k_2}{k_1+k_2} \exp\left(-\frac{k_1+k_2}{k_2}\frac{t}{T_{12}}\right) - \frac{k_1}{k_1+k_2} \exp\left(-\frac{k_2}{k_1+k_2}\frac{t}{T_{23}}\right) \right\} \\ \beta_{2(t)} = \beta_3 \left\{ 1 + \frac{k_1}{k_1+k_2} \exp\left(-\frac{k_1+k_2}{k_2}\frac{t}{T_{12}}\right) - \frac{k_1}{k_1+k_2} \exp\left(-\frac{k_2}{k_1+k_2}\frac{t}{T_{23}}\right) \right\} \\ \beta_{3(t)} = \beta_3 \end{cases} .$$

(2-35)

Thus the magnetization recovery is observed as the sum of two exponential functions of time ;

$$\frac{M(\infty) - M(t)}{M(\infty)} = \frac{k_2}{k_1+k_2} \exp\left(-\frac{k_1+k_2}{k_2}\frac{t}{T_{12}}\right) + \frac{k_1}{k_1+k_2} \exp\left(-\frac{k_2}{k_1+k_2}\frac{t}{T_{23}}\right) .$$

(2-36)

Therefore we can obtain two relaxation times, which we define $T_{12)ob}$ and $T_{23)ob}$. These observed relaxation times are different from the intrinsic relaxation times. The relations between the intrinsic values and the observed values are from (2-36) ;

$$T_{12)ob} = \frac{k_2}{k_1 + k_2} T_{12}$$

$$T_{23)ob} = \frac{k_1 + k_2}{k_2} T_{23} \quad . \qquad (2\text{-}37)$$

Fig. 3-c shows the behavior of the magnetization recovery in this case. In this figure the intercept of the second magnetization recovery line corresponding to $T_{23)ob}$ at $t = 0$, which is denoted by R, is

$$R = \frac{k_1}{k_1 + k_2} \quad . \qquad (2\text{-}38)$$

This is the prefactor of the second term in (2-36). This value can be obtained in the experiment as well as $T_{12)ob}$ and $T_{23)ob}$, when k_1 and k_2 are the same order.

Fig. 3

Three Bath Model and Magnetization Recovery

(3-a)

k_1, k_2 and k_3 are the energy constants of the 1-bath, 2-bath and 3-bath respectively.

T_{12} and T_{23} are the relaxation times between each bath.

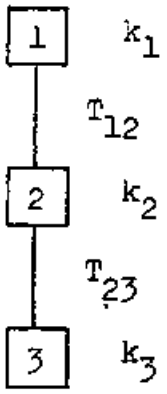

(3-b)

$$\frac{k_2}{k_1} T_{12} \gg T_{23}$$

$$\frac{M(\infty) - M(t)}{M(\infty)}$$

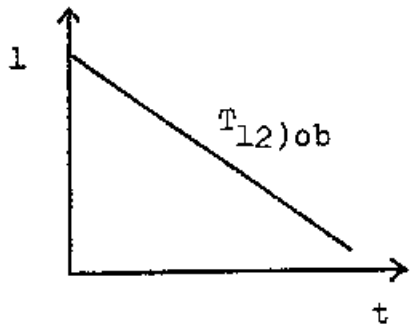

$$T_{12})ob = T_{12}$$

(3-c)

$$\frac{k_2}{k_1} T_{12} \ll T_{23}$$

$$\frac{M(\infty) - M(t)}{M(\infty)}$$

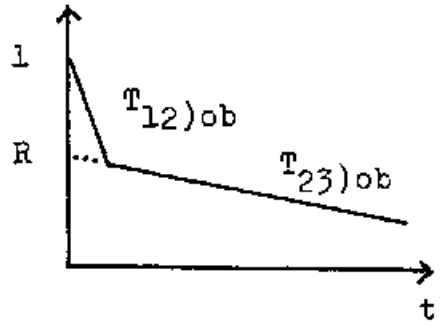

$$T_{12})ob = \frac{k_2}{k_1 + k_2} T_{12}$$

$$T_{23})ob = \frac{k_1 + k_2}{k_2} T_{23}$$

$$R = \frac{k_1}{k_1 + k_2}$$

§ 4 Relaxation Time in Solid ^{3}He

4-1 Spin Lattice Relaxation Time

In this section we review the typical spin lattice relaxation times T_1 in solid ^{3}He. The mechanisms which control the spin lattice relation times are different in several temperature ranges. The typical temperature variation of T_1 is shown in Fig. 4. In this figure we separate five temperature regions designated by I-a, I-b, II-a, II-b and III. The temperature dependence of T_1 is explained by the several kinds of excitation systems (heat baths) and their couplings between them. This is called bath model. The baths are coupled by a weak interaction with each other, so that the process between the baths becomes to be a bottleneck of the energy flow. This characteristic time is observed as the relaxation time T_1 in the NMR experiment.

The relaxation times in regions I-a, I-b and II-a are independent of the small amount of ^{4}He impurities. But in regions II-b and III ^{4}He impurities play an important role on the relaxation times.

In region I-a, the high temperature region, the

energy dumped into the Zeeman bath by the rf pulse is delivered to the vacancy bath through the agency of the dipole field. The topology of the energy flow process is shown in Fig. 4. Reich[2] successfully used the treatment of diffusion by Bloembergen, Purcell and pound[31], to describe the relaxation process in this region. The relaxation is occurred by the modulation of the dipole interaction between the nuclear magnetic moments due to the vacancy motions. The vacancy bath is tightly coupled with the lattice phonon bath through the vacancy phonon coupling.

The spin lattice relaxation time T_1 in this temperature range is calculated as follows[22]. We take the Hamiltonian describing the coupled Zeeman-vacancy system to be

$$\mathcal{H} = \mathcal{H}_Z + \mathcal{H}_V + \mathcal{H}_{ZV} \quad , \tag{2-39}$$

where $\mathcal{H}_Z$ is the Zeeman Hamiltonian and $\mathcal{H}_V$ is the vacancy Hamiltonian. $\mathcal{H}_{ZV}$ is a perturbation Hamiltonian which couples the Zeeman and the vacancy bath, and in this case is the dipole interaction

$$\mathcal{H}_d = \frac{1}{2} \sum_i \sum_j \left[\frac{\mu_i \cdot \mu_j}{r_{ij}^3} - \frac{3(\mu_i \cdot r_{ij})(\mu_j \cdot r_{ij})}{r_{ij}^5} \right] \tag{2-40}$$

Using the well known density matrix method, the relaxation time is obtained

$$\frac{1}{T_1} = \frac{2}{3} M_2 \left(\frac{\tau_v}{1 + \omega_0^2 \tau_v^2} + \frac{4 \tau_v}{1 + 4 \omega_0^2 \tau_v^2} \right) \tag{2-41}$$

$$\frac{1}{\tau_v} = z \omega_v x_v \quad , \tag{2-42}$$

where M_2 is the Van Vleck second moment and ω_v is the frequency for tunneling of a ^{3}He particle into a neighboring vacancy site in solid He^3. x_V is the concentration of vacancies in solid He^3 and is expressed by the formation energy Δ of a vacancy as

$$x_V = \exp\left(- \frac{\Delta}{k_B T} \right) \quad . \tag{2-43}$$

As temperature is lowered, the vacancy concentration goes toward zero. Thus the mechanism due to the vacancy motion becomes less dominant.

In region I-b, the energy in the Zeeman bath flows to the exchange bath by the modulation of dipole interaction due to the exchange motion of ^{3}He atoms instead of the vacancy motion[32]. Therefore in this case the spin variables rather than the special variables of the dipole Hamiltonian which is the case in region I-a

fluctuate randomly with time. Because the exchange motion is independent of temperature, the relaxation time in this region is temperature independent and this region is called the exchange plateau region.

The total Hamiltonian in this system is

$$\mathcal{H} = \mathcal{H}_Z + \mathcal{H}_T + \mathcal{H}_{ZT} \quad . \tag{2-44}$$

$\mathcal{H}_T$ is the exchange Hamiltonian given by (2-14). $\mathcal{H}_{ZT}$ is also the dipole interaction (2-40). By the similar calculation in the case of the relaxation from the Zeeman to the vacancy bath, the spin lattice relaxation time is given for a powder of crystallites by

$$\frac{1}{T_1} = J(\omega_0) + 4\, J(2\omega_0) \quad . \tag{2-45}$$

$J(\omega_0)$ is the Fourie transformation of the correlation function of spins, so-called the spectral function. If we assume the correlation function to be a Gaussian, $J(\omega_0)$ is

$$J(\omega_0) = \frac{\sqrt{2\pi}\, M_2}{3\omega_T} \exp\left(-\frac{\omega_0^2}{2\omega_T^2}\right) \quad , \tag{2-46}$$

where

$$\omega_T^2 = \frac{M_4}{M_2} \tag{2-47}$$

and for the Lorentzian correlation function, $J(\omega_0)$ is

$$J(\omega_0) = \frac{\pi M_2}{3\omega_T} \exp\left(-\frac{\omega_0}{\omega_T}\right) , \tag{2-48}$$

where

$$\omega_T^2 = \frac{M_4}{2M_2} \tag{2-49}$$

The second moment M_2 and the fourth moment M_4 are evaluated for bcc and hcp crystals as follows.

$$M_2 = \begin{cases} 22.796 \\ 22.610 \end{cases} \times \left(\frac{10^{10}}{V^2}\right) \text{sec}^{-2} \qquad \begin{matrix} \text{(bcc)} \\ \text{(hcp)} \end{matrix} \tag{2-50}$$

$$M_4 = \begin{cases} 517.76 \\ 951.68 \end{cases} \times 10^{10} \left(\frac{J^2}{V^2}\right) \text{sec}^{-4} \qquad \begin{matrix} \text{(bcc)} \\ \text{(hcp)} \end{matrix} \tag{2-51}$$

where V is the molar volume in cm^3/mol. The relations between ω_T and J for both correlation functions are

Gaussian

$$\omega_T = \begin{cases} 4.76\ J & \text{(bcc)} \\ 6.48\ J & \text{(hcp)} \end{cases} \qquad (2\text{-}52)$$

Lorentzian

$$\omega_T = \begin{cases} 3.36\ J & \text{(bcc)} \\ 4.58\ J & \text{(hcp)} \end{cases} \qquad (2\text{-}53)$$

The magnitude of exchange interaction J can be derived from the measurement of T_1 or T_2 in this region[33]. J is also derived by the thermodynamic measurements, such as the susceptibility measurements[34)-36)], dP/dT measurements[37),38)] and the nuclear relaxation heat capacity measurements[6),39)].

In the exchange plateau region, the exchange bath is tightly coupled with the phonon bath, thus the exchange bath is always at the lattice temperature. But as the temperature is lowered, the exchange bath is not strongly coupled with the phonon bath, because the number of phonons or vacancies decrease. As a consequence, the process from the exchange bath to the phonon bath or vacancy bath becomes a new bottleneck of the energy flow. In the process, since the numbers of the phonons or vacancies

are related to the relaxation mechanism, the relaxation time is temperature dependent. We denote this temperature range of the relaxation time by region II (II-a and II-b) in Fig. 4.

In region II-a, the vacancy motions play a dominant role on the relaxation mechanism and the energy in the exchange bath flows to the vacancy bath which is tightly coupled with the phonon bath. The relaxation time of this process depends on the number of vacancies and is not influenced by ^{4}He impurities.

In region II-b, as the number of vacancies decreases, the relaxation process from the exchange bath to the phonon bath becomes to be observed. The relaxation time of this process is affected by a small amount of ^{4}He impurities. Furthermore in this temperature region, it has been observed that there exists a large energy constant which depends on the ^{4}He concentration. The pioneering authors[3),5),6),12)] attempted to analyze the relaxation time by the Griffiths theory[40)], but the theory does not explain the effects of the ^{4}He impurities. They did not observe the ^{4}He concentration dependence of the relaxation time.

For bcc solid ^{3}He in this temperature region, Giffard et al.[7)], Bernier[8)] and Bernier et al.[11)] have studied

the relaxation time in the samples with various concentrations of ^{4}He impurities. In order to explain the impurity effects on the relaxation behavior, Guyer et al.[14),22)], Bernier et al.[15)] and Nakajima et al.[16)] proposed the idea of the phonon scattering by ^{4}He impurities. The large energy constant accompanied by the existance of ^{4}He impurities has been interpreted by introducing the ^{4}He - ^{4}He interaction bath. For bcc samples with ^{4}He impurities of less than 2.0×10^{-3}, the relaxation behaviors have been explained by these theories. But Bernier et al.[11)] have found the existance of another large heat bath and long relaxation time, which were not measured systematically. In addition, the nonexponential recovery of the magnetization was observed at the lower temperature for bcc samples. The temperature range where the nonexponential recovery of the magnetization is observed is denoted as region III in Fig. 4.

On the other hand for hcp solid ^{3}He in region II there is no systematic data on the effects of ^{4}He impurities, and some experimental results[6),8),12),13)] seems to be different from those of bcc solid or to be inconsistent with each other. One of the differences is the temperature dependence of the relaxation time, which is T^{-7} for hcp solid and T^{-n} with $n \simeq 8 \sim 9$ for bcc solid. The relaxation process

due to the vacancy motion in region II-a and the nonexponential recovery of the magnetization have not been observed in hcp phase.

We have studied the relaxation behaviors in region II-a, II-b and III mainly in hcp phase.

4-2 Spin Spin Relaxation Time

T_2, the characteristic time for decay of the transverse magnetization, is a measure of the time required for the spins to come to equilibrium among themselves. The individual spins move in the transverse plane relative to one another due to the local field. Energetically the process by which the equilibrium is established among spins involves energy transfer within only the Zeeman system. The typical temperature variation of T_2 is shown in Fig. 4 with T_1.

In region I-a the irreversible motion of the spins in the transverse plane is caused by the fluctuations in the local field due to the motions of vacancies in solid. The interaction between the spins is the dipole interaction. T_2 is obtained by calculating the time evolution of the transverse component of magnetization using the density matrix method[22] and is expressed as

$$\frac{1}{T_2} = M_2 \tau_v \left(1 + \frac{5}{3} \frac{1}{1 + \omega_0^2 \tau_v^2} + \frac{2}{3} \frac{1}{1 + 4 \omega_0^2 \tau_v^2} \right) \qquad (2\text{-}54)$$

The physical content of this result is the same as that

of Eq. (2-41) for T_1 in region I-a. T_2 in region I-a is temperature dependent. This is due to the temperature dependence of τ_v, which is related to x_v, the concentration of the vacancies. As temperature is lowered, T_2 becomes short until the particle motions which cause the dipole field to fluctuate are principally the exchange motions.

In region I-b, the important particle motion which fluctuates the dipole field is the exchange motion of He^3 atoms. Using the Gaussian approximation for the exchange correlation function, T_2 is expressed as

$$\frac{1}{T_2} = \frac{\sqrt{2\pi}}{3} \frac{M_2}{\omega_T} \left\{ \frac{3}{2} + \frac{5}{2} \exp\left[-\frac{1}{2} \left(\frac{\omega_0}{\omega_T} \right)^2 \right] + \exp\left[-2 \left(\frac{\omega_0}{\omega_T} \right)^2 \right] \right\} \qquad (2\text{-}55)$$

ω_T, which is proportional to J, is temperature independent, so T_2 is independent of temperature in this region.

T_2 in these two regions is independent of a small concentration of ^4He impurities.

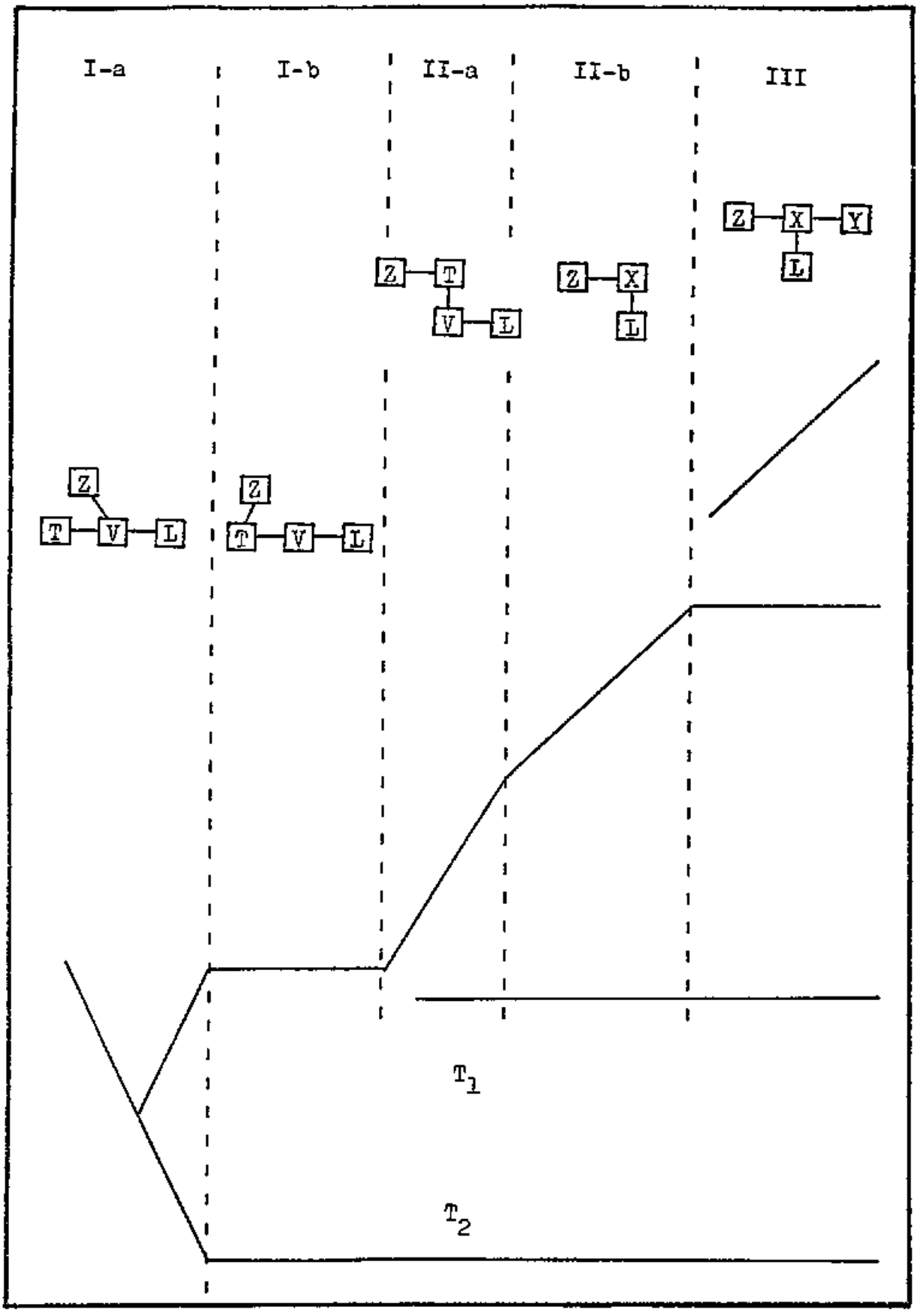

Fig. 4

Typical Temperature Variation of
Relaxation Time in Solid ^3He

§ 5 Relaxation Theory between the Exchange Bath and the Phonon Bath

In this section we show the relaxation mechanisms from the exchange bath to the phonon bath or the vacancy bath.

The relaxation time between the baths is calculated by treating the weak coupling interaction between them as a perturbation. When we denote the main Hamiltonians of the a-bath and the b-bath by $\mathcal{H}_a$ and $\mathcal{H}_b$ respectively, and the perturbation Hamiltonian by $\mathcal{H}_{ab}$, the relaxation time T_{ab} from the a-bath to the b-bath is calculated, following the well known density matrix method[22),44)];

$$\frac{1}{T_{ab}} = \frac{1}{\hbar^2 k_a} \int_0^\infty dt \; \mathrm{tr}\left(e^{-\beta(\mathcal{H}_a+\mathcal{H}_b)} \left[\mathcal{H}_a, \mathcal{H}_{ab(0)}\right]\left[\mathcal{H}_a, \mathcal{H}_{ab(t)}\right] \right) , \tag{2-56}$$

where

$$\mathcal{H}_{ab}(t) = \exp\left[\frac{i(\mathcal{H}_a+\mathcal{H}_b)t}{\hbar}\right] \mathcal{H}_{ab} \exp\left[-\frac{i(\mathcal{H}_a+\mathcal{H}_b)t}{\hbar}\right] \tag{2-57}$$

and β is the inverse temperature of the b-bath and is

assumed to have a fixed value. The Hamiltonians have the following commutation relations.

$$\left[\mathcal{H}_a , \mathcal{H}_b \right] = 0$$

$$\left[\mathcal{H}_a , \mathcal{H}_{ab} \right] \neq 0$$

$$\left[\mathcal{H}_b , \mathcal{H}_{ab} \right] \neq 0$$

5-1 Exchange-Vacancy Relaxation

The atomic jump due to the vacancy motion is one of the mechanisms for relaxing the exchange energy because the motion fluctuates the exchange field. Garwin et al.[3], Guyer et al.[22] and Richards[45] calculated the relaxation time in this case. The main Hamiltonians of the baths are identified as

$$\mathcal{H}_a \longrightarrow \mathcal{H}_T = \hbar J \sum_{ij} \mathbf{I}_i \cdot \mathbf{I}_j \tag{2-58}$$

$$\mathcal{H}_b \longrightarrow \mathcal{H}_V \tag{2-59}$$

and the perturbation Hamiltonian is

$$\mathcal{H}_{ab} \longrightarrow \mathcal{H}_{TV} = \hbar J \sum_{ij} \Delta\alpha_{ij}\, \mathbf{I}_i \cdot \mathbf{I}_j \quad , \tag{2-60}$$

where $\Delta\alpha_{ij} = \alpha_{ij} - \langle\alpha_{ij}\rangle$, and α_{ij} is unity if the sites i and j are both occupied by ^{3}He atoms and zero otherwise. Substituting these Hamiltonians to eq. (2-56), Richards obtained the relaxation time as

$$\frac{1}{T_{TV}} = 2\,(z-1)/\tau_c \quad , \tag{2-61}$$

where τ_c is the mean time in which the vacancy stays

at one lattice site and is related to ω_v and ϕ as

$$\frac{1}{\tau_c} = \omega_v e^{-\phi/k_B T} \qquad (2\text{-}62)$$

where ω_v is the frequency with which a ^{3}He atom tunnels into a vacancy site.

5-2 Exchange modulation

The exchange interaction varies very rapidly with the interatomic distance, and thus the lattice vibrations modulate the exchange interaction between the spins. This leads to a coupling between the exchange and phonon baths. Griffiths[40] considered this relaxation mechanism and Richards[45] extended the calculation by including the correlations between the different pairs of spins.

The main Hamiltonians of the baths are the ^3He - ^3He exchange bath and the phonon bath;

$$\mathcal{H}_a \longrightarrow \mathcal{H}_T = \hbar \sum_{i,j} J_{ij}\, \mathbb{I}_i \cdot \mathbb{I}_j \qquad (2\text{-}63)$$

$$\mathcal{H}_b \longrightarrow \mathcal{H}_P \quad . \qquad (2\text{-}64)$$

In eq. (2-63) we keep only the nearest neighbor interaction. The coupling Hamiltonian $\mathcal{H}_{ab}$ is described by

$$\mathcal{H}_{ab} = \hbar \sum_{i,j} \Delta_{ij}\, A_{ij} \quad . \qquad (2\text{-}65)$$

A_{ij} is a function of the spin variables,

$$A_{ij} = \mathbb{I}_i \cdot \mathbb{I}_j \qquad (2\text{-}66)$$

and has the commutation relations as

$$[\, A_{ij} \,,\, \mathcal{H}_T \,] \neq 0$$

$$[\, A_{ij} \,,\, \mathcal{H}_P \,] = 0 \quad .$$

Δ_{ij} is a function only of the lattice variables,

$$\Delta_{ij} = J_{ij}\,(\mathbb{r}_{ij}) - J_{ij}\,(\mathbb{r}^{o}_{ij}) \quad , \qquad (2\text{-}67)$$

where $J_{ij}(\mathbb{r}_{ij})$ is the exchange interaction between spins $\mathbb{I}_i$ and $\mathbb{I}_j$ which are separated by a distance $\mathbb{r}_{ij}$, and $\mathbb{r}^{o}_{ij}$ is the equilibrium distance. The commutation relations are

$$[\, \Delta_{ij} \,,\, \mathcal{H}_T \,] = 0$$

$$[\, \Delta_{ij} \,,\, \mathcal{H}_P \,] \neq 0 \quad .$$

Substituting eq. (2-63),(2-64) and (2-65) into (2-56), and using the commutation relations, the invariant property of the trace and the partial integration, we obtain

$$\frac{1}{T_1} = \frac{\hbar^2}{k_T}\left\{\sum_{ij}\sum_{kl}\int_0^\infty \langle \Delta_{ij}(0)\,\frac{d^2}{dt^2}\Delta_{kl}(-t)\rangle \left\{A_{ij}(0)\,A_{kl}(-t)\right\} dt \right.$$

$$\left. + \sum_{ij}\sum_{kl}\langle \Delta_{ij}(0)\,\frac{d}{dt}\Delta_{kl}(-t)\rangle\Big|_{t=0}\left\{A_{ij}(0)\,A_{kl}(0)\right\}\right\}$$

(2-68)

where the $\langle Q \rangle$ indicates a thermal equilibrium average with repect to the lattice variables;

$$\langle Q \rangle = \frac{\mathrm{tr}\left[\exp(-\beta \mathcal{H}_p)\, Q\right]}{\mathrm{tr}\,\exp(-\beta \mathcal{H}_p)} \qquad (2\text{-}69)$$

and $\{ Q \}$ is the average value for a spin operator;

$$\{ Q \} = \frac{\mathrm{tr}\, Q}{\mathrm{tr}\, 1} \qquad (2\text{-}69)$$

The quantity Δ_{ij} defined in (2-67) is discribed for the small departure of $\mathcal{H}_{ij}$ from equilibrium as

$$\Delta_{ij} = \sum_s \frac{\partial J_{ij}(\mathcal{H}_{ij})}{\partial x_{ij}^s}\, u_{ij}^s + \frac{1}{2}\sum_{r,s}\frac{\partial^2 J_{ij}(\mathcal{H}_{ij})}{\partial x_{ij}^r\, \partial x_{ij}^s}\, u_{ij}^r\, u_{ij}^s + \cdots ,$$

(2-70)

where x_{ij}^s (s = 1,2,3) are the Cartesian components of $\mathcal{H}_{ij}$ and u_{ij}^s is the s th component of $\mathcal{U}_{ij}$. $\mathcal{U}_{ij}(t)$ is

described in terms of phonon creation and annihilation operators as

$$u_{ij}(t) = \mathbf{r}_{ij} - \mathbf{r}^{o}_{ij}$$

$$= \sum_{\mathbf{q},\lambda} \left(\frac{\hbar}{2Nm\omega_{\mathbf{q}\lambda}} \right)^{1/2} \mathbf{e}_{\mathbf{q}\lambda}$$

$$\times \left\{ c_{\mathbf{q}\lambda} e^{-i\omega_{\mathbf{q}\lambda}t} \left(e^{i\mathbf{q}\cdot\mathbf{r}_i} - e^{i\mathbf{q}\cdot\mathbf{r}_j} \right) + c^{\dagger}_{\mathbf{q}\lambda} e^{i\omega_{\mathbf{q}\lambda}t} \left(e^{-i\mathbf{q}\cdot\mathbf{r}_i} - e^{-i\mathbf{q}\cdot\mathbf{r}_j} \right) \right\} \tag{2-71}$$

where $\omega_{\mathbf{q}\lambda}$ is the angular frequency of the phonon with wave vector $\mathbf{q}$ and branch λ, $\mathbf{e}_{\mathbf{q}\lambda}$ the unit polarization vector, N the number of atoms and m is the atomic mass of ^{3}He. Then we need to calculate the matrix elements of $\langle \Delta_{ij}(0)\, \Delta_{kl}(-t) \rangle$ in the phonon state space $|n_q)$.
The first term in (2-70) gives the single phonon process and the second gives the two phonon process (Raman process). Because the experimental results indicate that the two phonon process is dominant, we consider only this process. In general the two phonon process is more dominant than the single phonon process at low temperature because all the phonons in the spectrum can take part in the two phonon process, but only the low energy phonon can do in the single phonon process.

The summation over phonon state is replaced by an integral and a Debye spectrum is assumed for which phonon velocity v is independent of the direction of propagation and polarization. In the two phonon process, the phonon will be significant for ω and ω' of order of $k_B T/\hbar$ and for energy change $|\omega - \omega'| \lesssim J$. And since $\hbar J \ll k_B T$, we may set $\omega' = \omega$ and $q' = q$. According to the above assumptions, the second term in eq. (2-68) becomes zero and we obtain

$$\frac{1}{T_1} = -\frac{1}{k_T}\frac{3}{32}\frac{\hbar^4 V^2}{\pi^3 m^2 N^2 v^6}\int_0^\infty d\omega\ \omega^2\, n_q(n_q+1)$$
$$\times \sum_{ijk}{}' \Big[(J_{ij}^2 - J_{ij}J_{ik})\, L_{jk,jk}\, f^2_{jk,jk}(\theta)$$
$$- (J_{ij}^2 - J_{ij}J_{jk})\, L_{ik,jk}\, f^2_{ik,jk}(\theta)$$
$$+ J_{ij}J_{jk}\,(L_{ij,ik}\, f^2_{ij,ik}(\theta) - L_{ij,jk}\, f^2_{ij,jk}(\theta))\Big], \qquad (2\text{-}72)$$

where $\sum_{ijk}{}'$ indicates that i, j and k must be different. V is the volume and

$$n_q = \frac{1}{e^{\beta\hbar\omega_q} - 1} \qquad (2\text{-}73)$$

is the thermal equilibrium occupation number of the q phonon mode. The quantity $f_{ij,kl}(q)$ is defined by

$$f_{ij,kl}(q) = \frac{\sin qr_{ik}}{qr_{ik}} + \frac{\sin qr_{jl}}{qr_{jl}} - \frac{\sin qr_{jk}}{qr_{jk}} - \frac{\sin qr_{il}}{qr_{il}} \quad . \tag{2-74}$$

This term comes from the integral over the angles;

$$\int_0^{2\pi} d\varphi \int_0^{\pi} d\theta \sin\theta \; e^{\pm iq\mathcal{R}} = \frac{2\pi \sin qr}{qr} \quad . \tag{2-75}$$

The quantity $L_{ij,kl}$ is defined by

$$L_{ij,kl} = \sum_{r,s} \frac{\partial^2 J_{ij}}{\partial x_{ij}^r \partial x_{ij}^s} \frac{\partial^2 J_{kl}}{\partial x_{kl}^r \partial x_{kl}^s} \quad . \tag{2-76}$$

If it is assumed that $J_{ij}(\mathcal{R}_{ij})$ is a function only of the magnitude r_{ij} and $J'' \gg J'/a$, where the primes denote derivative and a is the nearest neighbor distance, $L_{ij,kl}$ can be calculated as follows.

$$\begin{aligned} L_{ij,ij} &= J''^2_{ij} \\ L_{ij,jk} &= J''_{ij} J''_{jk} \cos^2\theta_{ijk} \\ L_{ij,ik} &= J''_{ij} J''_{ik} \cos^2\theta_{jik} \\ L_{ik,jk} &= J''_{ik} J''_{jk} \cos^2\theta_{ikj} \quad , \end{aligned} \tag{2-77}$$

where θ_{ijk} is the angle (i,j,k). For $f_{ij,kl}(q)$, in the long wave approximation, we find

$$
\begin{aligned}
f_{ij,ij}(q) &= \tfrac{1}{3}\, q^2 a^2 \\
f_{ij,jk}(q) &= -\tfrac{1}{3}\, q^2 a^2 \cos\theta_{ijk} \\
f_{ik,jk}(q) &= \tfrac{1}{3}\, q^2 a^2 \cos\theta_{ikj} \\
f_{ij,ik}(q) &= \tfrac{1}{3}\, q^2 a^2 \cos\theta_{jik} \quad .
\end{aligned}
\tag{2-78}
$$

Substituting (2-77) and (2-78) into (2-72), we have

$$
\frac{1}{T_1} = -\frac{1}{k_T}\,\frac{1}{96}\,\frac{\hbar^4 V^2 a^4}{\pi^3 m^2 N^2 v^{10}}\left(\frac{k_B T}{\hbar}\right)^7 \times \int_0^\infty y^6 \frac{e^y}{(e^y-1)^2}\, dy \times B \quad , \tag{2-79}
$$

where

$$
B = \sum_{ijk}{}' \left[J_{ij}\left(J_{ij} - J_{ik}\right) J_{jk}'^2 - J_{ij}' J_{jk}' \cos^4\theta_{ijk}\left(J_{ik}^2 - J_{ik}J_{jk} - J_{ij}J_{ik} + J_{ij}J_{jk}\right)\right] . \tag{2-80}
$$

When it is assumed that $J_{ij} = J$, if (i,j) pair is nearest neighbor and $J_{ij} = 0$ for otherwise,

$$B = \begin{cases} 0.523 \\ 0.846 \end{cases} \times J^2 J''^2 Nz(z-1) \quad \begin{matrix} \text{(hcp)} \\ \text{(bcc)} \end{matrix} \qquad (2\text{-}81)$$

Thus the result is finally for hcp solid ^{3}He

$$\frac{1}{T_1} = 9.56 \times 10^{-35} J''^2 \frac{T^7}{\theta^{10}} \qquad (2\text{-}82)$$

and for bcc solid ^{3}He

$$\frac{1}{T_1} = 8.78 \times 10^{-35} J''^2 \frac{T^7}{\theta^{10}} \qquad (2\text{-}83)$$

5-3 Enhanced Exchange Modulation

The relaxation mechanisms mentioned in section 5-1 and 5-2 are independent of ^{4}He impurities. We extend the mechanism described in section 5-2 by introducing the enhanced exchange interaction between ^{3}He atoms near the ^{4}He impurities according to the following consideration.

The atomic wave functions of ^{3}He near the ^{4}He atom will be deformed due to the difference of the atomic sizes between a ^{3}He atom and a ^{4}He atom in the solid. The deformations may cause the enhanced exchange interaction between the ^{3}He atoms in the neighborhood of a ^{4}He atom. Let us suppose that the influence of a ^{4}He atom is restricted to the ^{3}He atoms which are nearest neighbors of a ^{4}He atom, and the exchange interaction is assumed to be effective only between the nearest neighboring ^{3}He atoms. That is, if both ^{3}He atoms at site i and j are the nearest neighbors of a ^{4}He atom,

$$J_{ij} = J_E \Lambda_{ij} \qquad (2\text{-}84)$$

and otherwise

$$J_{ij} = J_N \Lambda_{ij} \quad , \qquad (2\text{-}85)$$

where Λ_{ij} is unity if i and j are nearest neighbor with each other and zero otherwise.

Here we should pay attention to the difference of the crystal structures between the hcp and bcc solids. For hcp structure a ^{4}He atom in the crystal has 12 nearest neighboring ^{3}He atoms and some of them are also nearest neighbors with each other, as pictured in Fig. 5. There are 24 enhanced pairs around a ^{4}He atom. For bcc structure, however, the 8 nearest neighboring ^{3}He atoms around a ^{4}He atom have no nearest neighboring bonds with each other. Therefore for the bcc solid ^{3}He, eq. (2-84) is always zero and so the enhanced exchange interaction does not exist in this phase. The relaxation mechanism due to the enhanced exchange interaction is effective only in the hcp solid ^{3}He.

When we calculate the summution (2-80) carefully for the hcp crystal structure, we have

$$B = N\{69.0\, J_N^2\, J_N''^2 + x\,(-597\, J_N^2 J_N''^2 + 93.6\, J_E^2 J_E''^2 + 330\, J_E^2 J_N''^2 + 240\, J_N^2 J_E''^2 - 180\, J_E J_N J_N''^2 - 96.5\, J_E J_N J_E'' J_N'')\} \qquad (2\text{-}86)$$

Thus the relaxation time is in the hcp solid ^{3}He

$$\frac{1}{T_1} = -\frac{1}{k_o}\frac{1}{96}\frac{\hbar^4 \nu^2 a^4}{\pi^3 m^2 N^2 \nu^{10}}\int_o^\infty y^6 \frac{e^y}{(e^y-1)^2}dy \times B$$

$$= -\frac{\hbar^2}{k_o} 6.22 \times 10^{-36} \left(\frac{T^7}{\Theta^{10}}\right) \times B \quad , \tag{2-87}$$

where k_o is the sum of the energy constants of the normal exchange part and the enhanced exchange part,

$$k_o = k_N + k_E = -\frac{3}{8} Nz(\hbar J_N)^2 - \frac{3}{4} 24Nx(\hbar J_E)^2 \quad , \tag{2-88}$$

where we assumed that the normal exchange part and the enhanced exchange part are in good thermal equilibrium with each other.

It should be emphasized that $T_1 \propto T^{-7}$ and T_1 depends on the ^{4}He impurities.

Previously Richards et al.[6] and Bernier et al.[41),8)] applied the idea of the enhanced exchange to explain the ^{4}He impurity effects in solid ^{3}He. According to the analysis by Bernier et al., the experimental results in the bcc solid ^{3}He could be explained, if the 56 pairs of ^{3}He around a ^{4}He atom were assumed to have the enhanced exchange constant J_E which was about seven times as large

as J. But the theoretical estimate[42] for bcc phase indicated that the enhanced exchange was only $J_E \lesssim 1.6J$ and the similar conclusion was obtained by the analysis of the pressure measurement[43] and that of the susceptibility measurement[60] both in the bcc solid ^{3}He with ^{4}He impurities. However as mentioned above, in hcp phase the enhanced exchange effect can be expected to exist.

5-4 Phonon Scattering by ^{4}He Impurities

In order to explain the ^{4}He impurity effect on the relaxation time, Guyer et al. [14), 22)], Bernier et al.[15)] and Nakajima et al. [16)] have considered the relaxation mechanism from the exchange bath to the phonon bath due to the phonon scattering by ^{4}He impurities.

Here we calculate the relaxation time of this mechanism, following to the similar treatment with the calculation developed by Richards[45)]. Let us take the ^{3}He - ^{3}He and ^{3}He - ^{4}He exchange Hamiltonians and the phonon Hamiltonian as the main Hamiltonians,

$$\mathcal{H}_a \longrightarrow \mathcal{H}_T + \mathcal{H}_{34} = \hbar J \sum_{i,j} \mathbb{I}_i \cdot \mathbb{I}_j + \hbar J_{34} \sum_{\Delta} b^{+}_{R+\Delta} b_R \qquad (2\text{-}89)$$

$$\mathcal{H}_b \longrightarrow \mathcal{H}_P \quad , \qquad (2\text{-}90)$$

where b_R is the annihilation operator of a ^{4}He atom at the site R. $R + \Delta$ denotes the nearest neighboring site of the site R. The perturbation Hamiltonian which describes the phonon scattering by a ^{4}He impurity atom due to the mass difference in the solid is given by

$$\mathcal{H}_{4p} = \frac{1}{2}\sum_{R} \Delta m\, \dot{u}_R^2\, n_R$$

$$= \frac{\Delta m}{4Nm}\sum_{R}\sum_{qq'}\sum_{\lambda\lambda'} \hbar\,(\omega_{q\lambda}\,\omega_{q'\lambda'})^{1/2}\, e_{q\lambda}\, e_{q'\lambda'}$$

$$\times\left(c_{q\lambda}\, c^{+}_{q'\lambda'}\, e^{i(q-q')R} + c^{+}_{q\lambda}\, c_{q'\lambda'}\, e^{-i(q-q')R}\right) n_R \quad , \tag{2-91}$$

where $\Delta m = m_4 - m_3$, $n_R = b_R^{+} b_R$ and C_q^{+} is the creation operator of the phonon with wave vector q and palarization λ . When we define the phonon part Δ_R and the particle part A_R by

$$\Delta_R = \frac{1}{4Nm_3}\sum_{qq'}\sum_{\lambda\lambda'} \hbar\,(\omega_{q\lambda}\,\omega_{q'\lambda'})^{1/2}\, e_{q\lambda}\, e_{q'\lambda'}$$

$$\times\left(c_{q\lambda}\, c^{+}_{q'\lambda'}\, e^{i(q-q')R} + c^{+}_{q\lambda}\, c_{q'\lambda'}\, e^{-i(q-q')R}\right) \tag{2-92}$$

and

$$A_R = \Delta m\; n_R \quad , \tag{2-93}$$

eq. (2-91) is expressed as

$$\mathcal{H}_{4p} = \sum_{R} \Delta_R\, A_R \tag{2-94}$$

The a-bath is considered to consist of the ^3He - ^3He and ^3He - ^4He exchange and to be $\mathcal{H}_a = \mathcal{H}_T + \mathcal{H}_{34}$. But since $[\mathcal{H}_T , \mathcal{H}_{4p}] = 0$, only $\mathcal{H}_{34}$ is effective in this relaxation mechanism.

Substituting the main Hamiltonians (2-89), (2-90) and the perturbation Hamiltonian (2-94) into the formula of the relaxation time (2-56), we have a following equation which is similar to eq. (2-68).

$$\frac{1}{T_1} = \frac{\hbar^2}{k_{34}} \Big[\sum_R \sum_{R'} \int_0^\infty \langle \Delta_R(0) \frac{d^2}{dt^2} \Delta_{R'}(-t) \rangle \{ A_{R(0)} A_{R'(-t)} \} dt + \sum_R \sum_{R'} \langle \Delta_{ij}(0) \frac{d}{dt} \Delta_R(-t) \rangle \Big|_{t=0} \{ A_R(0) A_{R'}(0) \} \Big] . \tag{2-95}$$

For the phonon part, using $(\mathcal{C}_\lambda \cdot \mathcal{C}_{\lambda'})^2 = 3$ and $C_q^+ C_q |n_q\rangle = n_q |n_q\rangle$, we obtain

$$\langle \Delta_R(0) \Delta_{R'}(-t) \rangle = \frac{3}{8N^2 m_3^2} \sum_{qq'} \hbar^2 \omega_q \omega_{q'} \times \Big[(n_q + 1) n_{q'} e^{i(q-q')(R-R')} e^{i(\omega_q - \omega_{q'})t} + n_q (n_{q'} + 1) e^{-i(q-q')(R-R')} e^{-i(\omega_q - \omega_{q'})t} \Big] . \tag{2-96}$$

The summation over phonon state is replaced by an integral as

$$\sum_{q} \longrightarrow \frac{V}{(2\pi)^3} \int_0^{2\pi} d\varphi \int_0^{\pi} \sin\theta \, d\theta \int_0^{q_D} q^2 \, dq \quad .$$

The integral of the angular part is easily calculated as

$$\int_0^{\pi} d\theta \sin\theta \int_0^{\pi} d\theta' \sin\theta' \; e^{\pm i(q-q')R}$$

$$= \frac{4 \sin qr \sin q'r'}{q q' r^2} \quad , \qquad (2\text{-}97)$$

where $R = R - R'$. Thus eq. (2-95) becomes

$$\frac{1}{T_1} = - \frac{\hbar^2}{k_{34}} \frac{3\hbar^2 V^2}{2(2\pi)^4 N^2 m_j^2 v^6} \sum_{R} \sum_{R'} \int_0^{\infty} \omega^6 d\omega \frac{\sin^3 qr}{q^2 r^2} n_q(n_q+1)$$

$$\times \int_0^{\infty} d\Omega \; \Omega^2 \int_0^{\infty} dt \left\{ A_R(0) A_{R'}(-t) \right\} \left(e^{i\Omega t} + e^{-i\Omega t} \right) \quad ,$$

(2-98)

where $\Omega = \omega - \omega'$. To obtain this equation we performed the similar estimations as for ω and ω' that were mentioned above eq. (2-72).

$$F(\Omega) = 2 \int_0^{\infty} \left\{ A_R(0) A_{R'}(-t) \right\} e^{i\Omega t} \, dt \quad . \qquad (2\text{-}99)$$

and assume $F(-\Omega) = F(\Omega)$. The inverse Fourie transformation is expressed by

$$f(t) = \frac{1}{2\pi}\int_0^\infty F(\Omega)\, e^{-i\Omega t}\, d\Omega$$

$$= \left\{ A_R(0)\ A_{R'}(-t) \right\} \qquad (2\text{-}100)$$

and we have

$$\frac{d^2}{dt^2} f(t)\Big|_{t=0} = -\frac{1}{\pi}\int_0^\infty \Omega^2 F(\Omega)\, d\Omega \quad . \qquad (2\text{-}101)$$

eq. (2-100) and (2-101) yield

$$\int_0^\infty \Omega^2 F(\Omega)\, d\Omega = -\pi \frac{d^2}{dt^2}\left\{ A_R(0)\ A_{R'}(-t) \right\}\Big|_{t=0} \quad . \qquad (2\text{-}102)$$

Substituting eq. (2-99) into the left hand side of eq. (2-102) and calculating the right hand side, the integral over Ω and t in eq. (2-98) is expressed by

$$\int_c^\infty d\Omega\, \Omega^2 \int_0^\infty dt \left\{ A_R(0)\ A_{R'}(-t) \right\} \left(e^{i\Omega t} + e^{-i\Omega t} \right)$$

$$= -\frac{\pi}{\hbar^2}\left\{ \left[\mathcal{H}_{34}\ ,\ A_R(0) \right] \left[\mathcal{H}_{34}\ ,\ A_{R'}(0) \right] \right. \quad . \qquad (2\text{-}103)$$

Using Fermi commutation relations

$$\left[b_R \, , \, b_{R'}^{+} \right]_+ = \delta_{RR'}$$

$$\left[b_R \, , \, b_{R'} \right]_+ = \left[b_R^{+} \, , \, b_{R'}^{+} \right]_+ = 0 \qquad (2\text{-}104)$$

and $\left\{ b_R^{+} \, b_R \right\} = x$, we obtain

$$\left\{ \left[\mathcal{H}_{34} \, , \, A_R \right] \left[\mathcal{H}_{34} \, , \, A_{R'} \right] \right\}$$

$$= 2(\hbar J_{34} \Delta m)^2 \, x(1 - x) \, z(\delta_{R,R-\Delta} - \delta_{RR'}) \, . \qquad (2\text{-}105)$$

Substituting eq. (2-103) and (2-105) into (2-98), and using the long wave approximation and $k_{34} = - zNx(1 - x)(\hbar J_{34})^2$, T_1 is described as

$$\frac{1}{T_1} = \frac{1}{(2\pi)^3} \left(\frac{V}{N} \right)^2 \left(\frac{\Delta m}{m_3} \right)^2 \frac{a^2}{v^9} \left(\frac{k_B T}{\hbar} \right)^9 \int_0^{\infty} \frac{y^8 e^y}{(e^y - 1)^2} \, dy \, , \qquad (2\text{-}106)$$

where

$$\int_0^{\infty} \frac{y^8 e^y}{(e^y - 1)^2} \, dy = 40484 \, .$$

For hcp solid ^{3}He this is written as

$$\frac{1}{T_1} = 1.44 \times 10^{18}\, T\left(\frac{T}{\theta}\right)^8 \left(\frac{\Delta m}{m_3}\right)^2 \qquad (2\text{-}107)$$

and for bcc solid ^{3}He

$$\frac{1}{T_1} = 1.36 \times 10^{18}\, T\left(\frac{T}{\theta}\right)^8 \left(\frac{\Delta m}{m_3}\right)^2 . \qquad (2\text{-}108)$$

It should be noticed that $T_1 \propto T^{-9}$.

This result is identical with that by Bernier et al.[15], if $\Delta m/m_3$ is replaced by S which was introduced as a coupling constant between the ^{4}He impurity and the phonon. Nakajima et al.[16] calculated the relaxation time of this mechanism by the transition matrix method. Their result is also identical with the above result. Guyer et al.[22] obtained the relaxation time which was proportional to T^{-7}, by the density matrix method. They considered the motions of ^{4}He impurities in solid ^{3}He as the mass fluctuation waves and included all the correlations of the mass differences. Using the random phase approximation for the random distribution of the ^{4}He impurities, they assumed

$$\sum_{RR'} \left\{ A_R(0)\, A_{R'}(t) \right\}_{MFW} \exp\left[i(\mathbf{q} - \mathbf{q}') \cdot (\mathbf{R} - \mathbf{R}') \right]$$

$$= \sum_{R} \left\{ A_R(0)\, A_R(t) \right\}_{MFW} \quad .$$

But Nakajima et al.[16] pointed out that the mass fluctuation wave was not a good excitation. When the localized model is applied for the motions of ^{4}He impurities and thus the correlation is restricted within the same site and the nearest neighboring site, the result is identical with eq. (2-106).

Fig. 5

Crystal Structures of BCC and HCP

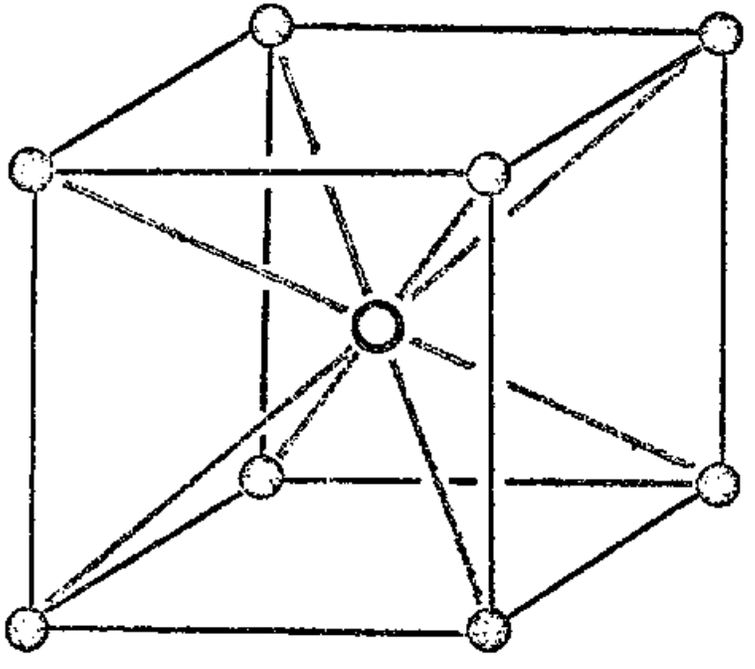

BCC

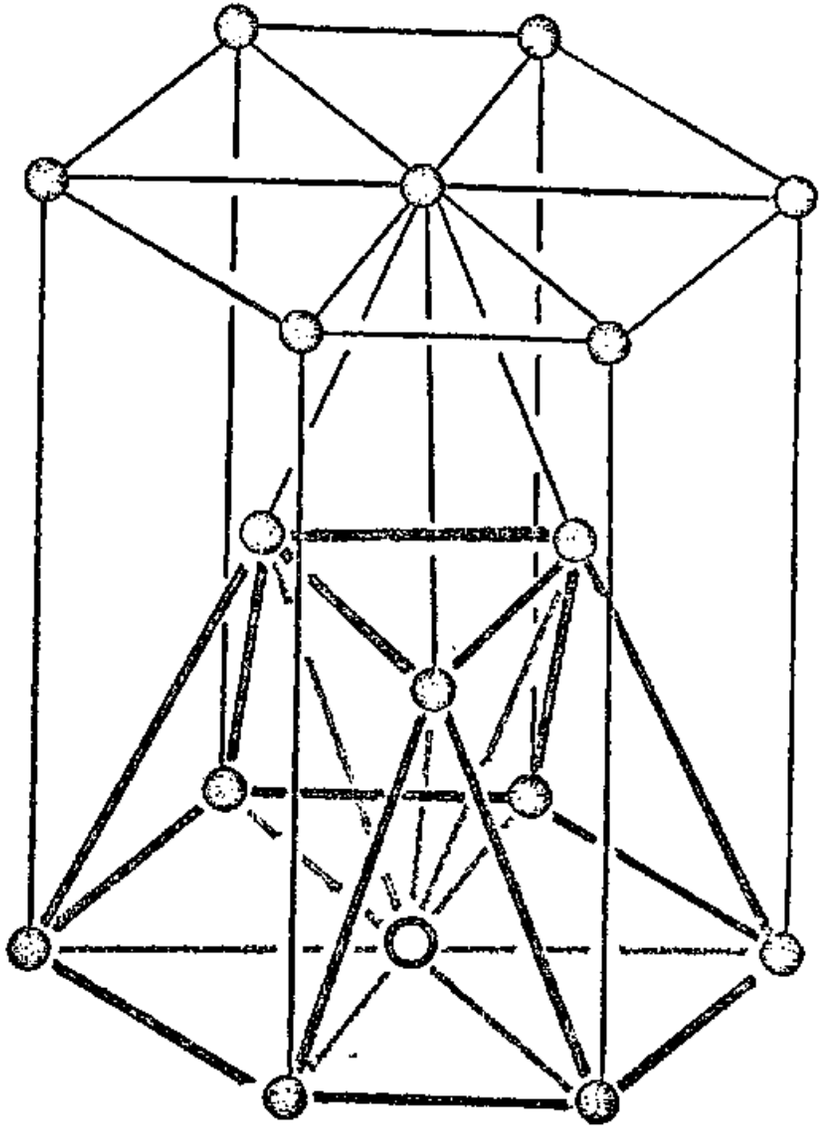

HCP

CHAPTER III

EXPERIMENTAL

§ 1 Cryostat

Dewars were of conventional glass design, with extended tail assembly entering into the gap of the electric magnet. The outer Dewar contained liquid N_2. The inner Dewar which contained liquid ^4He was about 890 mm long in all and 86 mm i.d. The tail was about 390 mm long and 35 mm i.d. Temperature from 4.2 K to 1.2 K was attained by pumping liquid ^4He in this Dewar. We constructed a cryostat, which immersed in liquid ^4He, as shown in Fig. 6. We could attain temperature between 1.2 K and 0.4 K by pumping liquid ^3He in a pot inside a vacuum can. The sample ^3He was introduced through a cupronickel capillary tube (0.15 mm i.d., 1.0 mm o.d.) to a sample cell. The sample cell shown in Fig. 7 was made of Kel-F that is easily machinable. He atoms can penetrate through the Kel-F wall by diffusion at room temperature and it could be detected by a leak detector. But below liquid N_2 temperature there was no leak. The sample cell and the metal parts were connected by screws and they were fastened by finger tight. The sample cell

was attached firmly by a copper supporter to the pot of the ^{3}He refrigerator.

The NMR coils, the transmitter coil and the receiver coils, were wound around the outside of the sample cell which had dimensions of 3 mm i.d., 6 mm o.d. and 50 mm long. Cares were taken to allow no ferromagnetic or supperconducting materials not to disturb the magnetic field and no metal to avoid eddy current heating near the NMR sample cell.

The pressure of the sample was measured by means of a strain gauge invented by Straty and Adams[46], which is also shown in Fig. 7. This consisted of a capacitor formed by a thin diaphragm and a regid plate. Their surfaces were polished by Al_2O_3 polishing powder (0.05 μ). The gauge was made of Be-Cu because this metal obeys the Hooke's law up to high pressure at low temperature. The upper part of this gauge was made of oxygen free high conductivity copper (OFHC) that has large thermal conductivity. The doughnut type mayler sheet of 30 thick was placed between the outer body and the lower plate to insulate electrically and they were fastened by nylon screws. The dimensions of the sample chamber in this pressure gauge were 6 mm i.d., 2mm thick and 0.2 cc. It is easiest to measure the capacitance by the capacitance bridge, but for the lack of this instrument we formed the oscillation circuit by using a backward

diode (BD6) in the low temperature part[53]. The circuit is described in Fig. 8. The heat power of this circuit was about 10 μW. The sample pressure was measured through the frequency of the oscillator. The change of the frequency per 1 kg/cm^2 is about 20 KHz. The stability of the circuit was $\pm$ 2 Hz for a long time, so the sensitivity was about 2×10^{-4} kg/cm^2. The reproducibility of this gauge was good for the heat cycle between He temperature and N_2 temperature but not good between the low temperature and the room temperature.

We have used two germanium resistance thermometers. The one was attached by the GE cement on the copper supporter just above the sample cell for the purpose of measuring the temperature of the sample. The other was cemented on the liquid ^{3}He pot. Associating it with the manganin heater wound around the pot, we composed the feedback circuit to stabilize the temperature. The thermometers were calibrated against the ^{3}He vapor pressuure and the suceptivility of solid ^{3}He which obeys the Curie's law. The calibration was futher checked by taking the melting curve of solid ^{3}He and comparing it with the data by Grilly[51].

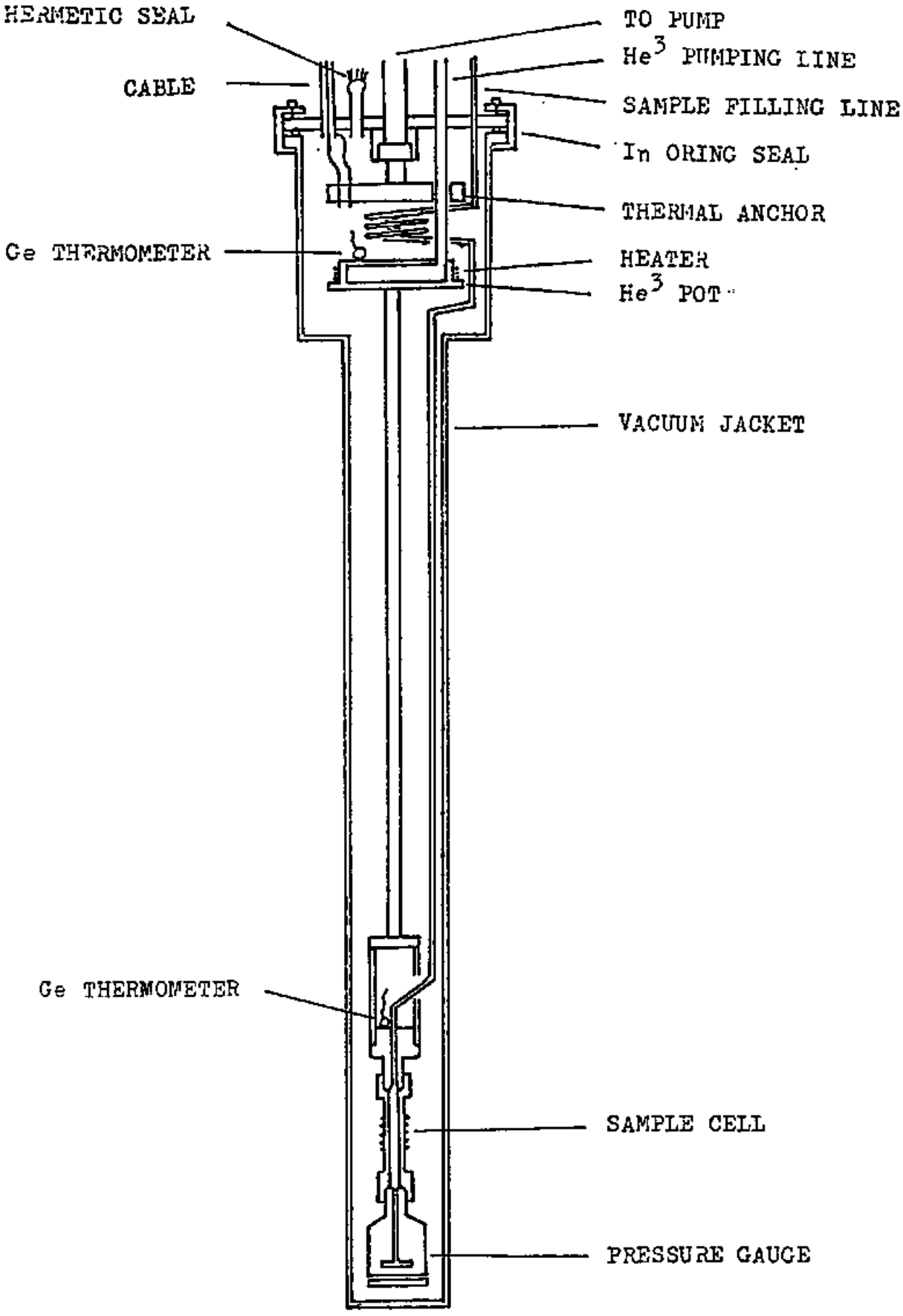

Fig. 6

Main Part of Cryostat

Fig. 7

Sample Cell and Strain Pressure Gauge

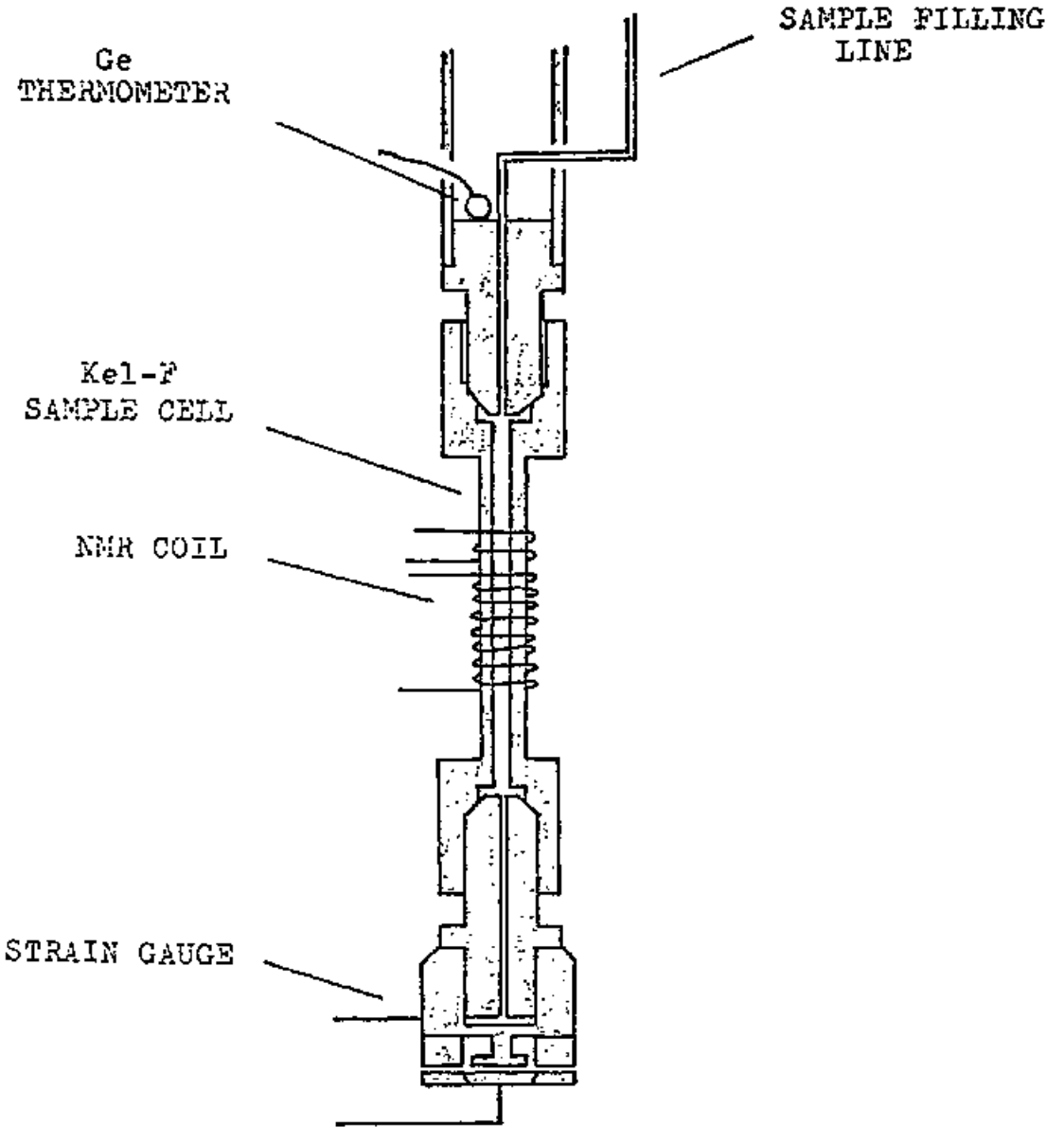

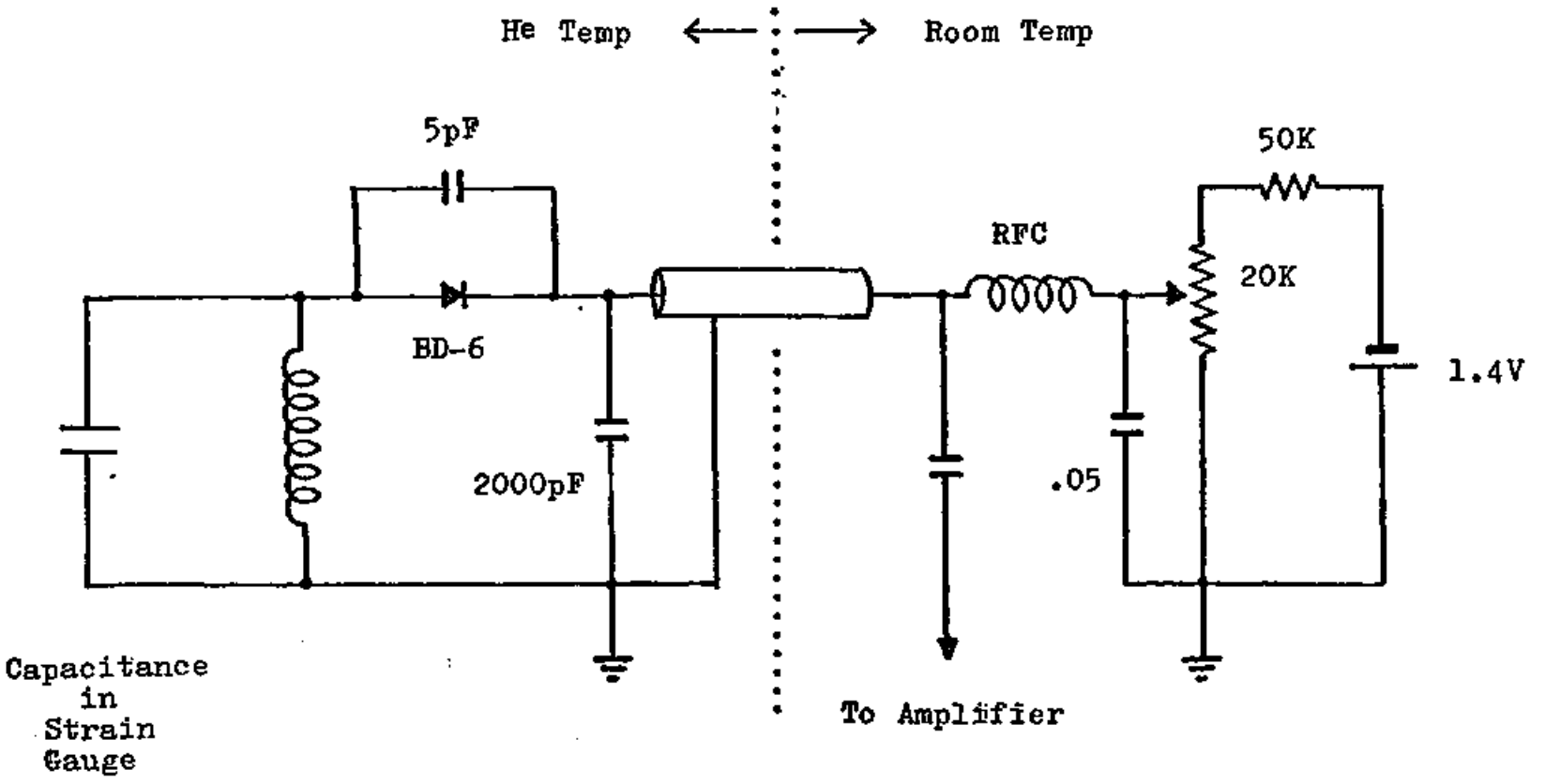

Fig. 8

Oscillation Circuit for the Strain Pressure Gauge

§ 2 Gas Handling systems

We have constructed the gas handling systems to prepare the sample solid Helium. They consisted mainly of a pressure unit, a sample storage unit and a flashing unit, as shown in Fig. 9.

We used about 3.5 liters ^{3}He gas for samples and it was stored in the sample storage unit. This unit was separable from the main system and movable in order to utilize also for the sample purification systems.

A cryopump was placed between the sample storage unit and the pressure unit. It had a copper cell around which the manganin heater was wound. Being cooled down to about 1.2 K by pumping liquid ^{4}He, the cell could inhale about 90% ^{3}He in the storage tanks. Then ^{3}He sample was transferred to the pressure unit by warming the cell up to the liquid N_2 temperature.

Pressure was generated by the oil pressure pumps which were operated by hands. The oil was silicone (Toshiba Silicone TSF 451). The pressure of the oil was measured by two Bourdon gauges. The one could measure up to 50 kg/cm^2 and the other up to 200 kg/cm^2.
A commercial pressure gauge (Texas Instrument Inc. Model 145 with Type 7 capsule) was used as the pressure standard.

The compressed oil in turn pushed the mercury in a steinless steel U-tube, which compressed the helium gas. To prevent the entrance of the mercury into the low temperature part, the level was monitored by means of a electric level meter. The sensers of the level meter were straight steinless steel wires, which were put into the U-tube from the top. The wires with different length were insulated with each other and the U-tube body. The electric circuit was constructed with them to put the lamps on, when the level of the mercury went up and the lower tip of the wire was immersed in it.

We also measured the level of the mercury by the γ ray method. The scintillation counter was placed against the γ ray source through the U-tube. The counter and the source could move up and down with the same height. The level of the mercury could be measured by the change of the counts due to the absorption of the γ ray by the mercury.

A steinless steel capillary carried the compressed gas from the U-tube to the cryostat. We have made a trap (① in Fig. 9) to avoid the mercury vapor going into the cryostat. It was packed with fine copper wires and was cooled by liquid N_2. This trap was also useful for avoiding the disaster of the mercury pathing into the cryostat at the high pressure.

There were other three traps (②, ③ and ④ in Fig. 9) between the storage tanks and the cryostat to absorb impurity gases such as nitrogen, oxygen and vapor. The traps ② and ④ were packed with molecular sieves and the trap ③ was filled with fine copper wires. They were cooled by liquid N_2.

We equipped the flashing unit to flash the sample filling line by ^3He gas before the experiment. We prepared about 2 liters ^3He gas for this operation.

Fig.9 Gas Handling Systems

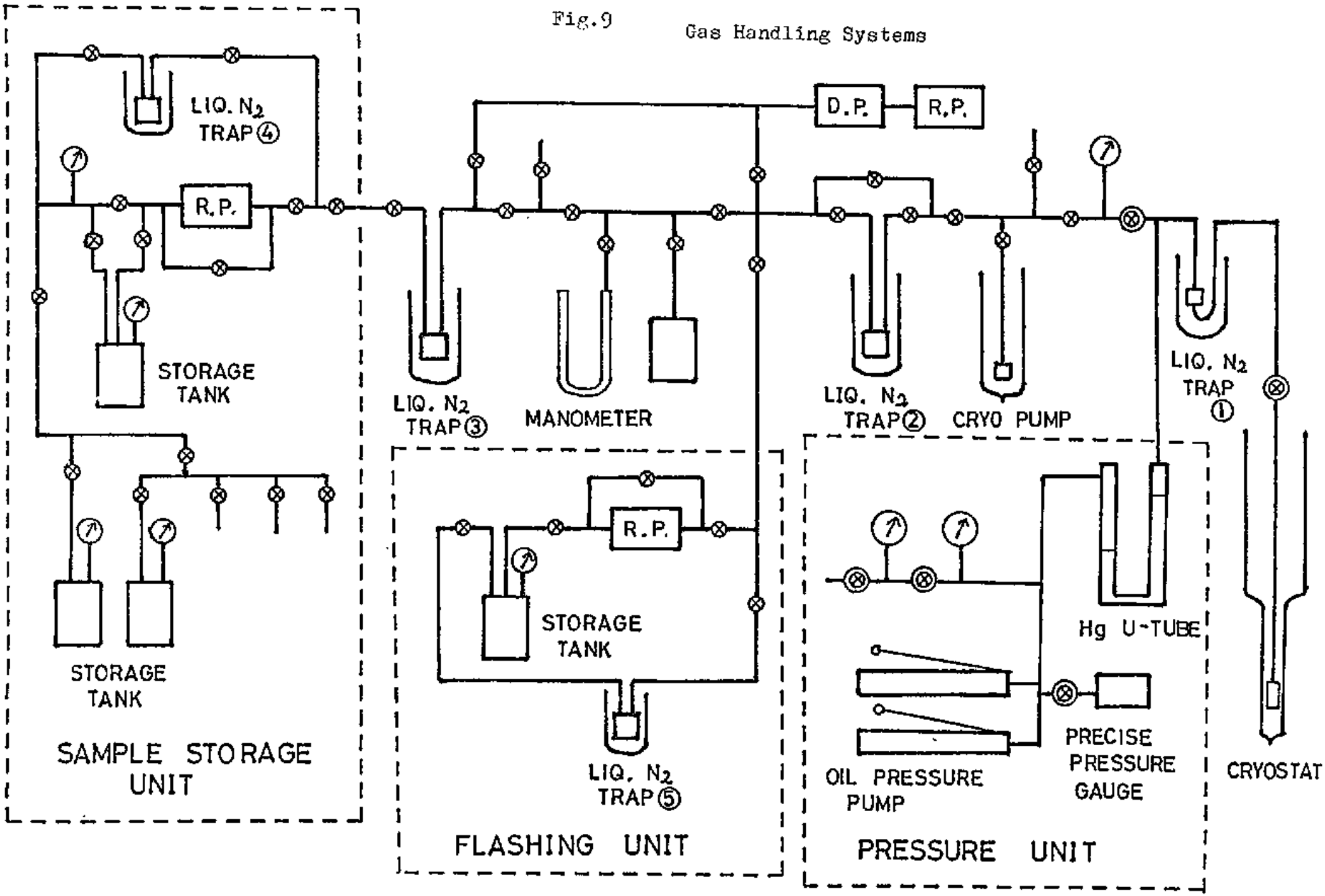

§ 3 Experimental Procedure for Sample

We got ^{3}He gas whose concentration was 99.9%. We made gaseous samples with high concentrations of ^{4}He by adding the known amount of ^{4}He gas. The purer samples were prepared by purification apparatus.

We constructed a rectifying column as shown in Fig. 10, following the reports by R.P Giffard et al.[47),48)]. The rectifying column was a 120 mm long and 10 mm o.d. steinless steel tube containing steinless steel mesh (200 meshs per 1 inch square). The top of the column was made of copper and was in good thermal contact with the ^{4}He bath at about 1.2 K. The evapolator which was made of copper was positioned at the bottom of the column. Its volume was 6,6 cc and the liquid ^{3}He in this evapolator corresponded to the gaseous ^{3}He of 4.6 litters at room temperature. The manganin heater (70 Ω) was wound around it. Carbon resistance thermometers (47 Ω) were fixed on the top and the bottom of the column for temperature measurement.

In operation the liquid ^{3}He in the evapolator was pumped out and the heat power was supplied to the heater of the order of 1 mW to keep the temperature difference between the bottom and the top of the column about 1 mK. The helium mixture climbed the column changing from vapor

to dew or vice versa over and over again on the mesh and thereby was rectified. As we had no attachable analyzer and could not monitor the concentration of ^{4}He in the returning gas, we could not search the best conditions to obtain the pure ^{3}He efficiently. But we collected about 90% of the initial gas and could reduce the concentration of ^{4}He impurity down to 30 or 20% at one run.

The concentration of ^{4}He in the sample was determined by means of the mass spectrometer (type CH4 made by Atlas K.K.) before and after the run of the experiment. The lower limit of the ^{4}He concentration which we could analyze by this analyzer was about 2×10^{-6}. The precision of this instrument was about 10^{-3}.
The difference between the ^{4}He concentrations of the sample before and after the experiments was within about 5%.

Prior to each series of experimental runs, two days were spent for cleaning up the sample filling lines to avoid the contamination with air which caused to block the fine capillary in the low temperature parts. After pumping out for one day to remove the outgas in the system, we flashed the system by using the flashing unit. First we filled the sample lines with the ^{3}He gas at about one half atmosphere. Then we pumped out the ^{3}He gas for one or two hours, and eliminated air contained in

the returning gas by the trap ⑤. These flashing processes were repeated about ten times. By means of this procedure a small amount of air could be rejected and was replaced by ^{3}He. It was a tedious preparation but was necessary not to block the fine capillary in the cryostat.

After flashing about five or six times we began to precool the cryostat by liquid nitrogen. About half a day was spent for the precooling. Then we transferred liquid ^{4}He from the vessel to the Dewar.

We next show the way how we formed the sample solid ^{3}He. The ^{3}He gas in the sample storage tanks was transferred to the mercury U-tube by the cryopump. Then we compressed the sample gas by the mercury U-tube and the oil pressure pump. The pressure of the oil was monitored by the two Bourdon gauges. This pressure, however, was different from that of the sample gas because of the difference of the mercury levels in both sides of the U-tube. We measured the level of the mercury by the γ ray method, and estimated the gas pressure from the oil pressure and the mercury level difference.
The observational error of the mercury level was about $\pm$ 3 mmHg, which corresponded to $\pm$ 10^{-2} kg/cm^2 of the gas pressure.

Till the gas pressure reached to 3.0 kg/cm^2, the high pressure value just above the cryostat was closed.

It was because we were afraid that the concentration of the sample in the U-tube at room temperature became different from that in the cryostat at 4.2 K. The sample ^{3}He was forced to enter into the cryostat. Then we calibrated the strain pressure gauge in the cryostat at 4.2 K and obtained the relations between the frequency of the strain gauge and the pressure of the sample. After solidification of the sample, the pressure of the sample could be measured only by the strain gauge.

The next procedure was to solidify the sample. We used so-called blocked capillary method to form solid sample. First at 4.2 K we compressed sample ^{3}He, which was liquid state at this temperature, up to the pressure corresponding to the desired molar volume. The PVT relation on the melting curve of ^{3}He is known from the published data[49),50),51)]. Then the sample was cooled by pumping liquid ^{4}He in the inner Dewar. When the temperature was lowered, the capillary was blocked by the solid ^{3}He sample in the region where the temperature was first reduced to the melting point. This region is thought to be near the surface of liquid ^{4}He. Once the capillary is blocked, the molar volume in the sample cell remains constant and the state of the sample changes along the melting curve. We could easily observe the moment of the block according to an abrupt decrease of the sample

pressure monitored by the strain gauge in the cryostat. Then we reduced the temperature rapidly until all the sample changed to solid. It took about one hour from the blocking to the solidification of all the sample in the cell.

After the solidification was completed in the sample cell, in order to anneal the sample, we increased the temperature slowly just above the melting point. Then the sample was cooled again slowly below the melting point. This procedure was repeated about three times. It took about two hours for one cycle. The molar volume of the solid sample was determined from the measured melting pressure using the PV relation reported by Grilly and Mills[49].

Then we reduced the temperature down to 1.2 K which was the lowest temperature obtained by pumping liquid ^{4}He. ^{3}He gas for coolant was slowly introduced to the pot in the vacuum can and was liquefied at this temperature. About 1.5 liters ^{3}He gas was prepared for this coolant. Simaltaneously we began to pump out the exchange ^{4}He gas in the vacuum can to isolate the liquid ^{3}He pot and the sample cell thermally from the liquid ^{4}He bath. We waited at least three hours in this situation till we began to decrease temperature below I.2 K.

We observed the relaxation behaviors mainly at the ^{3}He temperature. During the NMR measurement we first roughly controlled the pumping rate of ^{3}He by the needle value and then we operated the feedback temperature controller which fed the current to the heater wound around the ^{3}He pot. We could perform our NMR experiment at the ^{3}He temperature for about 18 hours until the liquid ^{4}He level went down below the top of the vacuum can.

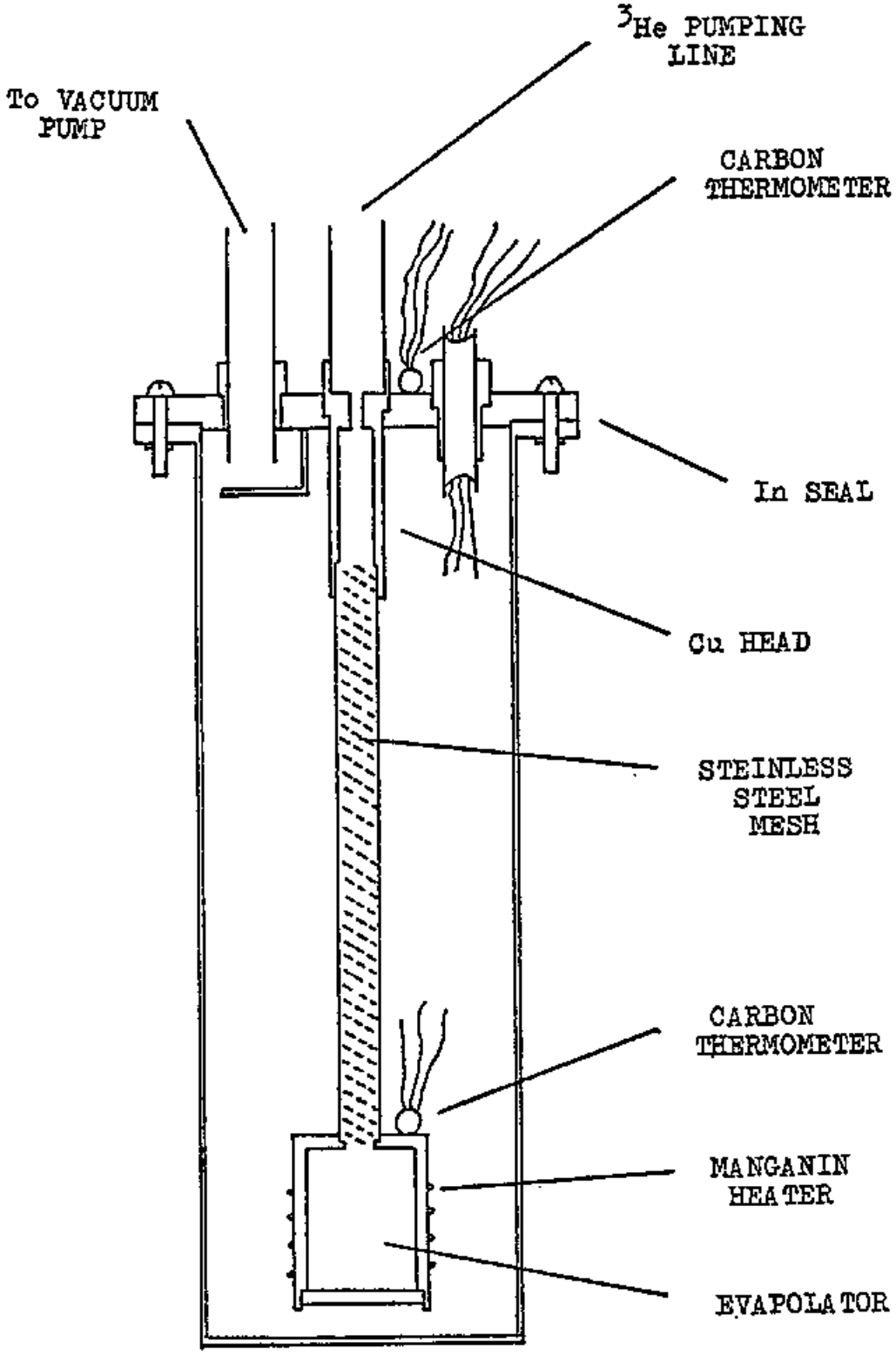

Fig. 10

^{3}He Rectification Column

§ 4 NMR Apparatus

The nuclear relaxation times T_1 and T_2 were measured by using a coherent pulsed NMR spectrometer. The range of frequency was 1~4.2 MHz. The blockdiagram of the NMR apparatus used in this experiment is shown in Fig. 11. The main parts of this apparatus consisted of the trigger generator, the exciter, the receiver system, the data acquisition system, the data display system, the electric magnet and the proton controller. Almost all the systems were constructed by the I.C. or transistors. The trigger generator and the data acquisition system were programmed by the microcomputer.

The trigger generator programmed by the microprocessor generated the trigger sequences to observe the free induction decay signals or the spin echo signals. It also provided the trigger pulses for the memory syncroscope and the sample holding system. The pulse generator which was composed of the monostable multivibrators produced the pulse which had the suitable pulse width for 90° pulse. The 90° pulse means that the pulse satisfies the relation of

$$\int_0^{t_p} \gamma H_1 \, dt = \frac{\pi}{2} \quad , \tag{3-1}$$

where t_p is the pulse width and H_1 is the magnitude of

the component of circularly polarized rf field rotating with the frequency ω_0. In the exciter the continuous rf wave from the signal generator was gated by the pulse and was amplified. Then the rf pulse was transmitted to the coil in the cryostat. The pulse width was about 20 μsec for the 90° pulse. The transmitter coil was wound around the sample cell. The coil had dimensions of 6 mm diameter and about 15 mm long, and was 5 turns of copper wire. On this construction the oscillating magnetic field in the coil was estimated to be about 4 Gauss. The receiver coil was 140 turns of the copper wire.

The NMR signal was amplified by the preamplifier mounted on the head of the cryostat. The variable capacitor in this amplifier and the receiver coil composed the tank circuit to tune the resonant frequency. The gain was about 25 dB. The output impedance was converted to 50 Ω . Then the signal was attenuated suitably not to saturate the main amplifier. In the main amplifier the signal was detected by the diode and was amplified. The gain was about 60 dB. Both the preamplifier and the main amplifier were of the narrow band type. The NMR signal was shown on the memory syncroscope. In addition we constructed the sample holding systems in order to store the data automatically. This system held the height of

the free induction decay signal and the output voltage was coverted to the degital values by the degital volt meter. The degitalized signal was arranged by the microcomputer and the data were written on the teletype.

A electric magnet which had a flux stablizer was used. The homogeneity was 10^{-6} per 10 mm and the stability was 10^{-7} for a short time scale and 10^{-5}/hour for a long time scale. It was very important to stabilize the magnetic field to measure the long relaxation times. A proton NMR controller was used for the experiment at 3 MHz, which developed the stability to 10^{-6}/hour for a long time scale.

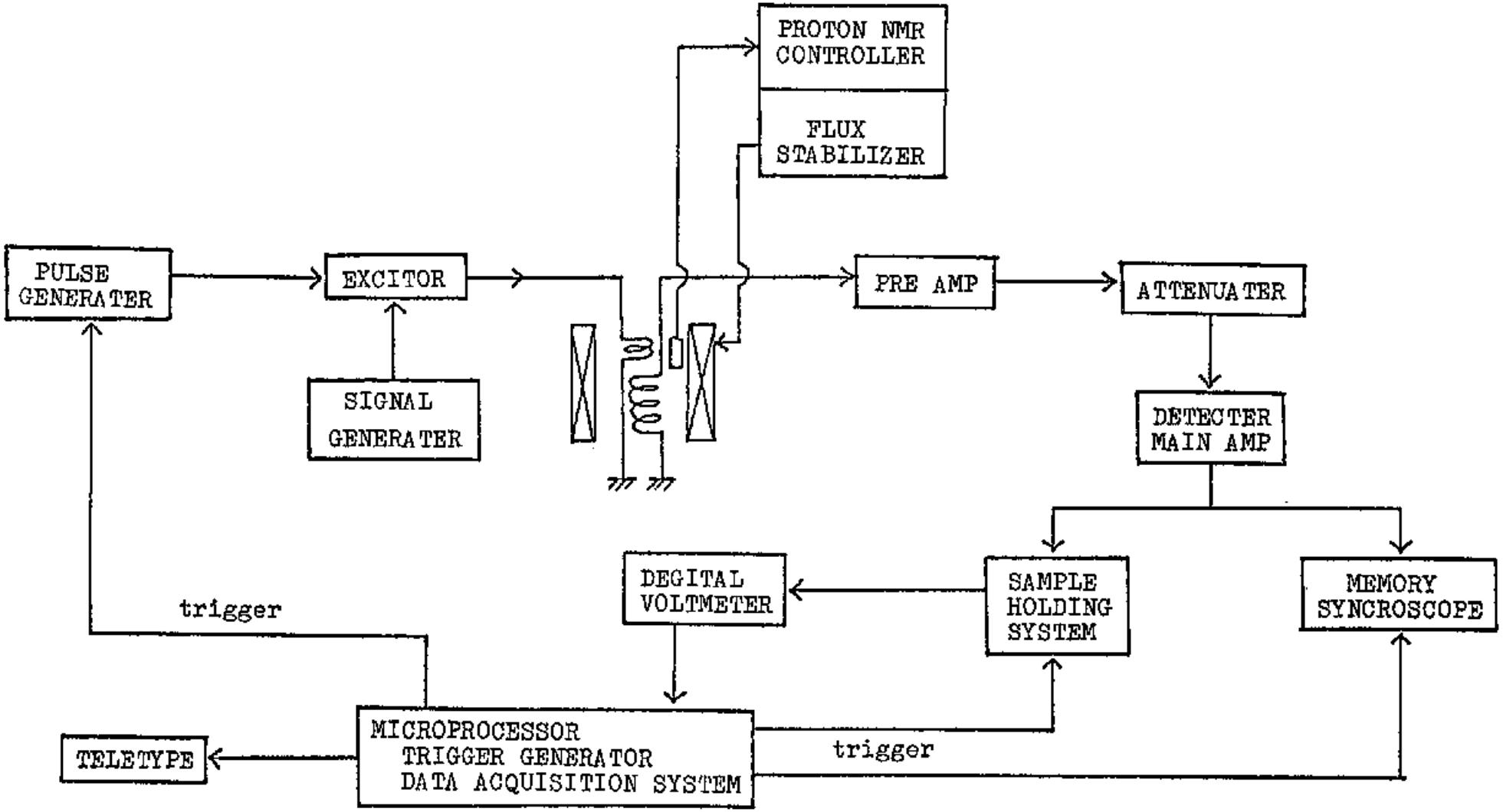

Fig. 11

Blockdiagram of NMR Apparatus

§ 5 Experimental Procedure for NMR

In this section we describe the adjustments of the NMR apparatus and the methods of the measurements of the relaxation times.

Before the measurements at every experiment we adjusted the NMR apparatus. The adjustments mention below were performed when the solid sample was formed and the temperature was at about 1.2 K where the magnetization recovery was a single exponential function of time and the spin lattice relaxation time was short (order of 1 sec). First we locked the magnetic field whose magnitude was determined from the relation, $H_0 = \omega_0/\gamma$, for the frequency at which we wanted to take data. We found the just resonance condition by means of canceling the beats between a free induction signal and a leak wave from the excitor. Next we tuned the excitor and the preamplifier with the resonant frequency by adjusting the variable capactances. Then we searched the 90° condition for the rf pulse. The height of the free induction signal is maximum when the tipping angle is 90°. The dead time of the receiver after the rf pulse was about 100 μsec and there was a very small ringing after that.

After these adjustments we ascertained whether the magnetization recovery was a single exponential function

of time in the exchange plateau region. Owing to the degitalized apparatus, we could measure the magnetization signals with the precision of the one part of 10^3.

Next we will describe the methods of T_1 and T_2 measurements. For the measurement of T_1 we used the two pulse method and the multipulse saturation method.[11] The pulse sequences of these methods are shown in Fig. 12. The two pulse method we used was the conventional 90° - 90° pulse one. After waiting for a time of more than five times T_1, in which the spin system comes to thermal equilibrium with the phonon system, the pulse sequence 90° - 90° was applied. We measured the heights of free induction decay signals just after the pulses as a function of the pulse interval, t. If there is only one relaxation time, the relaxation time T_1 is obtained from the equation,

$$M(t) = M(\infty)\ (1 - e^{-t/T_1}) \quad , \qquad (3\text{-}2)$$

where M(t) is the height of free induction decay signal after the second pulse and $M(\infty)$ is that after the first pulse.

If there is an intermediate bath between the Zeeman bath and the phonon bath, the magnetization recovery is expressed by the sum of the exponential functions mentioned in chapter II, § 3. Also in this case, the relaxation

times can be measured by the two pulse method. But when the energy constant of the intermediate bath is very large compared with that of the Zeeman bath, and the relaxation time between the intermediate bath and the phonon bath is very long, the multipulse saturation method is very useful. By means of this method we can obtain both the longest relaxation time and the energy constant of the intermediate bath. After waiting for the spin system to be in thermal equilibrium with the lattice, we apply the 90^{o} pulse train, whose pulse interval τ is shorter than the relaxation time between the intermediate bath and the lattice but is longer than the relaxation time between the Zeeman bath and the intermediate bath. On this condition the rf energy is stored in the Zeeman bath and the intermediate bath, and the baths approach asymptotically to the state that the energy dumped from the rf pulse is equal to the energy which flows away from the intermediate bath to the lattice by the relaxation process.

The height of the free induction decay signal M_n just after the $(n + 1)$ pulse $(n = 0,1,2...)$ is calculated as follows. Let's consider the system which consists of the Zeeman bath Z, the phonon bath L and the intermediate bath X. We assume the relaxation time T_{ZX} between the Zeeman bath and the intermediate bath is enough

shorter than the relaxation time T_{XL} between the intermediate bath and phonon bath. We note that the energy E of a bath except for the phonon bath is expressed as $E = k\beta$ in the high temperature approximation, where k and β is the energy constant and the inverse temperature of the bath respectively. We call here the Zeeman bath and the intermediate bath in the lump as a floating system, whose energy constant is $k_S = k_Z + k_X$. $\beta_n(t)$ stands for the inverse temperature of the floating system at a time t after the n th pulse. Before the n th pulse the floating system is in equilibrium with an inverse temperature $\beta_{n-1}(\tau)$ because we choose the pulse interval τ such as $T_{ZX} \ll \tau \ll T_{SL}$. Since the Zeeman bath at temperature $\beta_{n-1}(\tau)$ gets energy of $-k_Z \beta_{n-1}(\tau)$ from the n th 90^o pulse, considering the energy conservation law, we have

$$k_S \beta_{n-1}(\tau) - k_Z \beta_{n-1}(\tau) = k_S \beta_n(\tau_1) \quad , \qquad (3\text{-}3)$$

where τ_1 is the order of T_{ZX} and we have neglected the relaxation characterized by T_{XL}. Because $\tau_1 \ll \tau$, $\beta_n(\tau_1)$ is taken as the initial condition for the relaxation from the floating system to the phonon bath and τ_1 can be neglected. After the n th pulse the time evolution of $\beta_n(t)$ is governed by

$$\frac{d\beta_{n(t)}}{dt} = -\frac{\beta_{n(t)} - \beta_L}{T_{SL}} \qquad (3\text{-}4)$$

and so

$$\beta_{n(t)} - \beta_L = (\beta_{n(o)} - \beta_L) \exp(-t/T_{SL}) \qquad (3\text{-}5)$$

Here β_L is the inverse temperature of the phonon bath. T_{SL} is the relaxation time between the floating system and phonon bath, and is equal to the observed relaxation time corresponding to T_{XL},

$$T_{SL} = \frac{k_S}{k_X} T_{XL} \qquad (3\text{-}6)$$

Combining (3-3) and (3-5), we get

$$\beta_{n(\tau)} - \beta_L = \left(\frac{k_S - k_Z}{k_S} \beta_{n-1(\tau)} - \beta_L \right) \times \exp\left(-\frac{\tau}{T_{SL}}\right) \qquad (3\text{-}7)$$

This recurrence equation has a solution as

$$1 - \frac{\beta_n(\tau)}{\beta_L} = \frac{(k_z/k_s)\exp(-\tau/T_{SL})}{1-\{1-(k_z/k_s)\}\exp(-\tau/T_{SL})} \times \left[1-\{(1-k_z/k_s)\exp(-\tau/T_{SL})\}^n\right] . \tag{3-8}$$

The height of the free induction decay signal M_n after the (n+1)th pulse is proportional to $\beta_n(\tau)$.
As $\tau \ll T_{SL}$, we have

$$1 - \frac{M_n}{M_0} = \frac{1}{1+(k_s/k_z)(\tau/T_{SL})} \times \left[1-\exp\left\{-n\left(\frac{\tau}{T_{SL}}+\frac{k_z}{k_s}\right)\right\}\right] , \tag{3-9}$$

if $k_s/k_z \gg 1$. When the other bath Y is coupling with the X bath with the relaxation time T_{XY}, Eq. (3-9) is also valid and $k_S = k_Z + k_X + k_Y$ in the case. if T_{ZX}, $T_{XY} \ll \tau \ll T_{SL}$ is satisfied.

Measuring M_n and M_o, we obtained k_S/k_Z and T_{SL} by the least square fit to Eq. (3-9) using a computer [52].

For the measurement of T_2, we applied the 90^o - 90^o pulse sequences and observed the echo height as a function of the interval time t between the two pulses. The echo height is express by

$$M(t) = Mo \exp(-\frac{2t}{T_2}) \tag{3-10}$$

Fig. 12

PULSE SEQUENCES

○ TWO PULSE METHOD

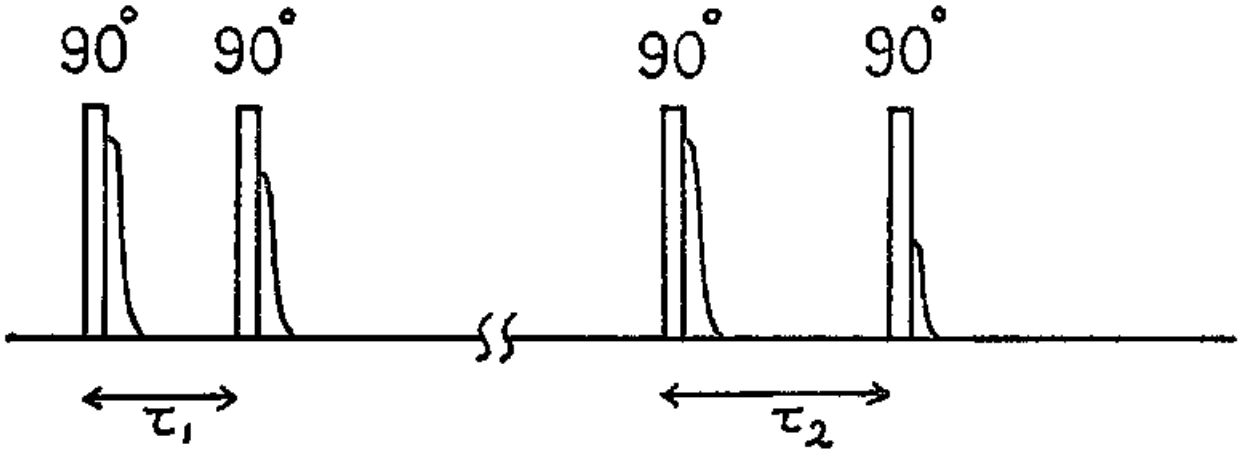

○ MULTI-PULSE SATURATION METHOD

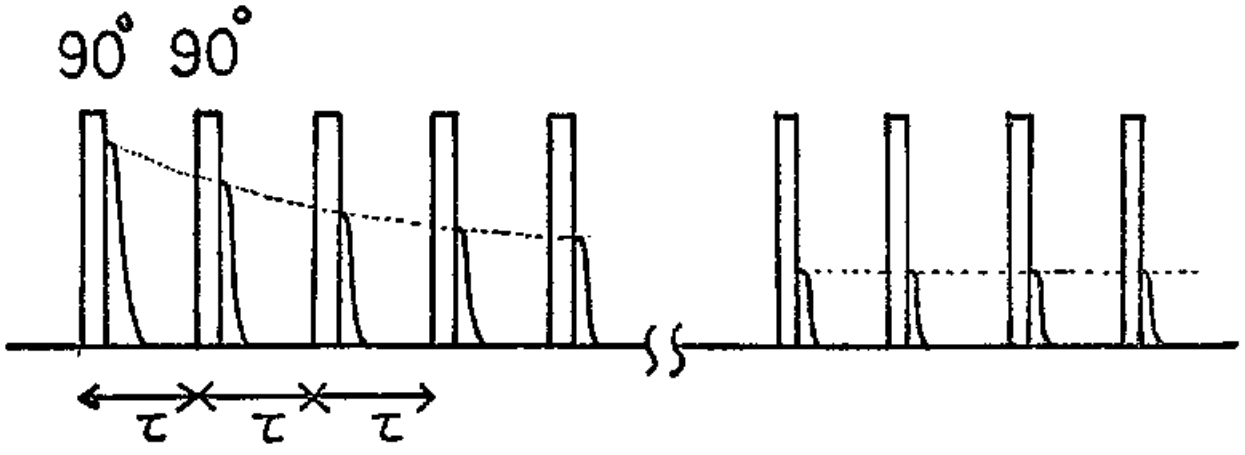

CHAPTER IV

EXPERIMENTAL RESULTS AND PHENOMENOLOGICAL MODEL

1 Introduction

We observed the nuclear spin lattice relaxation times mainly in hcp solid ^{3}He. The molar volume of these samples were 19.65, 19.4 and 19 1 cm^3/mol. 19.65 cm^3/mol is almost the largest molar volume in hcp phase and 19.1 cm^3/mol is the smallest molar volume that we could form by our pressure system. We took data for samples of 19.4 cm^3/mol most systematically. The molar volume of the bcc samples was 20.5 cm^3/mol.

The NMR frequency we systematically used for hcp phase was 3 MHz. For many samples we took data also at 1 MHz and for some samples at 4.2 MHz. The data in bcc phase were at 3 MHz. As the energy constant of the Zeeman bath depends on the NMR frequency, we can change the ratio of the energy constants between the Zeeman bath and the other bath by choosing the proper NMR frequency.

We observed also the spin spin relaxation time T_2 in both phases.

§ 2 Experimental Results in HCP Phase

In Fig. 13 we show the typical data of the temperature variation of the spin lattice relaxation times T_1 in hcp solid ^{3}He with ^{4}He impurities. The concentration of ^{4}He impurities is 4.2×10^{-3}, the molar volume of the sample is 19.4 cm^3/mol and the NMR frequency is 3 HMz. Following to Fig. 13, we describe the characters of the relaxation behavior in detail. We designate three temperature regions, I, II and III in the figure.

Region I where the temperature is above 1.1 K ($1/T = 0.9\ K^{-1}$) is the exchange plateau region and T_1 is independent of temperature. We denote T_1 in region I by T_I. The relaxation mechanism in this region has been already summarized in chapter II, § 4. The magnetization recovery in this region is a single exponential function of time as shown in Fig. 14-(1) and is expressed by

$$\frac{M(\infty) - M(t)}{M(\infty)} = \exp\left(- \frac{t}{T_I} \right) \quad . \qquad (4\text{-}1)$$

In Region II below about 1.1 K the magnetization recovery observed by means of the two pulse method is the sum of the two exponential functions,

$$\frac{M(\infty) - M(t)}{M(\infty)} = (1 - R)\exp(-t/T_{II-1}) + R\exp(-t/T_{II-2}) \qquad (4\text{-}2)$$

as shown in Fig. 14-(2). Therefore we can obtain two kinds of relaxation times, T_{II-1} and T_{II-2}. T_{II-1} is temperature independent, while T_{II-2} is temperature dependent. R in Eq. (4-2), which corresponds to the intercept obtained by extaporating the second magnetization recovery line to t = 0 in Fig. 14-(2), is temperature independent except for the transient region between region I and region II.

When the temperature is lowered below about 0.6 K ($1/T = 1.6\ K^{-1}$), region III, the behavior of the magnetization recovery observed by the two pulse method changes. That is, the first decay of the magnetization is the expotential function of time but the second is not, as shown in Fig. 14-(3). Hence we replot $(M(\infty) - M(t))/M(\infty)$ against $t^{1/2}$ as shown in Fig. 14-(3'), so that we can draw the straight line on the data points. Accordingly we settle T_{III-1} and T_{III-2} by fitting the magnetization recovery to the following equation,

$$\frac{M(\infty) - M(t)}{M(\infty)} = (1 - R')\exp(-t/T_{III-1}) + R'\exp\left[-(t/T_{III-2})^{\frac{1}{2}}\right] . \qquad (4\text{-}3)$$

We call the magnetization recovery which corresponds to T_{III-2} to be a nonexponential recovery. The behavior of the magnetization recovery changed gradually from region II to region III, but T_{III-2} does not necessarily continue to T_{II-2} because these two relaxation times, T_{II-2} and T_{III-2}, are obtained by fitting the recoveries to the different functions. T_{III-2} is temperature independent at sufficiently low temperature and T_{III-1} which corresponds to the magnetization recovery in the first stage is also temperature independent and is the same value as T_{II-1}.

During the course of the two pulse measurements, we found that the magnetization recovery was incomplete even after waiting some ten times T_{III-2}. We call this long relaxation time to be T_{III-3} and measured it by the multipulse saturation method. In Fig. 15 we show the gradual change of the magnitude of the free induction decay signal just after the pulse, M_n. T_{III-3} was observed only in region III where the nonexponential behavior of magnetization appeared. When we applied the multipulse saturation method in region II, the value we got was identical with that of T_{II-2} which was obtained by the two pulse method. T_{III-3} is temperature dependent as $T_{III-3} \propto T^{-7}$. This experiment is the first time that T_{III-3} is found to exist also in hcp phase, although in

bcc phase Bernier and Deville[11] became aware of its existance but not measured it.

In order to study the effects of ^{4}He impurity on the relaxation behaviors in solid ^{3}He, we observed the ^{4}He concentration dependence of the relaxation times and the prefactor R or R' at a very wide ^{4}He concentration range for the same molar volume 19.4 cm^3/mol at the same NMR frequency 3 MHz. In Fig. 16 we show the temperature dependence of relaxation times for samples whose ^{4}He concentrations are 2.0×10^{-5}, 7.0×10^{-5}, 1.6×10^{-4}, 2.8×10^{-4}, 5.8×10^{-4} and 1.2×10^{-3}. For these samples the region III did not appear in our temperature range. In region II of these samples we could not observe T_{II-1} at 3 MHz because R was almost unity. This suggests that the energy constant of the Zeeman bath is very large compared with that of the bath which receives the energy from the Zeeman bath. In order to measure the value R, we made the energy constant of the Zeeman bath to be small by reducing the NMR frequency to 1 MHz. The data at 1 MHz for the same samples are shown in Fig. 17. At this frequency the value of T_{II-1} and R could be measured. Since T_I in the exchange plateau region at 1 MHz is shorter by one order of magnitude than that at 3 MHz, we could observe T_{II-2} over the four or five orders of magnitude. The temperature dependence of T_{II-2} is found to be $T_{II-2} \propto T^{-7}$.

As for the ^{4}He concentration dependence of T_{II-2}, it is found from Fig. 16 and Fig. 17 that T_{II-2} decreases as the ^{4}He concentrations increase. The concentration dependence of T_{II-2} is expressed as $T_{II-2} \propto x^{-1}$ for $x \leq 1.2 \times 10^{-3}$. But it was found that T_{II-2} was insensitive to ^{4}He in the higher temperature part of region II for the samples with ^{4}He concentrations of 2.0×10^{-5} and 7.0×10^{-5}. The relaxation time in the pure limit was more strongly dependent on temperature than the ^{4}He dependent relaxation time.

T_{II-1} was not affected by ^{4}He impurities.

We show the data of solid ^{3}He with ^{4}He impurities of 3.00×10^{-3}, 4.75×10^{-3}, 6.83×10^{-3} and 1.47×10^{-2} in Fig. 18, 19, 20 and 21 respectively. The molar volume of these data is 19.4 cm^3/mol and the NMR frequency is 3 MHz. In contrast with the data of the samples whose ^{4}He concentrations were less than 1.2×10^{-3}, for these samples the values of R were not almost unity and T_{II-1} or T_{III-1} could be observed even at 3 MHz. These results suggest that the energy constant of the bath which receives the energy from the Zeeman bath becomes large with the increase of the ^{4}He concentrations. The data of samples containing ^{4}He impurities of 4.75×10^{-3} and 6.83×10^{-3} (Fig. 19 and Fig. 20) were very similar with

that of 4.20×10^{-3} except for the remarkable change of T_{III-2}. When the ^4He concentration was increased, T_{III-2} becomed short. Extremely for the sample of $x = 1.47 \times 10^{-2}$, T_{III-2} was shorter than T_{III-1}. Consequently region II did not appear between region I and region III.

As seen in these data, R, R', T_I, T_{II-1}, T_{III-1} and T_{III-2} were temperature independent except for the transient regions. These values for 19.4 cm^3/mol at 3 MHz and/or 1 MHz are tabulated in table I.

Fig. 13

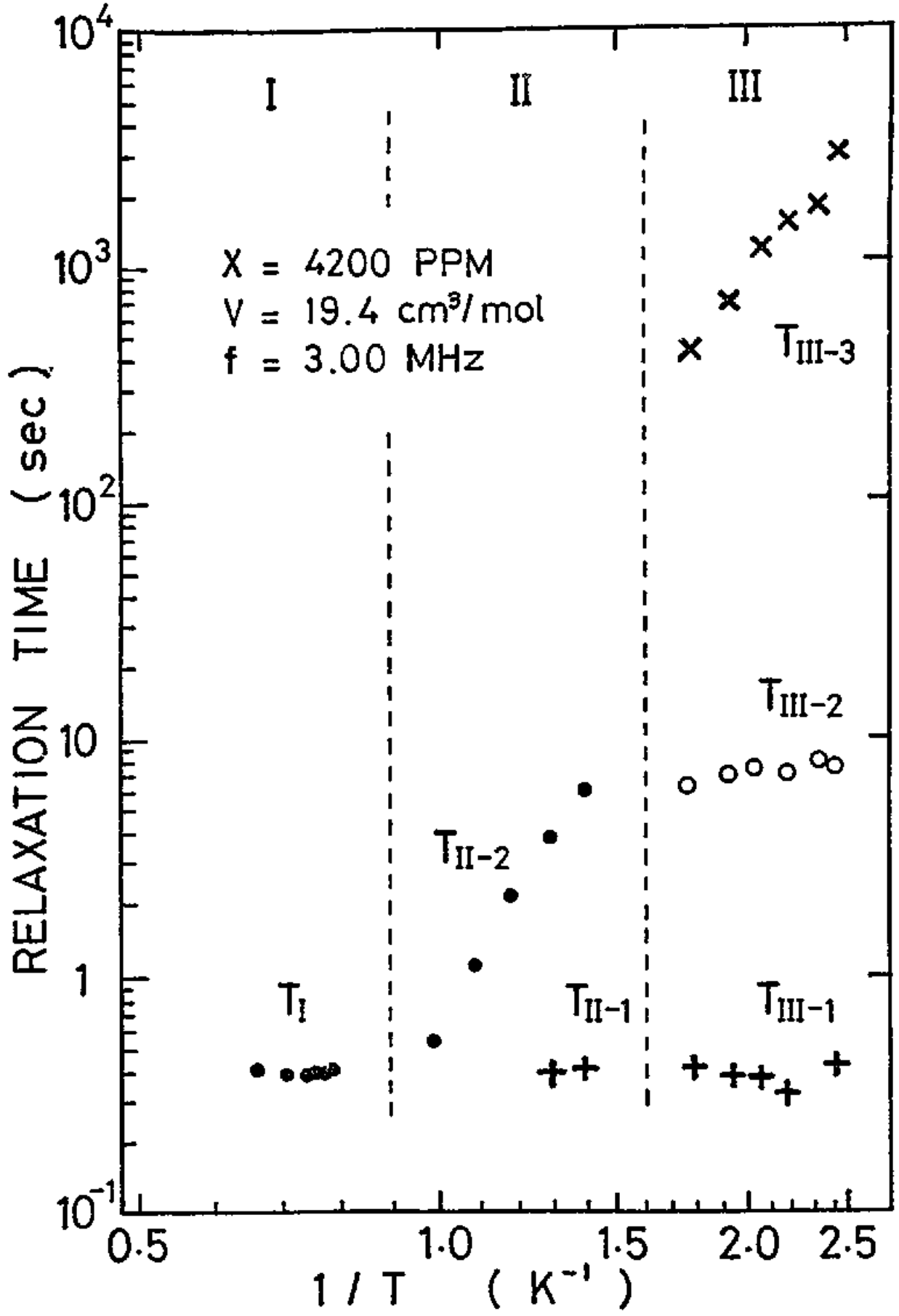
I
II
III
X = 4200 PPM
V = 19.4 cm³/mol
f = 3.00 MHz
T_{III-3}
T_{III-2}
T_{II-2}
T_I
T_{II-1}
T_{III-1}
RELAXATION TIME (sec)
10^4
10^3
10^2
10
1
10^{-1}
0.5
1.0
1.5
2.0
2.5
1 / T (K^{-1})

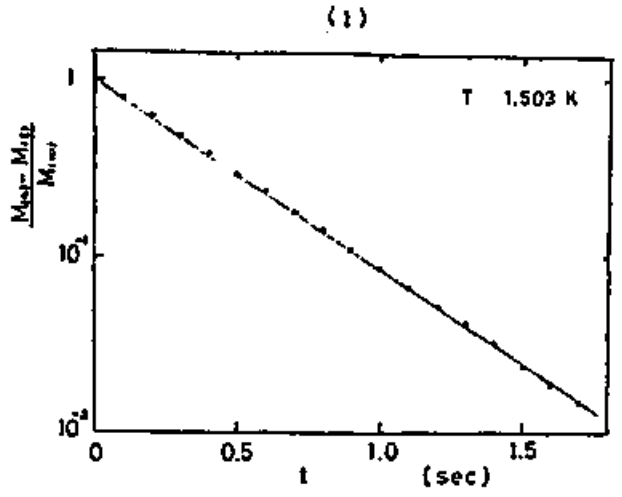

Fig. 14

Typical Magnetization Recoveries at Various Temperatures

HCP, V = 19.4 cm^3/mol

$x = 4.20 \times 10^{-3}$

$\omega_0/2\pi$ = 3.0 MHz

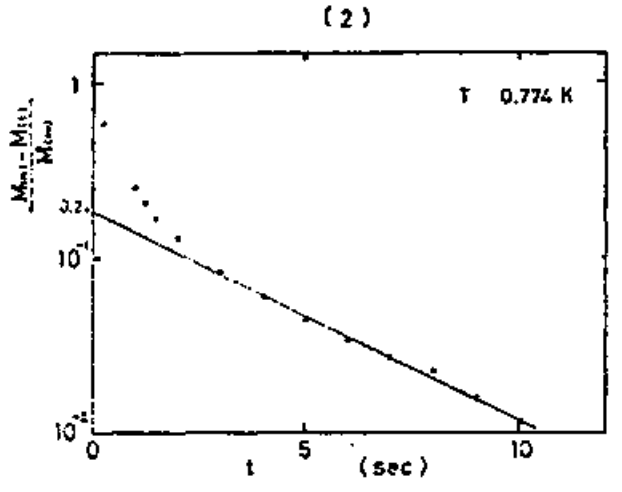

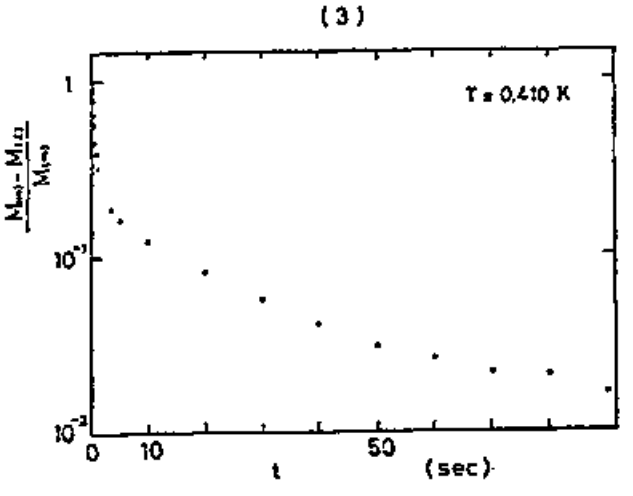

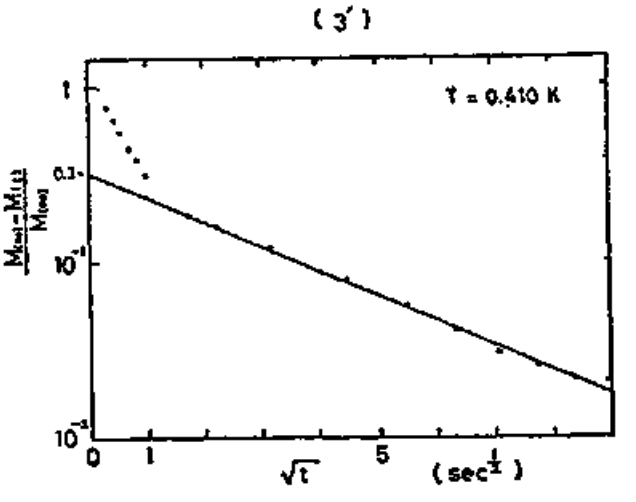

Fig. 15

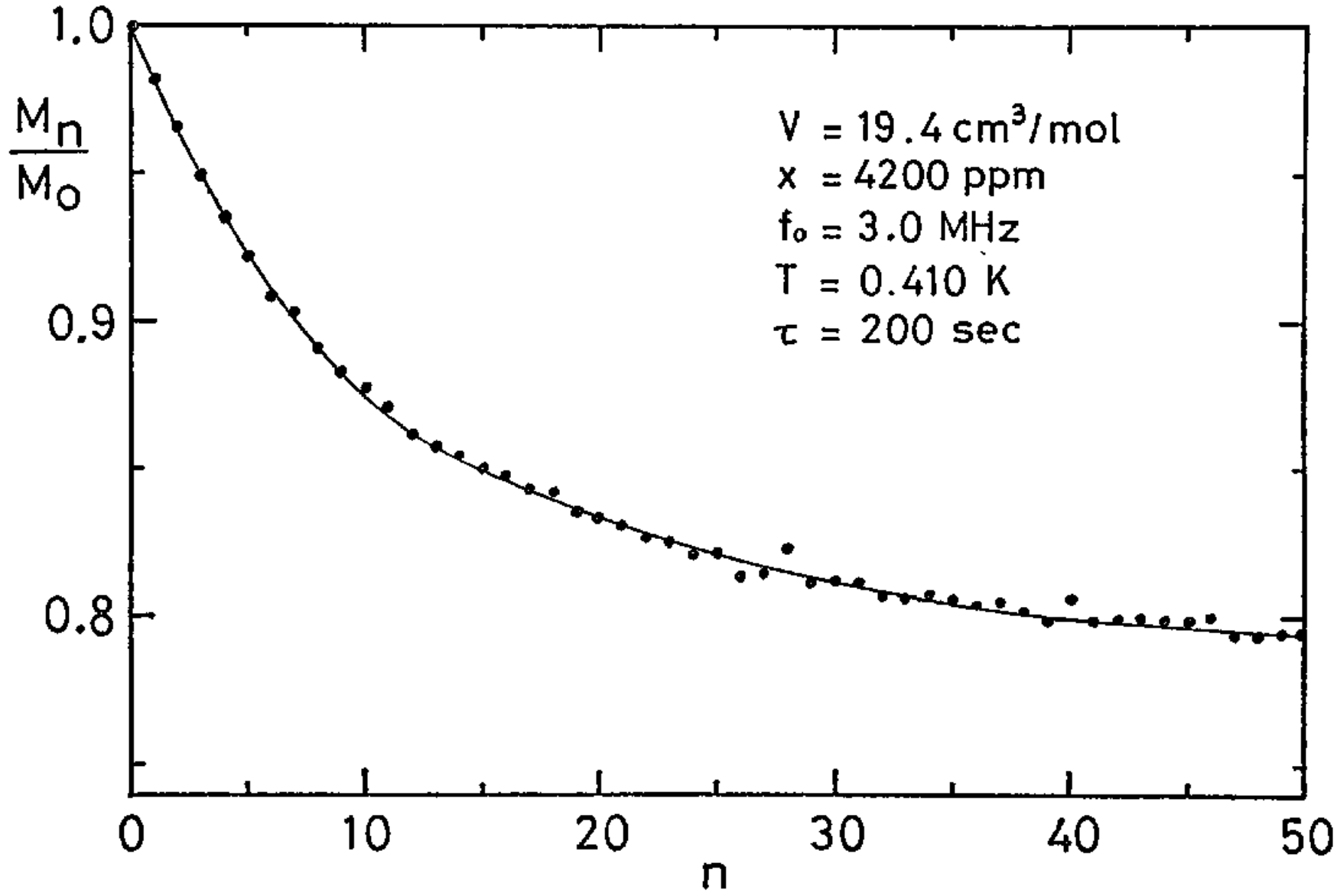
1.0
$\frac{M_n}{M_o}$
0.9
0.8
V = 19.4 cm³/mol
x = 4200 ppm
f_o = 3.0 MHz
T = 0.410 K
τ = 200 sec
0
10
20
30
40
50
n

Fig. 16

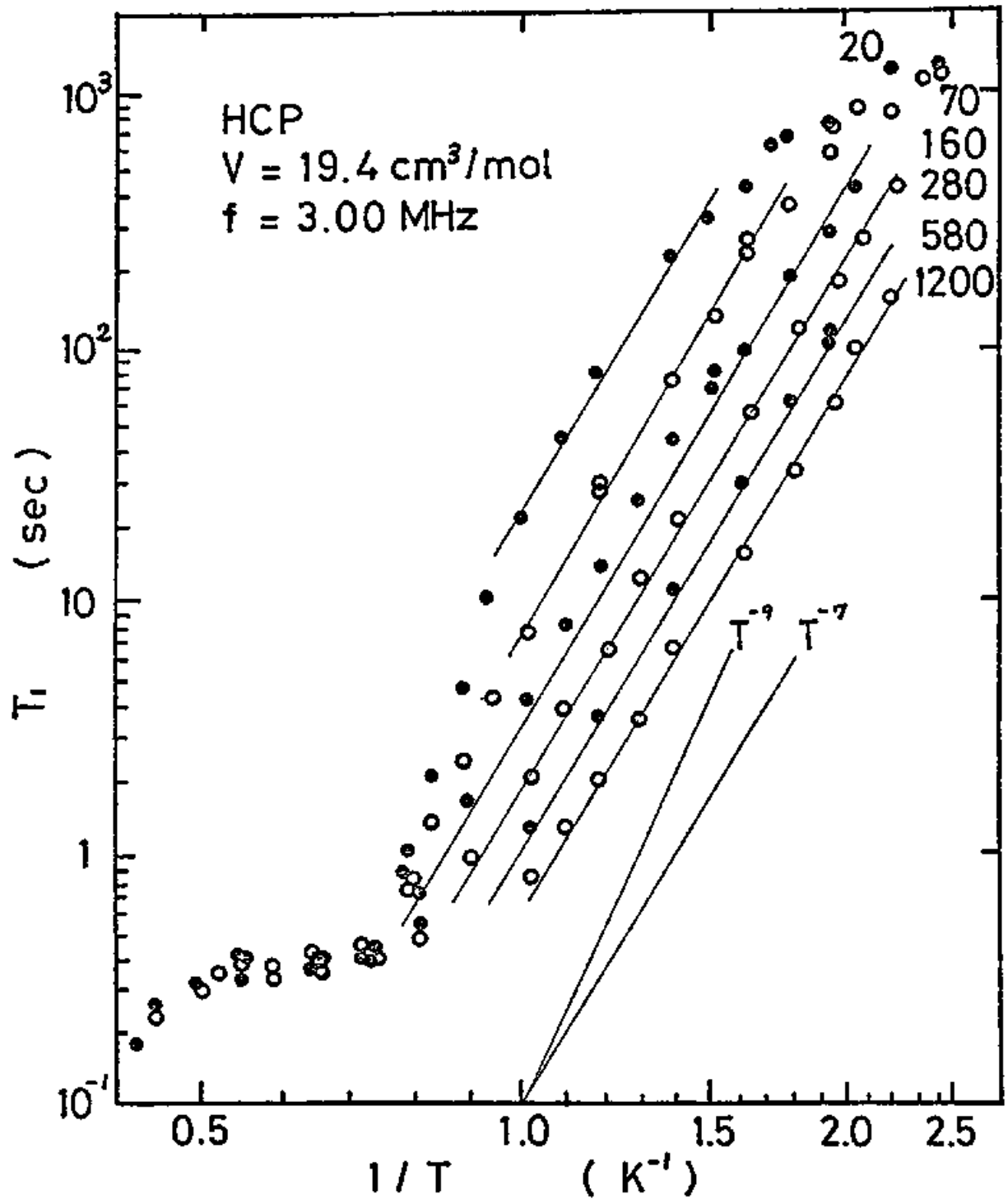
HCP
V = 19.4 cm³/mol
f = 3.00 MHz
20
70
160
280
580
1200
T⁻⁹
T⁻⁷
T₁ (sec)
10³
10²
10
1
10⁻¹
0.5
1.0
1.5
2.0
2.5
1 / T (K⁻¹)

Fig. 17

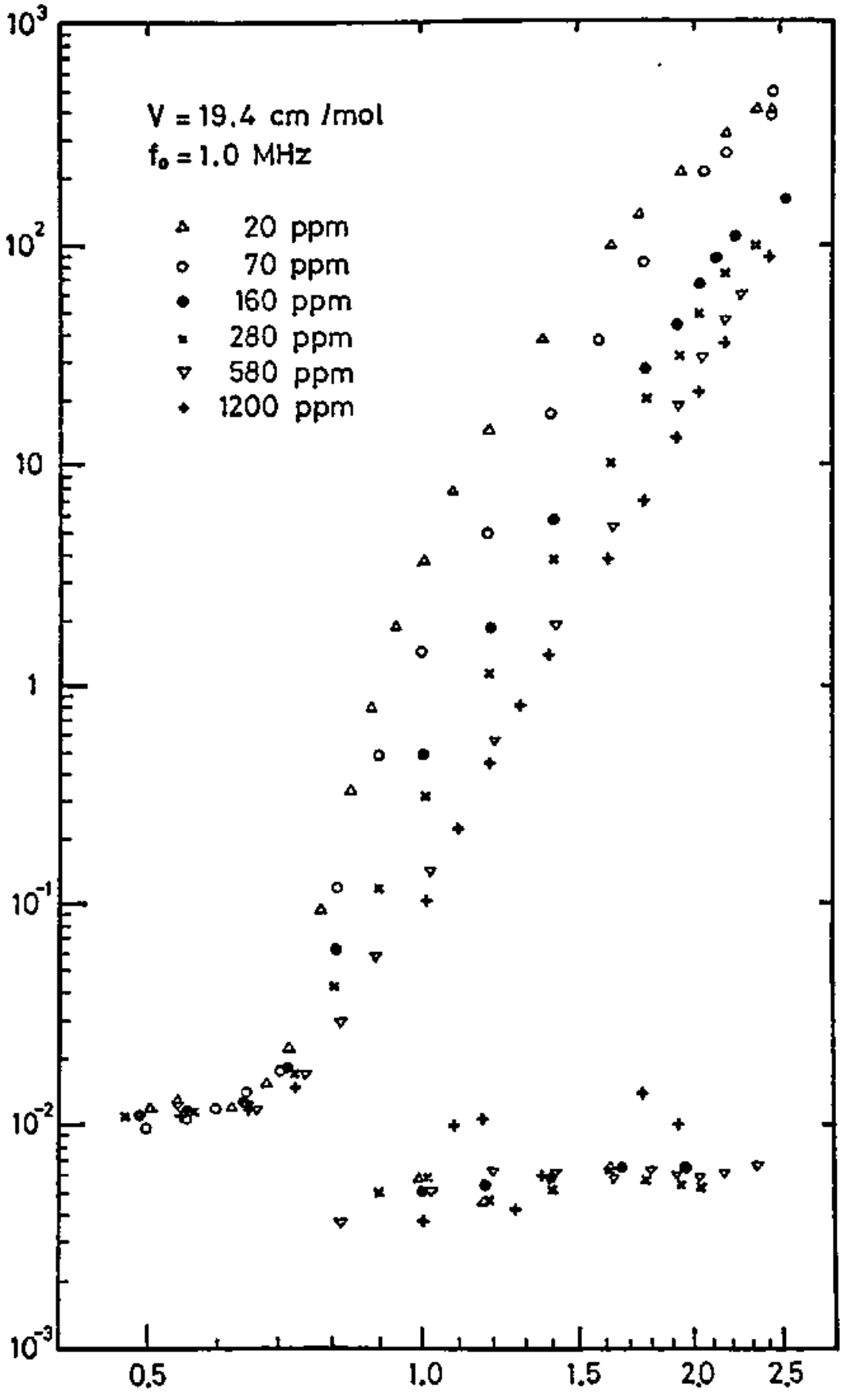
V = 19.4 cm /mol
f_o = 1.0 MHz
20 ppm
70 ppm
160 ppm
280 ppm
580 ppm
1200 ppm
10^3
10^2
10
1
10^{-1}
10^{-2}
10^{-3}
0.5
1.0
1.5
2.0
2.5

Fig. 18

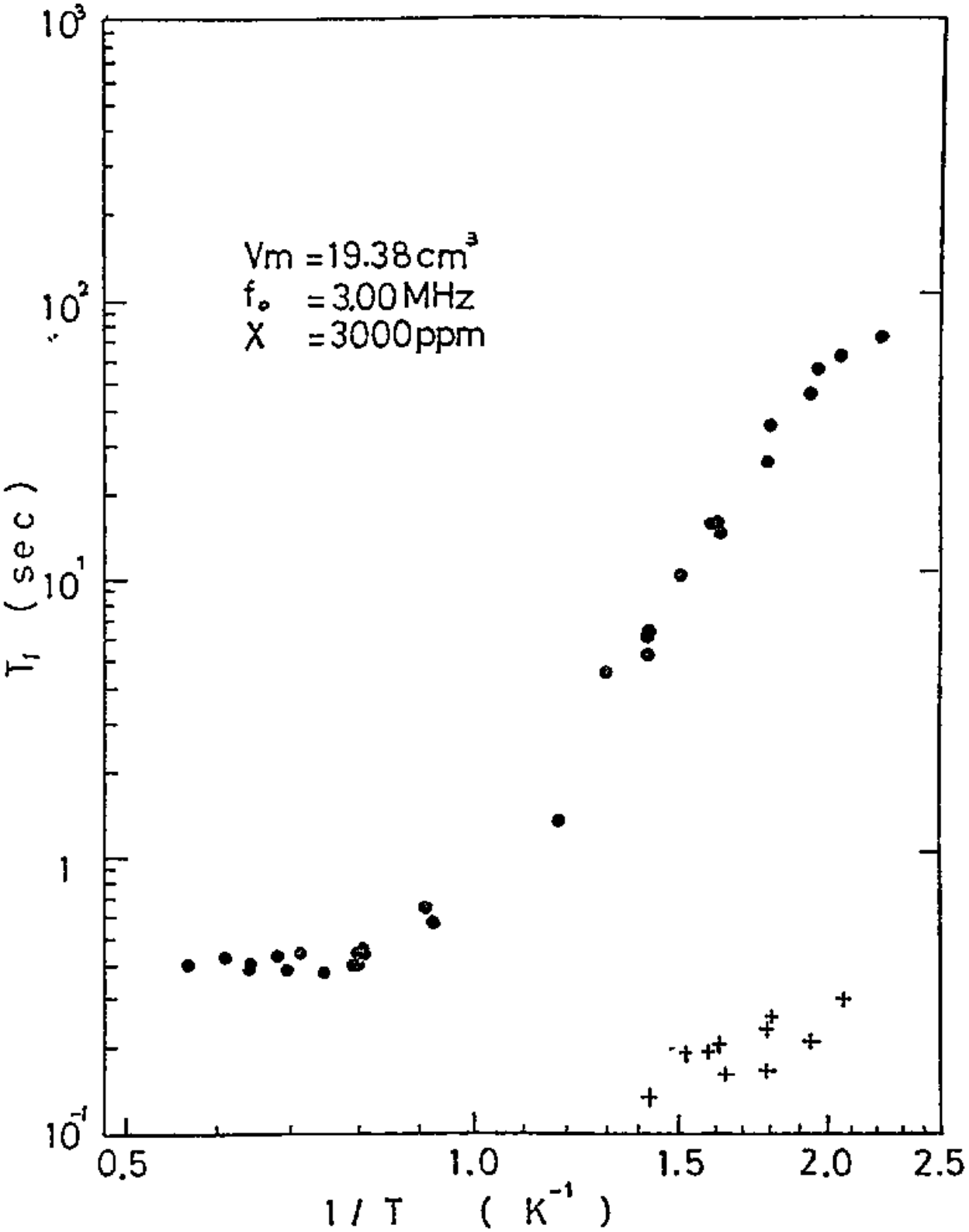
Vm = 19.38 cm³
f₀ = 3.00 MHz
X = 3000 ppm
T₁ (sec)
10³
10²
10¹
1
10⁻¹
0.5
1.0
1.5
2.0
2.5
1 / T (K⁻¹)

Fig. 19

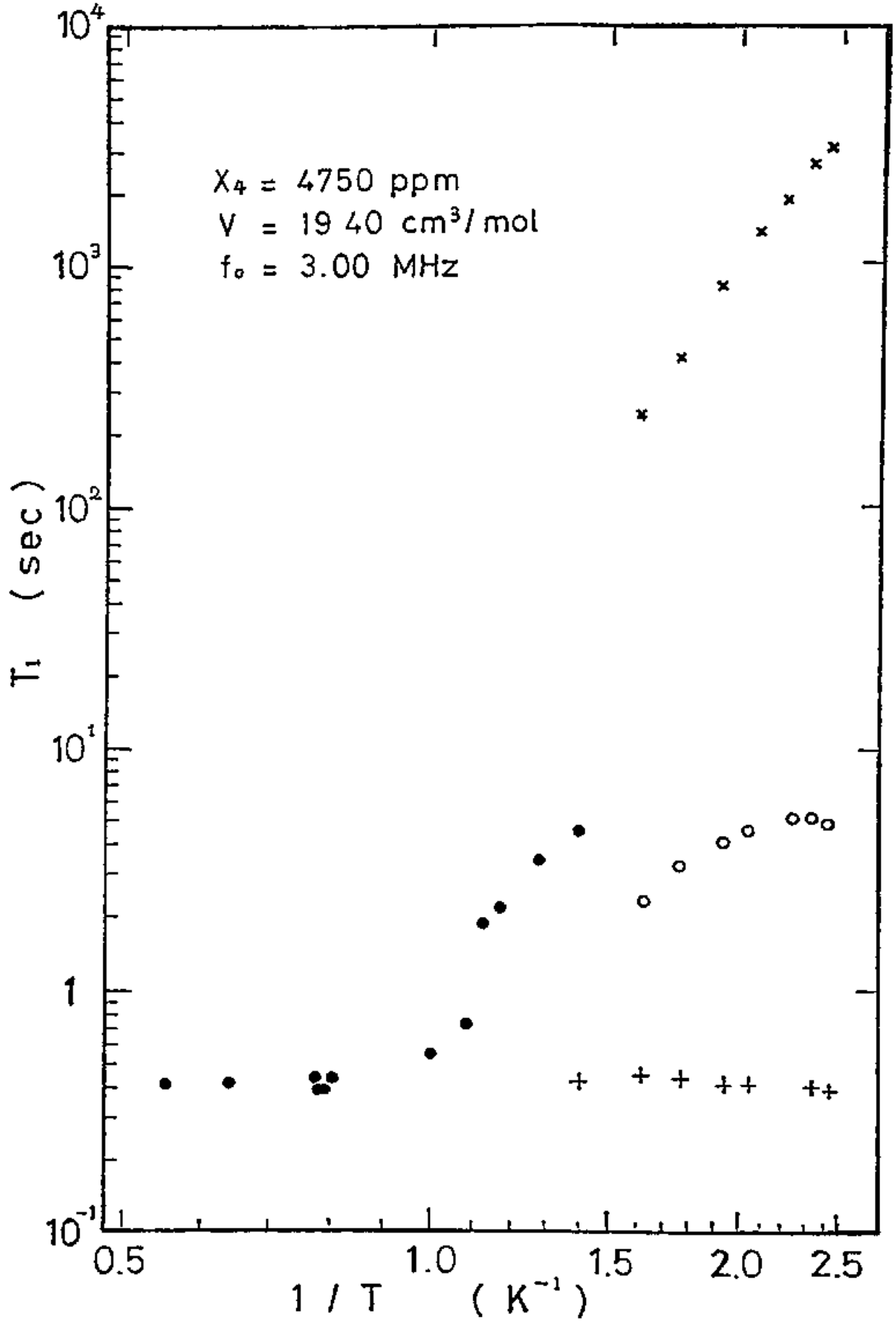
X_4 = 4750 ppm
V = 19 40 cm³/mol
f_o = 3.00 MHz
T_1 (sec)
10^4
10^3
10^2
10^1
1
10^{-1}
0.5
1.0
1.5
2.0
2.5
1 / T (K^{-1})

Fig. 20

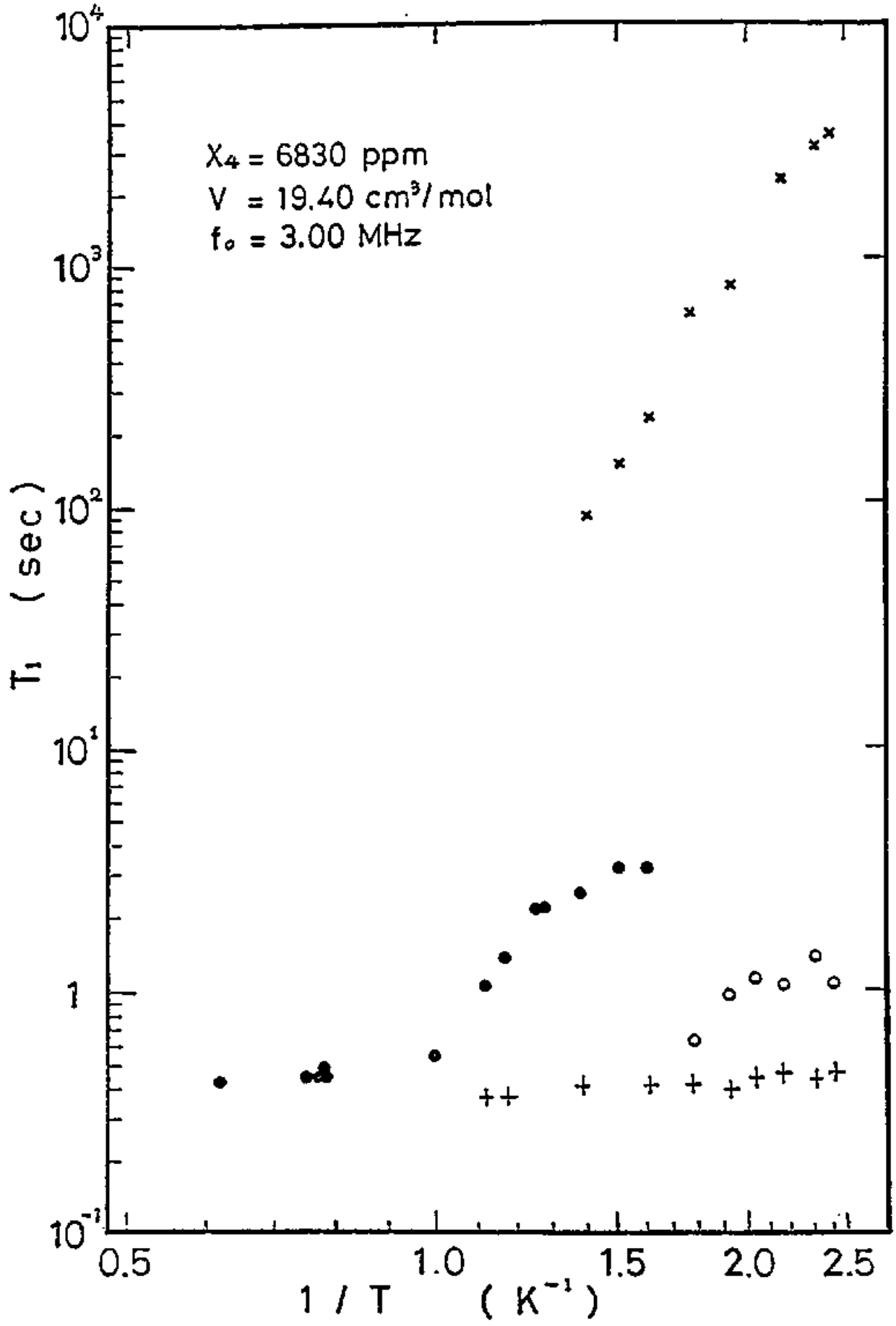
X_4 = 6830 ppm
V = 19.40 cm³/mol
f_o = 3.00 MHz
T_1 (sec)
10^4
10^3
10^2
10^1
1
10^{-1}
0.5
1.0
1.5
2.0
2.5
1 / T (K^{-1})

Fig. 21

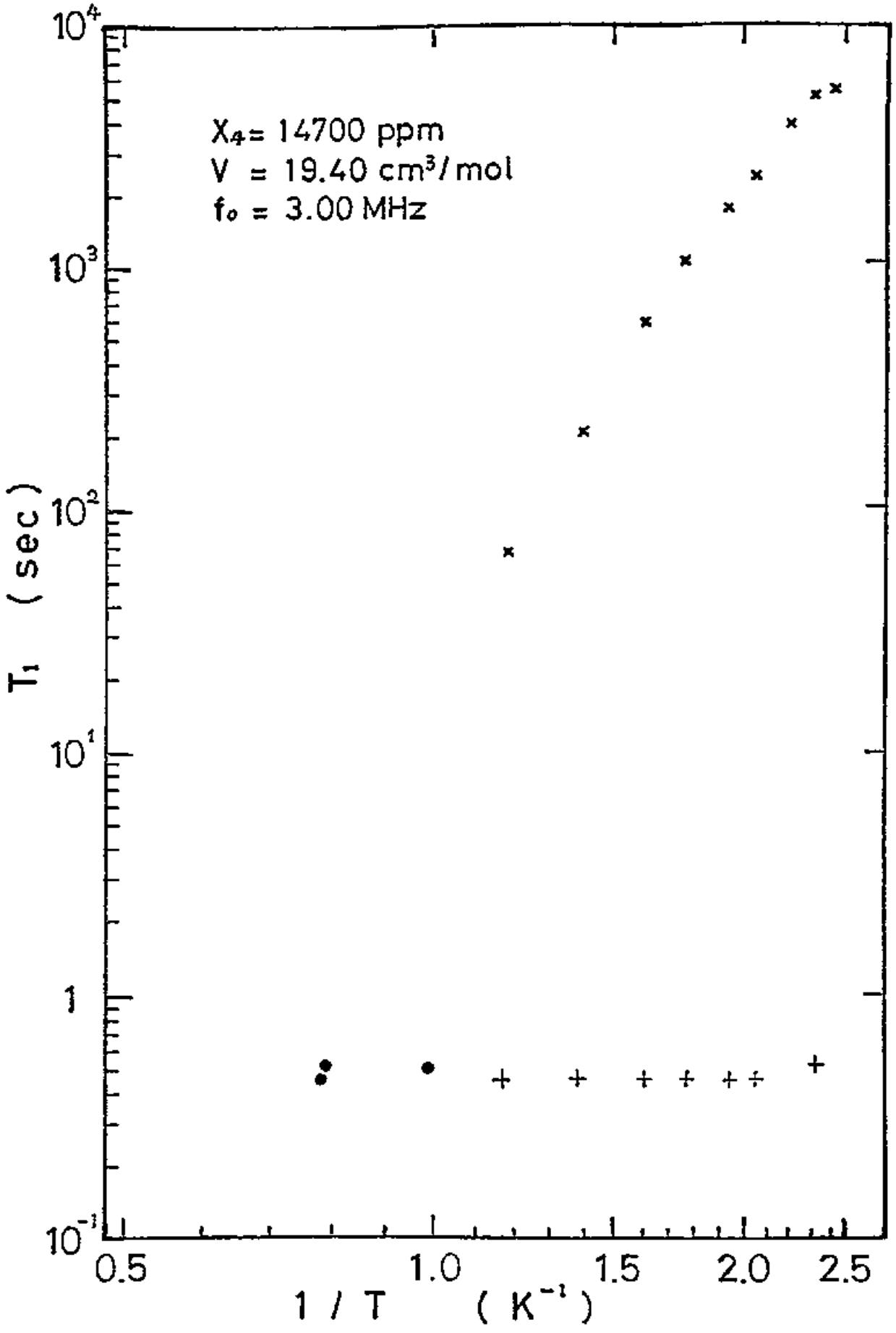
X_4= 14700 ppm
V = 19.40 cm³/mol
f_o = 3.00 MHz
T_1 (sec)
10^4
10^3
10^2
10^1
1
10^{-1}
0.5
1.0
1.5
2.0
2.5
1 / T (K^{-1})

Table I

Table Caption

Temperature Independent Values

HCP, $V = 19.4\ cm^3/mol$

k_X/k_Z were deduced from R or R' following to the equation of $k_X/k_Z = (1-R)/R$. The values of k_X/k_Z in the column marked * were the values at 3 MHz estimated from the values of R at 1 MHz, following to $k_Z \propto \omega_0^2$.
For samples of $x = 1.20 \times 10^{-3}$, 2.48×10^{-3} and 3.00×10^{-3} the behaviors of the magnetization recovery were expressed by the sum of three exponential functions of time, and the two kinds of intercepts were obtained.

Table I

x	T_I		T_{II-1}, T_{III-1}		T_{III-2}	R		R'	k_x/k_z		k_s/k_z
10^{-6}	3 MHz (sec)	1 MHz (sec)	3 MHz (sec)	1 MHz (sec)	(sec)	3 MHz	1 MHz	3 MHz	3 MHz *		
20	0.42	0.0125		0.0056		0.91	0.57			0.083	
70	0.43	0.011				1	0.57			0.083	
160	0.39	0.0117		0.0064		1	0.627			0.066	
280	0.34	0.012		0.0054		0.85	0.602		0.17	0.073	
580	0.40	0.0116		0.0060		0.88	0.58		0.14	0.081	
1200	0.41	0.0115		0.0079		0.82 0.72	0.38 0.25		0.22 0.39	0.18 0.33	
2480	0.42	0.0113	0.15	0.013		0.68 0.45	0.185 0.0815	0.76	0.47 1.22	0.49 1.25	
3000	0.43		0.35			0.53 0.31		0.50	0.89 2.23		
4200	0.39		0.42		8.0			0.39	1.6		52
4750	0.41		0.42		5.0			0.30	2.3		65
5460	0.50		0.42		2.8			0.30	2.3		
6830	0.44		0.43		1.1			0.24	3.2		120
14700	0.44		0.44		0.4						520

§ 3 Four Bath Model

From the fact that there are three kinds of relaxation times, we propose the four bath model as shown in Fig. 22. The four baths are the Zeeman bath, the X bath, the Y bath and the phonon bath. The X bath and the Y bath are introduced phenomenologically and will be discussed later. In our temperature region the phonon bath has the enough large energy constant and thereby can be regarded as the infinite heat reservoir.
The nonexponential recovery of the magnetization is supposed to correspond to the relaxation between the X bath and the Y bath. k_Z, k_X and k_Y denote the energy constants of each bath. T_{ZX} and T_{XL} are the intrinsic relaxation times between each bath. The special feature of this bath model is that the four baths do not connect in series but that the Y bath couples only with the X bath.

Here we show that this four bath model can reasonably explain the complicated temperature variations of the relaxation times in our experimental results. Though the relaxation process between the X bath and the Y bath is nonexponontial, in order to write down the rate equations, we assume temporarily the process is exponential. Then we have the rate equations for this model as

$$
\begin{cases}
\dfrac{d\beta_Z}{dt} = \dfrac{1}{T_{ZX}} \left(\beta_X - \beta_Z \right) \\
\dfrac{d\beta_X}{dt} = \dfrac{k_Z}{k_X} \dfrac{1}{T_{ZX}} \left(\beta_Z - \beta_X \right) + \dfrac{1}{T_{XY}} \left(\beta_Y - \beta_X \right) \\
\qquad\qquad + \dfrac{1}{T_{XL}} \left(\beta_L - \beta_X \right) \\
\dfrac{d\beta_Y}{dt} = \dfrac{k_X}{k_Y} \dfrac{1}{T_{XY}} \left(\beta_X - \beta_Y \right) \\
\dfrac{d\beta_L}{dt} = 0 \quad .
\end{cases}
\tag{4-4}
$$

we take the initial conditions which correspond to the two pulse method to be

$$
\begin{cases}
\beta_{Z(0)} = 0 \\
\beta_{X(0)} = \beta_{Y(0)} = \beta_L
\end{cases}
\tag{4-5}
$$

at $t = 0$. The solution of β_Z, which is proportional to the height of the magnetization signal, is obtained as

$$
\beta_{Z(t)} = \beta_L + C_1 e^{-\lambda_1 t} + C_2 e^{-\lambda_2 t} + C_3 e^{-\lambda_3 t} \quad .
\tag{4-6}
$$

where we define

$$\begin{cases} C_1 = -\beta_L \dfrac{(\lambda_1 - \rho_1\eta_{XY})(\lambda_2 - \eta_{ZX})(\lambda_3 - \eta_{ZX})(\lambda_2 - \lambda_3)}{(\rho_2\eta_{XY} - \eta_{ZX})(\lambda_1 - \lambda_2)(\lambda_2 - \lambda_3)(\lambda_3 - \lambda_1)} \\ C_2 = -\beta_L \dfrac{(\lambda_2 - \rho_2\eta_{XY})(\lambda_3 - \eta_{ZX})(\lambda_1 - \eta_{ZX})(\lambda_3 - \lambda_1)}{(\rho_2\eta_{XY} - \eta_{ZX})(\lambda_1 - \lambda_2)(\lambda_2 - \lambda_3)(\lambda_3 - \lambda_1)} \\ C_3 = -\beta_L \dfrac{(\lambda_3 - \rho_2\eta_{XY})(\lambda_1 - \eta_{ZX})(\lambda_2 - \eta_{ZX})(\lambda_1 - \lambda_2)}{(\rho_2\eta_{XY} - \eta_{ZX})(\lambda_1 - \lambda_2)(\lambda_2 - \lambda_3)(\lambda_3 - \lambda_1)} \end{cases} \tag{4-7}$$

$$\begin{cases} \rho_1 = \dfrac{k_Z}{k_X} \\ \rho_2 = \dfrac{k_X}{k_Y} \end{cases} \tag{4-8}$$

$$\begin{cases} \eta_{ZX} = \dfrac{1}{T_{ZX}} \\ \eta_{XY} = \dfrac{1}{T_{XY}} \\ \eta_{XL} = \dfrac{1}{T_{XL}} \end{cases} \tag{4-9}$$

λ_1, λ_2 and λ_3 are the inverse of the observed relaxation times and are the solutions of the next cubic equation.

$$\lambda^3 - (\eta_{ZX} + \eta_{XY} + \eta_{XL} + \rho_1\eta_{ZX} + \rho_2\eta_{XY})\lambda^2$$

$$+ (\eta_{ZX}\eta_{XY} + \eta_{ZX}\eta_{XL} + \rho_2\eta_{XY}\eta_{XL} + \rho_2\eta_{ZX}\eta_{XY}$$

$$+ \rho_1\rho_2\eta_{ZX}\eta_{XY})\lambda - \rho_2\eta_{ZX}\eta_{XY}\eta_{XL} = 0 \qquad (4\text{-}10)$$

Assuming that $T_{ZX} = 0.4$ sec, $T_{XY} = 10$ sec, $k_X/k_Z = 1.6$, $k_Y/k_Z = 49$ and T_{XL} is temperature dependent as $T_{XL} = 0.16\ T^{-7}$(sec), we solved Eq. (4-10) using the computer and obtained the observed relaxation times. The temperature variation of the calculated relaxation times are shown in Fig. 23 and the coincidence with the experimental results supports the four bath model to be good.

Next we derive the relations between the intrinsic relaxation times and the observed relaxation times, following the four bath model. In region I, where $((k_Z + k_X)/k_X)\ T_{XL} \ll T_{ZX}$ and therefore the X bath and the phonon bath L are in thermal equilibrium, the bottleneck of energy flow is the process between the Zeeman bath Z and the X bath. The observed relaxation time T_I is identical with T_{ZX},

$$T_I = T_{ZX} \qquad (4\text{-}11)$$

In region II, where the relation among T_{ZX} and T_{XL} is $T_{ZX} \ll ((k_Z + k_X)/k_X)\ T_{XL} \ll T_{XY}$, the energy does not flow to the Y bath and the X bath becomes to be in thermal equilibrium with the Z bath more early than with the L bath. The observed relaxation times are described by

$$T_{II-1} = \frac{k_X}{k_Z + k_X} T_{ZX} \qquad (4\text{-}12)$$

$$T_{II-2} = \frac{k_Z + k_X}{k_X} T_{XL} \quad . \qquad (4\text{-}13)$$

In region III, according to the temperature dependence of T_{XL}, $((k_Z + k_X)/k_X)\ T_{XL}$ becomes larger than T_{ZX} and T_{XY}. Therefore the energy in the X bath flows once to the Y bath before to the phonon bath L. The observed relaxation times in region III are expressed as

$$T_{III-1} = T_{II-1} = \frac{k_X}{k_Z + k_X} T_{ZX} \qquad (4\text{-}14)$$

$$T_{III-3} = \frac{k_Z + k_X + k_Y}{k_X} T_{XL} \quad . \qquad (4\text{-}15)$$

The prefactor R and R' in Eq. (4-2) and (4-3) are the same in region II and III,

$$R = R' = \frac{k_Z}{k_Z + k_X} \quad . \qquad (4\text{-}16)$$

Eq. (4-11) ~ (4-16) are all valid except for the transient regions.

On the multipulse saturation method, if the pulse interval τ is chosen to be much shorter than T_{III-3} but longer than the times in which the Z bath, the X bath and the Y' bath reach in thermal equilibrium with each other, the observed k_S is the sum of the energy constants of the Z, X and Y' baths,

$$k_S = k_Z + k_X + k_{Y'} \quad . \tag{4-17}$$

Fig. 22

Phenomenological Four Bath Model

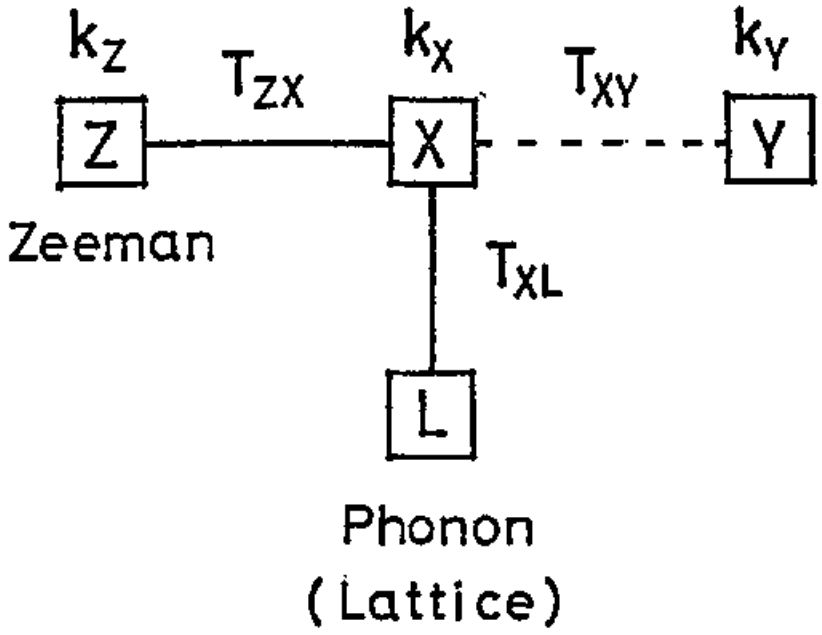

Z is the Zeeman bath. L is the phonon bath. The X bath and the Y bath are introduced phenomenologically. k_Z, k_X and k_Y are the energy constants of each bath. T_{ZX}, T_{XY} and T_{XL} are the intrinsic relaxation times between each bath. The relaxation process between the X bath and the Y bath corresponds to the nonexponential recovery of the magnetization.

Fig. 23

Computer Simulation of the Relaxation Behavior on the Basis of the Four Bath Model

Figure Caption

From the eq. (4-6), the behavior of the magnetization recovery is expressed by

$$\frac{M(\infty) - M(t)}{M(\infty)} = -\frac{C_1}{\beta_L} e^{-\lambda_1 t} - \frac{C_2}{\beta_L} e^{-\lambda_2 t} - \frac{C_3}{\beta_L} e^{-\lambda_3 t}$$

Following to eq. (4-6) ~ (4-10) and using the values of $T_{ZX} = 0.4$ sec, $T_{XY} = 10$ sec, $k_X/k_Z = 1.6$, $k_Y/k_Z = 49$ and $T_{XL} = 0.16\ T^{-7}$ sec, the values of λ_1, λ_2, λ_3, C_1, C_2 and C_3 were calculated by a computer. The curves represent the temperature variations of the relaxation times λ_1^{-1}, λ_2^{-1}, λ_3^{-1} and the intercepts R_1, R_2 at $t = 0$, where

$$R_1 = -\frac{C_2 + C_3}{\beta_L}$$

$$R_2 = -\frac{C_3}{\beta_L} .$$

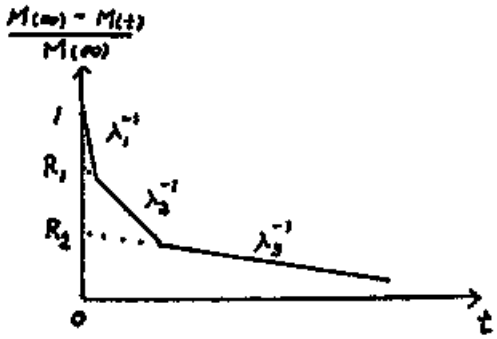

The dashed lines represent that the relaxation times on the line can not be observed in the experiment, because the prefacter C_i in the term of λ_i is very small.

Fig. 23

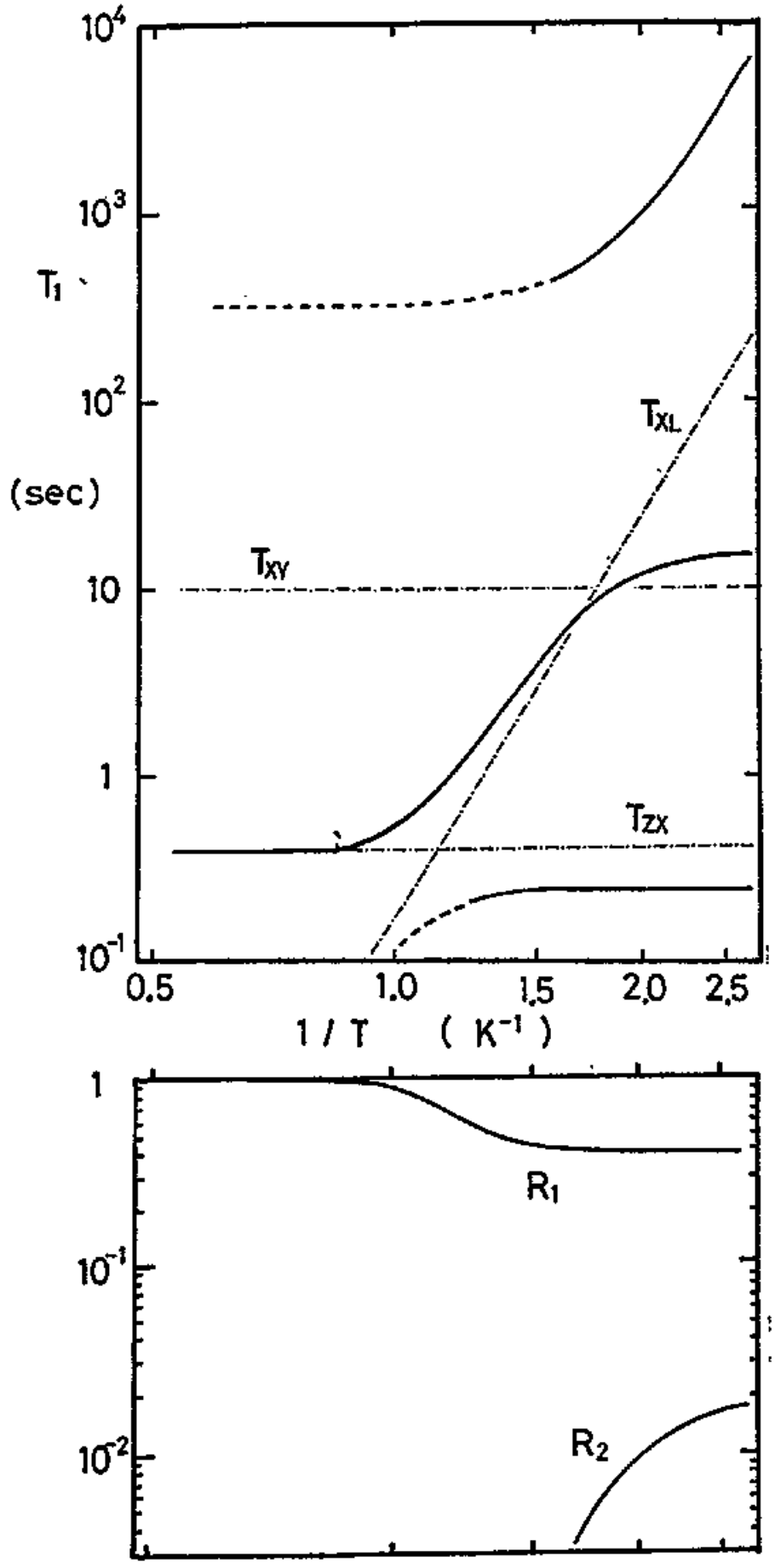
10^4
10^3
T_1
10^2
(sec)
10
1
10^{-1}
T_{XL}
T_{XY}
T_{ZX}
0.5
1.0
1.5
2.0
2.5
1 / T (K^{-1})
1
10^{-1}
10^{-2}
R_1
R_2

§ 4 Intrinsic Values

Using the equations (4-11)～(4-17), we can deduce the energy constants, k_X/k_Z and k_Y/k_Z, and the intrinsic relaxation times, T_{ZX} and T_{XL}, from our experimental results.

In Fig. 24 we show the ^{4}He concentration dependence of k_X/k_Z and k_S/k_Z for the samples of 19.4 cm^3/mol at 3 MHz. The values of k_X/k_Z at 3 MHz for $x \leq 1.2 \times 10^{-3}$ are estimated from the data at 1 MHz by using the relation, $k_Z \propto \omega_0^2$. The validity of this relation was confirmed experimentally. The values deduced from the data of other authors[6),11)] are also shown in Fig. 24 k_X is independent of ^{4}He concentrations below about $x = 5 \times 10^{-4}$, but above $x = 3 \times 10^{-3}$, k_X varies as x^2.

The intrinsic relaxation times T_{ZX} deduced from the observed T_{II-1}, T_{III-1} and k_X/k_Z are all about 0.4 sec at 3 MHz and they are identical with the Zeeman-exchange relaxation time T_I in the exchange plateau region (region I). Consequently we can conclude that the mechanism between the Zeeman bath and the X bath is identical with the mechanism in the exchange plateau region.

The relaxation times T_{II-2} and T_{III-3} are temperature dependent and are not continuous to each other. However, if we deduce the intrinsic relaxation time T_{XL}

from T_{II-2} and T_{III-3}, T_{XL} in region II and T_{XL} in region III connect smoothly with each other. This suggests that T_{II-2} and T_{III-3} attribute to the same relaxation mechanism between the X bath and the phonon bath, and that the apparent discontinuity between T_{II-2} and T_{III-3} is due to the difference of the contributing energy constants, when the relaxation times are observed. T_{II-2} and T_{III-3} are influenced by the ^4He impurities. The temperature and the ^4He concentration dependence of the deduced T_{XL} for V = 19.4 cm^3/mol at 3 MHz is expresseed as

$$T_{XL} = \frac{1 + 1.3 \times 10^6 \, x^2}{3.5 \times 10^4 \, x} \; T^{-n} \qquad (4\text{-}18)$$

with $n = 7.2 \pm 0.4$.

T_{XL} has a minimum at concentration of $x \simeq 1.0 \times 10^{-3}$.

T_{III-2} which corresponds to the nonexponential recovery of the magnetization is temperature independent but is strongly affected by ^4He impurities,

$$T_{III-2} \propto x^{-n} \qquad (4\text{-}19)$$

with $n = 3 \sim 4$. This nonexponential recovery is thought to be related to the characters of the X bath and the Y bath, and will be discussed later.

Next we will discuss the NMR frequency dependence of the relaxation times. When we compare the experimental results at 1 MHz (Fig. 17) with those at 3 MHz (Fig. 16) both for $x \leq 1.2 \times 10^{-3}$, all the relaxation times at 1 MHz are shorter than those at 3 MHz. In Region I, exchange plateau region, the frequency dependence can be understood by Eq. (2-45). In region II, T_{II-2} at 3 MHz are about 5.7 times larger than those at 1 MHz for the samples of $x \leq 5.8 \times 10^{-4}$. Let's compare the topological factor, $(k_Z + k_X)/k_X$ in eq. (4-13). The experimental results of k_X/k_Z at 3 MHz is 0.065 . Using $k_Z \propto \omega_0^2$ and supposing that k_X is independent of the NMR frequency, the topogical factor at 1 MHz is calculated to be 6.0 times smaller than that at 3 MHz. Consequently using eq. (4-13), T_{XL} deduced from the data at 1 MHz is equal to T_{XL} at 3 MHz within the experimental error, and it is found that the NMR frequency dependence is caused only by the energy constant of the Zeeman bath.

In order to study the frequency dependence of the relaxation times in region III, we took the data at 4.2 MHz for the samples with ^{4}He concentrations of 4.75×10^{-3} and 1.47×10^{-2}. In Fig. 25 we show the data of $x = 1.47 \times 10^{-2}$. T_{III-3} at 4.2 MHz are almost the same values as those at 3 MHz for both samples. This result is reasonably explained by our model as follows. For these

samples k_X and k_Y, are much larger than k_Z. Hence $k_S = k_Z + k_X + k_Y$ is almost insensitive to the NMR frequency. Since the relaxation mechanism between the X bath and the phonon bath will not depend on the NMR frequency, T_{XL} is expected to be independent of the frequency. Therefore the observed relaxation time $T_{III-3} = (k_S/k_X)\, T_{XL}$ should not be influenced by the frequency for these samples.

We also examined the molar volume dependence of the relaxation times and the energy constants. Fig. 26 shows the data of samples of 19.11, 19.38 and 19.63 cm^3/mol with ^4He impurities of 2.8×10^{-4}. The molar volume dependence in region I can be easily understood by the molar volume dependence of the ^3He - ^3He exchange constant J, following Eq. (2-45). The molar volume dependence of T_{II-2} or T_{III-3} would come from J and the Debye temperature. The molar volume dependence of T_{II-2} will be discussed with the relaxation mechanism in the next chapter.

For sample with ^4He concentration of 2.48×10^{-3}, we observed peculiar relaxation behaviors which could not be understood within a framework of the present four bath model. The magnetization recovery observed by the two pulse method was described by the sum of three exponential functions of time and thus three

kinds of relaxation times were obtained. The longest and the shortest relaxation times could be identified with T_{II-1} and T_{II-2}. However the second one was temperature independent and about 7 sec for V = 19.4 cm^3/mol at 3 MHz, which was too short compared with T_{III-2} expected for $x = 2.48 \times 10^{-3}$, and hence the second relaxation time could not be identified with any of other relaxation times mentioned above. Fig. 27 shows the temperature variation of the relaxation times for sample of $x = 2.48 \times 10^{-3}$.

It is noted that in Fig. 24 we plot two values of k_X/k_Z which were estimated by extapolating both the second and the third magnetization recovery to t = 0. The similar behavior of the magnetization recovery was observed for samples of $x = 1.20 \times 10^{-3}$ and 3.00×10^{-3}, though the interval of the second recovery was very narrow, so that the relaxation time could not be measured.

Fig. 24 Figure Caption

^{4}He concentration dependence of the energy constants k_X/k_Z, k_S/k_Z

The value of k_Z is taken at 3.0 MHz.

● + : Our data, HCP, V = 19.4 cm^3/mol, $\omega_0/2\pi$ = 3.0 MHz
The values of + are estimated from the data at 1.0 MHz, using $k_Z \propto \omega_0^2$.
For samples of $x = 1.20 \times 10^{-3}$ and 2.48×10^{-3} the behaviors of the magnetization recovery were described by the sum of three exponential functions of time. For these samples two kinds of values of k_X/k_Z which were estimated from two intercepts are plotted.

△ : Richards, Hatton and Giffard[6], HCP, V = 19.0 cm^3/mol.
The value is estimated from their data at 2.0 MHz.

▽ : Bernier and Deville[11], BCC, V = 20.5 cm^3/mol.
The value is estimated from their data at 1.5 MHz.

The dashed lines represent the values of

$$k_X/k_Z = k_T/k_Z = 18\ J^2/\omega_0^2 ,$$
$$k_X/k_Z = k_{44,X}/k_Z = 28.88\ C_X V_0^2 x^2/\omega_0^2$$
$$k_S/k_Z \doteqdot k_{44,Y}/k_Z = 28.88\ C_Y V_0^2 x^2/\omega_0^2$$

where $\omega_0/2\pi$ = 3.0 MHz, $J/2\pi \doteqdot 0.18$ MHz,
$V_0/2\pi$ = 930 MHz, $C_X \doteqdot 0.03$ and $C_Y \doteqdot 0.97$.

Fig. 24

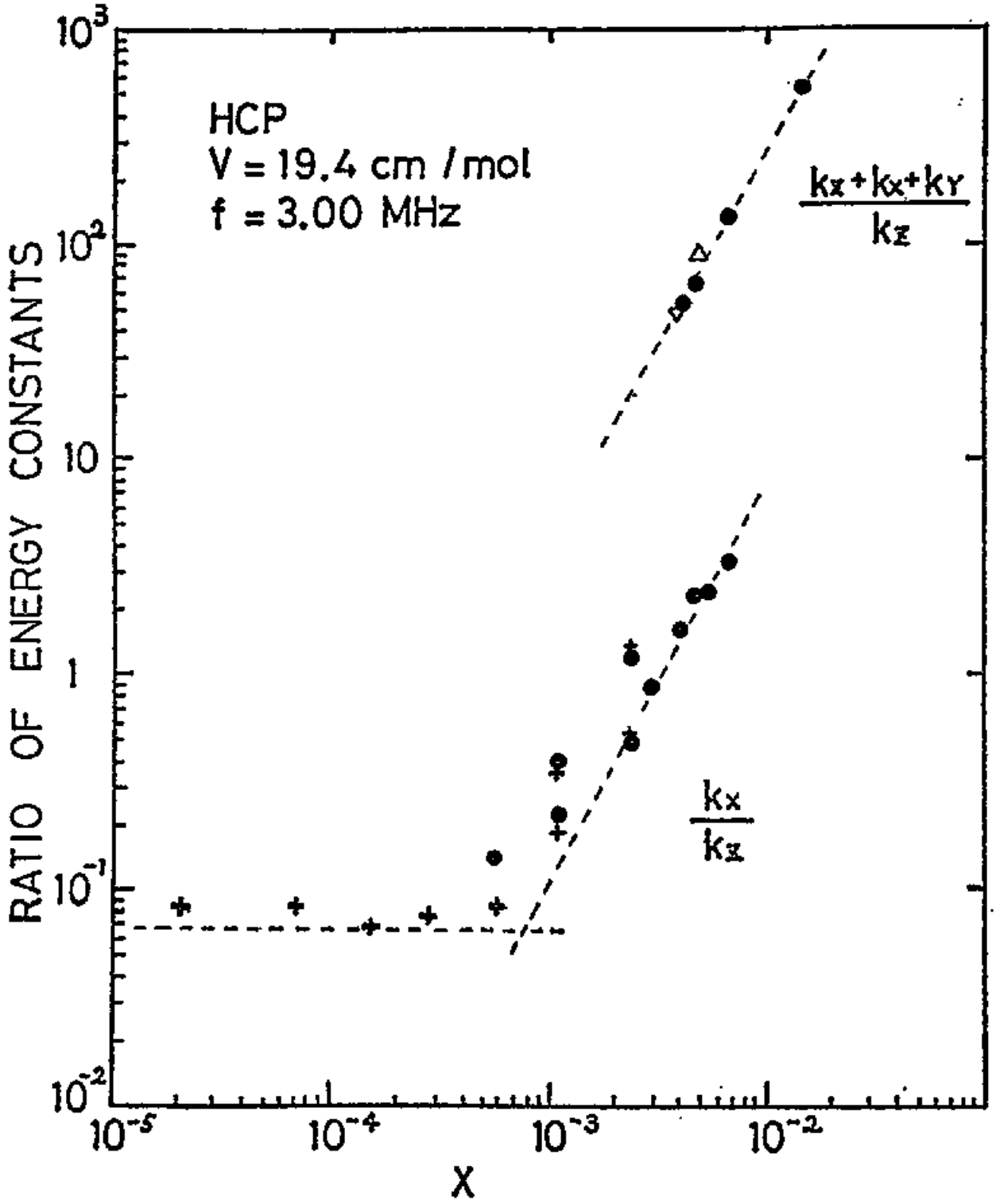
HCP
V = 19.4 cm / mol
f = 3.00 MHz
$\frac{k_z+k_x+k_y}{k_z}$
$\frac{k_x}{k_z}$
RATIO OF ENERGY CONSTANTS
X
10^3
10^2
10
1
10^{-1}
10^{-2}
10^{-5}
10^{-4}
10^{-3}
10^{-2}

Fig. 25

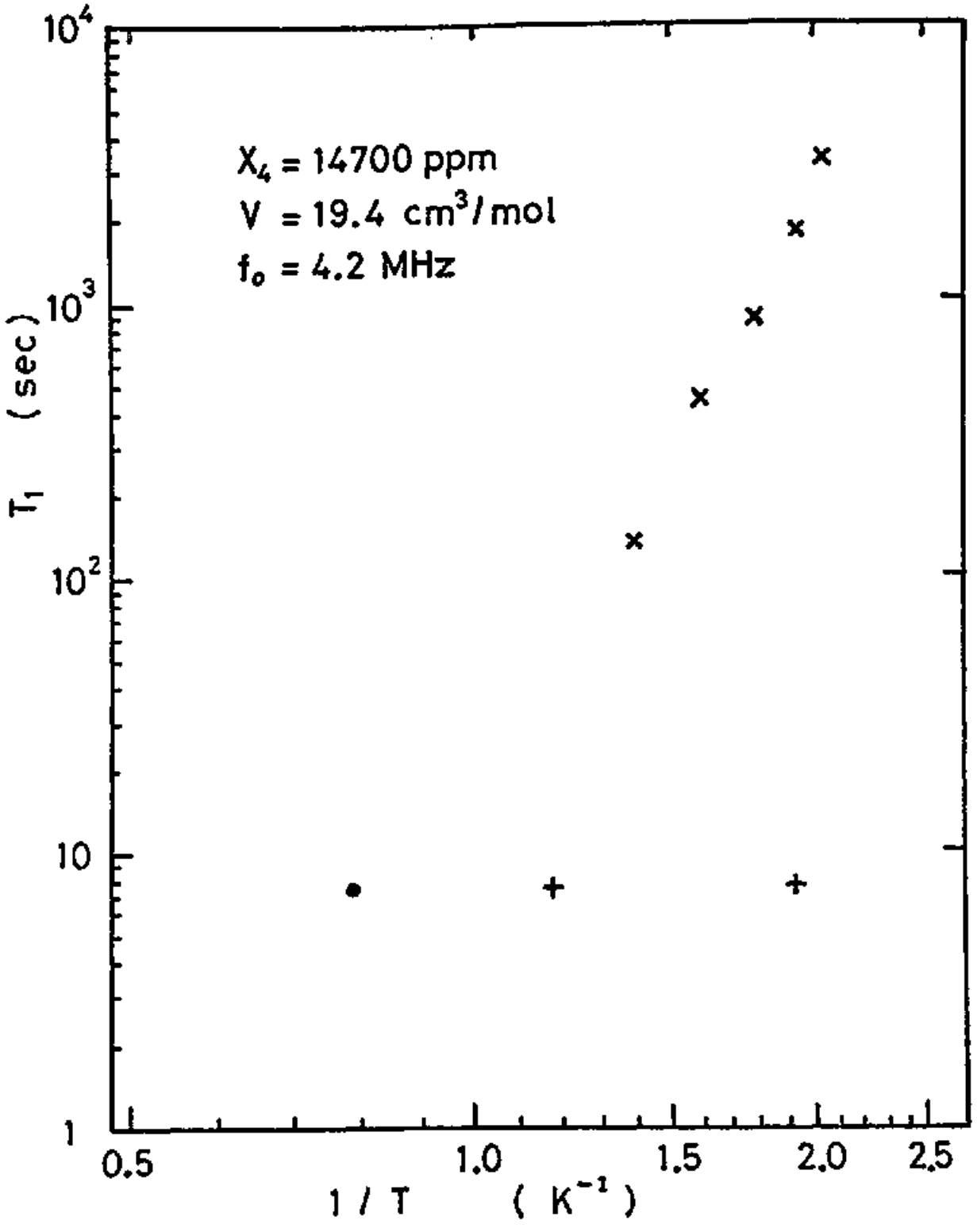
10^4
10^3
10^2
10
1
T_1 (sec)
X_4 = 14700 ppm
V = 19.4 cm^3/mol
f_o = 4.2 MHz
0.5
1.0
1.5
2.0
2.5
1 / T (K^{-1})

Fig. 26

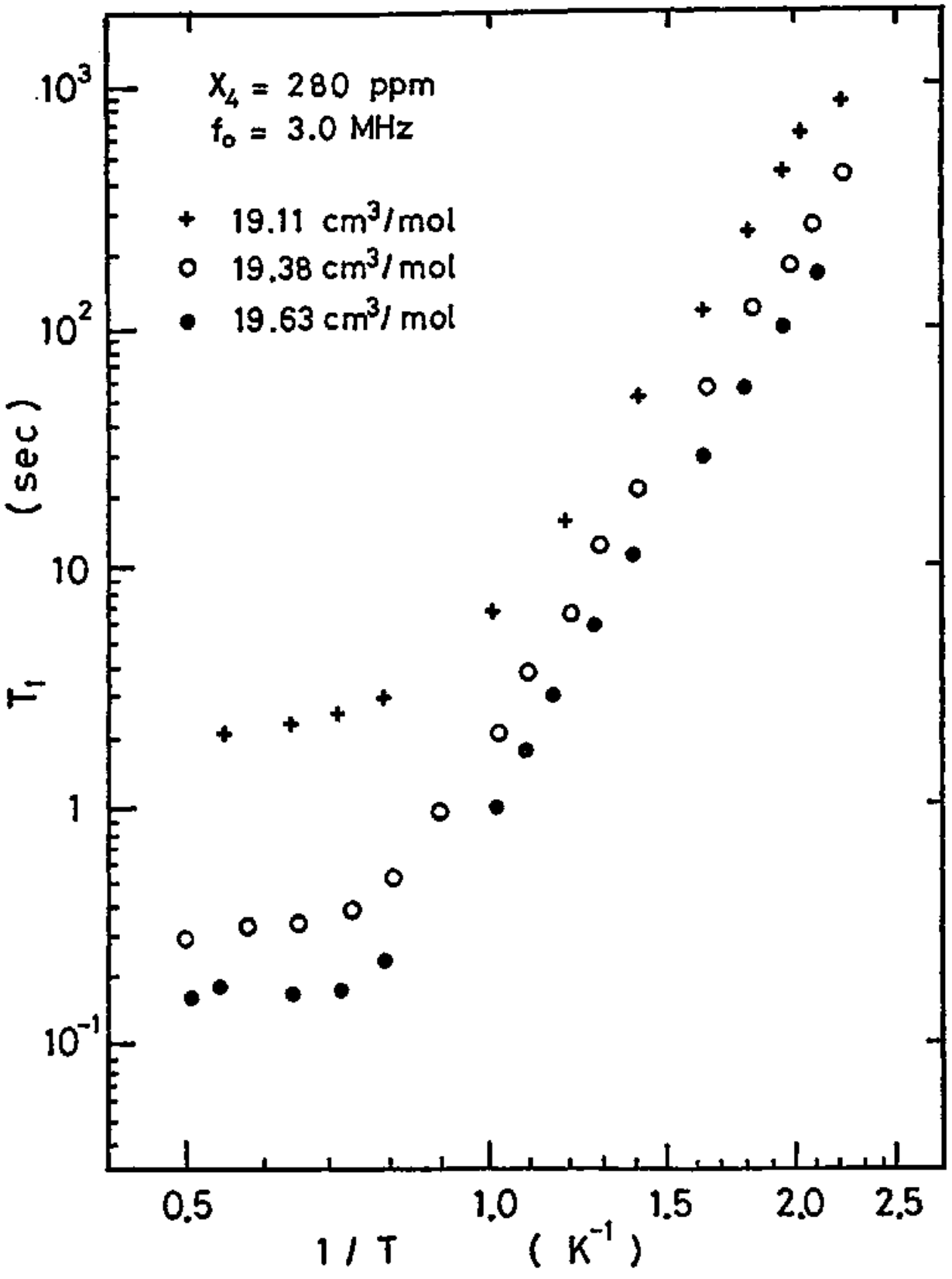
X_4 = 280 ppm
f_o = 3.0 MHz
+ 19.11 cm³/mol
○ 19.38 cm³/mol
● 19.63 cm³/mol
10^3
10^2
10
1
10^{-1}
T_1 (sec)
0.5
1.0
1.5
2.0
2.5
1 / T (K^{-1})

Fig. 27

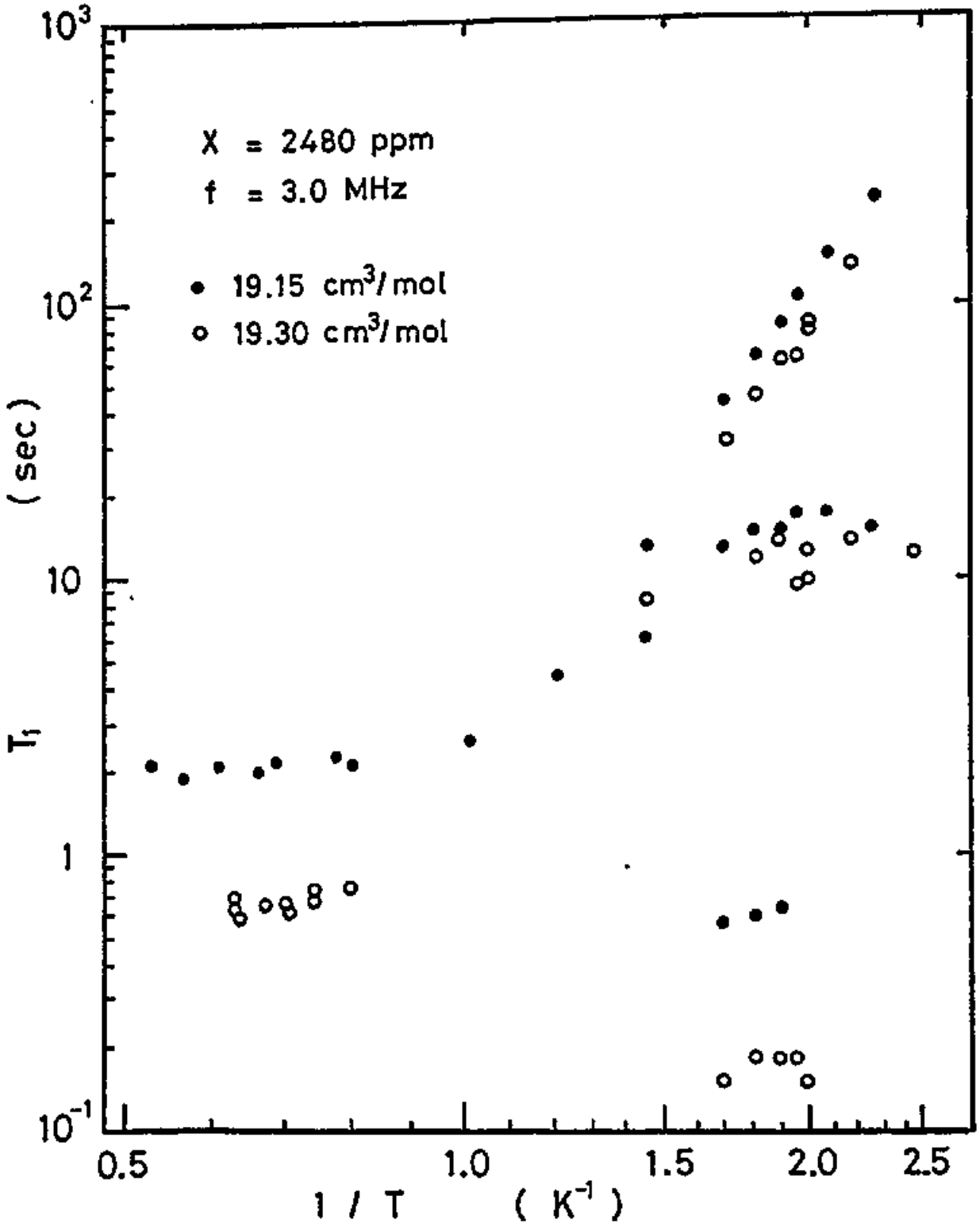
X = 2480 ppm
f = 3.0 MHz
• 19.15 cm³/mol
○ 19.30 cm³/mol
10^3
10^2
10
1
10^{-1}
T_1 (sec)
0.5
1.0
1.5
2.0
2.5
1 / T (K^{-1})

§ 5 Experimental Results in BCC Phase

In Fig. 28 we show the temperature variation of the relaxation times in bcc solid ^{3}He with ^{4}He impurities of 2.0×10^{-5}, 7.0×10^{-5}, 1.6×10^{-4}, 2.8×10^{-4}, 5.8×10^{-4}, 1.20×10^{-3} and 3.00×10^{-3}. The molar volume of them is 20.48 ± 0.3 cm^3/mol and the NMR frequency is 3 MHz. Above about 1.4 K ($1/T = 0.71$ K^{-1}) the relaxation times are temperature dependent. This region is the vacancy region. The relaxation times are temperature independent between 1.4 K ($1/T = 0.71$ K^{-1}) and 0.6 K ($1/T = 1.7$ K^{-1}). Here is the exchange plateau region. In these high temperature regions the relaxation times are not influenced by ^{4}He impurities and the magnetization recovery is a single exponential function of time. The relaxation times in these high temperature regions have been well understood and have been summarized in chapter II, § 4.

The relaxation times below about 0.6 K ($1/T = 1.7$ K^{-1}) are again temperature dependent and are influenced by ^{4}He impurities. This region corresponds to region II which we designate in the data of the hcp phase. The magnetization recoveries are the sum of two exponential functions of time and we can obtain two kinds of relaxation times and the prefactor R, as well as the case of the hcp

solid. We plot only T_{II-2} but not T_{II-1} in Fig. 28 for simplicity. T_I, T_{II-1} and R which are temperature independent are tabulated in table II.

In Fig. 28 there can be seen the pure limit relaxation time in the higher temperature part of region II. As for the pure limit, it will be analyzed in chapter V, § 1 with the data in hcp phase. As temperature is lowered, the relaxation time deviates from the pure limit and becomes to be influenced by ^{4}He impurities. The ^{4}He impurity dependent relaxation time becomes shorter when the ^{4}He concentration is increased, following $T_1 \propto x^{-1}$. It is difficult to judge the temperature dependence of this relaxation time from our data, because the temperature could not be reduced enough, but it seems that $T_{II-2} \propto T^{-n}$ with $7 \leq n \leq 9$.

Since in the bcc solid ^{3}He there is not the region III in our temperature range, the relaxation behaviors can be interpreted by the bath model which consists of the Zeeman bath, the X bath and the phonon bath.

Following to the bath model, the ratio of the energy constant between the X bath and the Zeeman bath is deduced not only from R (eq. 4-16) but also from the relation between T_{ZX} and T_{II-1} (eq. 4-12) independently. Here T_{ZX} is equal to T_I in the exchange plateau region. In Fig. 29 we show the ^{4}He concentration dependence of

the ratio, k_X/k_Z. As seen in this figure, the ratio calculated from R and that from T_I and T_{II-I} are in good agreement with each other. The emperical formula for the ratio of energy constant is described by

$$\frac{k_X}{k_Z} = 0.65 + 1.3 \times 10^5 x^2 \qquad (4\text{-}20)$$

The data obtained by Bernier[8] for samples of $V = 21.00$ cm^3/mol and 20.06 cm^3/mol in bcc phase are also shown in Fig. 29.

Fig. 28

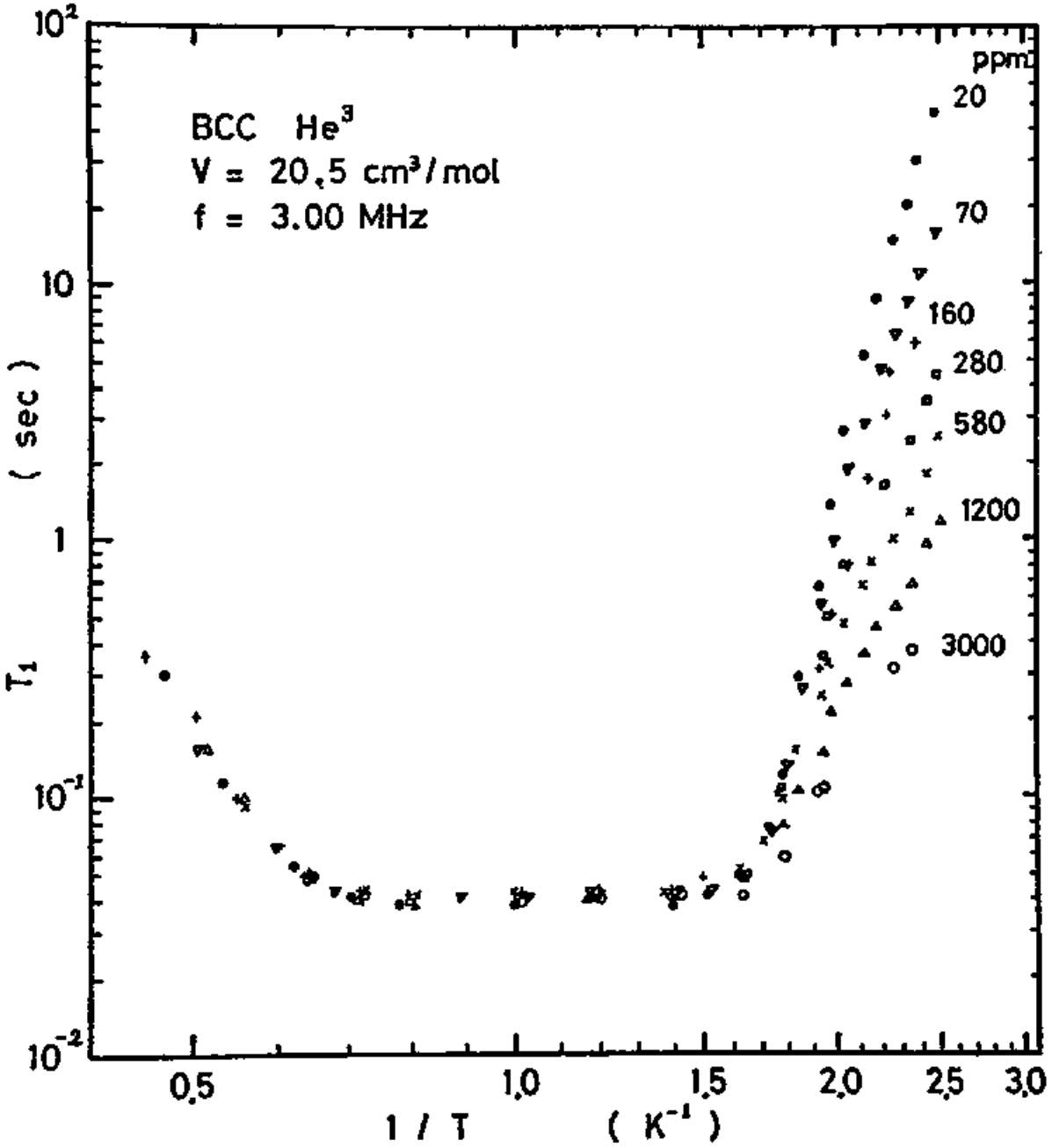
BCC He³
V = 20,5 cm³/mol
f = 3.00 MHz
ppm
20
70
160
280
580
1200
3000
T1 (sec)
10²
10
1
10⁻¹
10⁻²
0,5
1,0
1,5
2,0
2,5
3,0
1 / T (K⁻¹)

Table II

Temperature Independent Values

BCC, V = 20.5 cm^3/mol, $\omega_0/2\pi$ = 3.0 MHz

x 10^{-6}	T_I (msec)	T_{II-1} (msec)	R	k_X/k_Z		T_2 (msec)
				*	**	
20	40.5	15.5	0.544	0.838	0.620	15.6
70	40.9		0.614	0.629		14.8
160	42.0	19.0	0.59	0.695	0.826	13.7
280	39.8	14.8	0.56	0.786	0.592	14.3
580	41.0	16.1	0.56	0.786	0.646	13.9
1200	40.0	18.5	0.52	0.923	0.860	13.5
2480	41.0	21.7	0.51	0.961	1.12	14.0
3000	40.0	30.0	0.32	2.13	3.00	16.0

The values of k_X/k_Z were obtained by the following equations.

$$* \quad : \quad k_X/k_Z = (1-R)/R$$

$$** \quad : \quad k_X/k_Z = 1/(T_I/T_{II-1} - 1)$$

Fig. 29 Figure Caption

^{4}He concentration dependence of the energy constants for bcc solid ^{3}He

The values of ● and ○ are our data for bcc solid ^{3}He of $V = 20.5$ cm^3/mol at 3 MHz. The values of ● are estimated from $k_X/k_Z = (1-R)/R$. The values of ○ are estimated from $k_X/k_Z = 1/(T_{ZX}/T_{II-1} - 1)$.

The solid line represents the values of

$$\frac{k_X}{k_Z} = \frac{k_T + k_{34} + k_{44}}{k_Z} = \frac{12J^2 + 32J_{34}^2 + 24.4V_{0X}^2x^2}{\omega_0^2}$$

where $\omega_0/2\pi = 3.0$ MHz, $J/2\pi = J_{34}/2\pi = 0.7$ MHz and $V_{0X}/2\pi = 220$ MHz.

The values of △ and + were obtained by Bernier[8] for bcc samples of $V = 21.00$ and 20.06 cm^3/mol respectively. These values are at 3MHz estimated from his data at 2.19 MHz.

The dashed lines represent the values of

$$\frac{k_X}{k_Z} = \frac{k_T}{k_Z} = \frac{12J^2}{\omega_0^2}$$

where $J/2\pi = 1.19$ and 0.45 MHz for $V = 21.00$ and 20.06 cm^3/mol respectively, and $\omega_0/2\pi = 3.0$ MHz.

Fig. 29

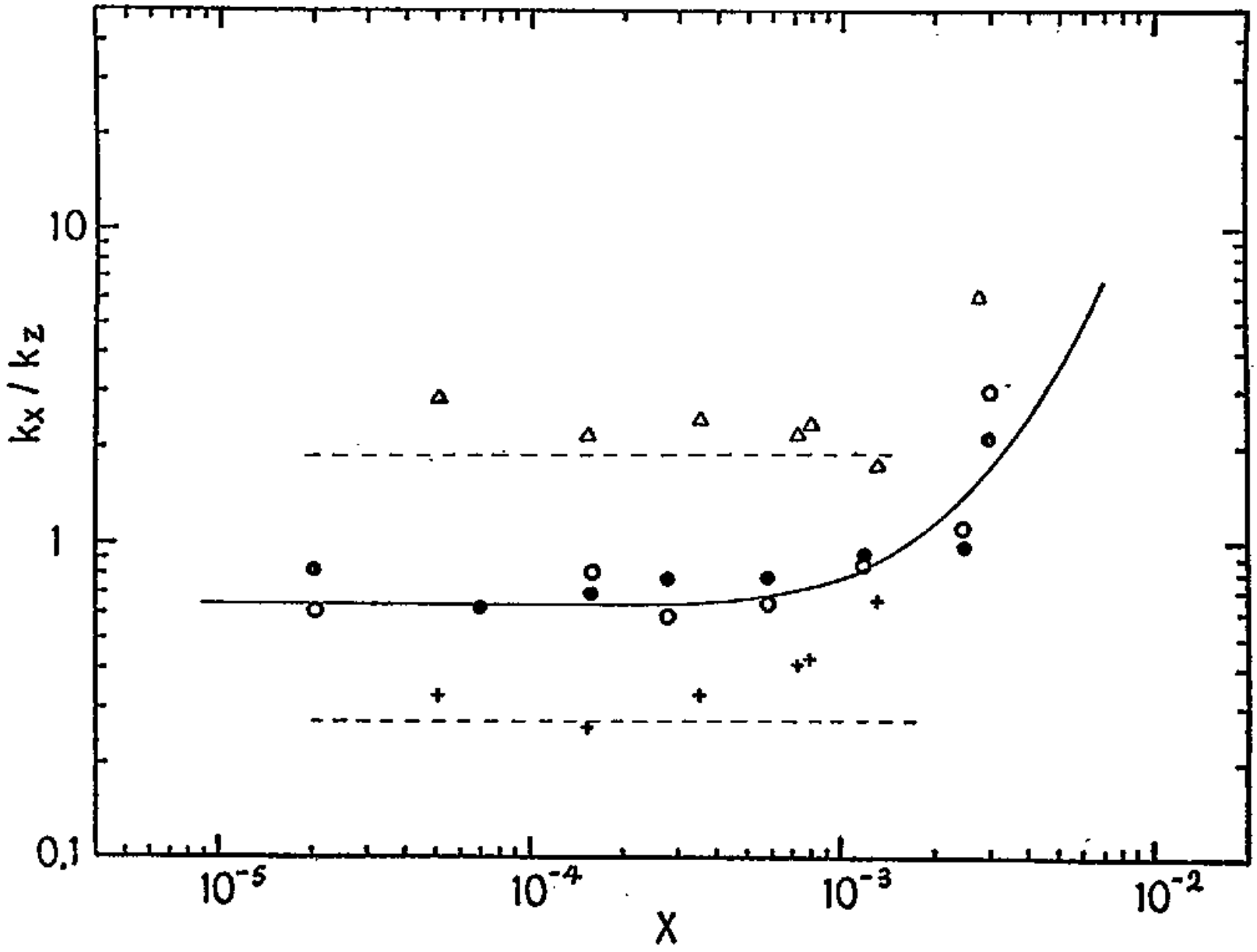

§ 6 Spin Spin Relaxation Time

Finally we note that both in hcp and bcc phases the spin spin relaxation times T_2 in region II and region III were the same values as those in the exchange plateau region and were not influenced by ^{4}He impurities. The results suggest that the spin spin relaxation process is governed by the ^{3}He - ^{3}He exchange interaction even in region II and III. Thus T_2 can be explained by the same way as discussed in chapter II, § 4. It is noticed that the spin spin relaxation mechanism does not accompany the energy transfer between the spin system and the thermal reservoir, thereby it is unneeessary to consider the energy baths which should be done in the case of the spin lattice relaxation process.

Fig. 30 shows the spin spin relaxation times for various molar volumes at $\omega_0/2\pi$ = 1.0, 2.0, 3.0 and 4.0 MHz. The molar volume dependence of the exchange interaction J deduced from T_2, using eq. (2-55), is shown in Fig. 34

Fig. 30

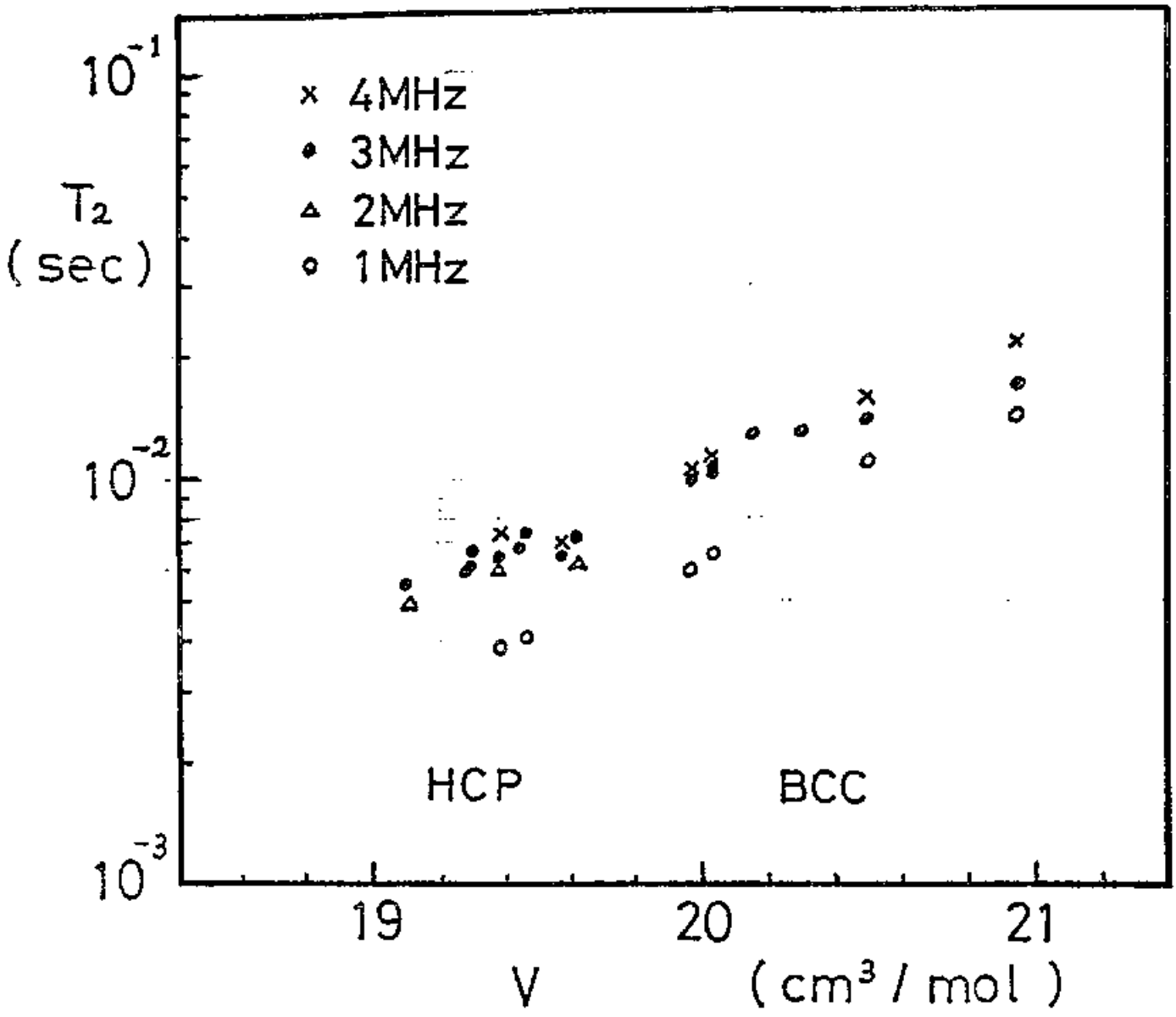

Fig. 34

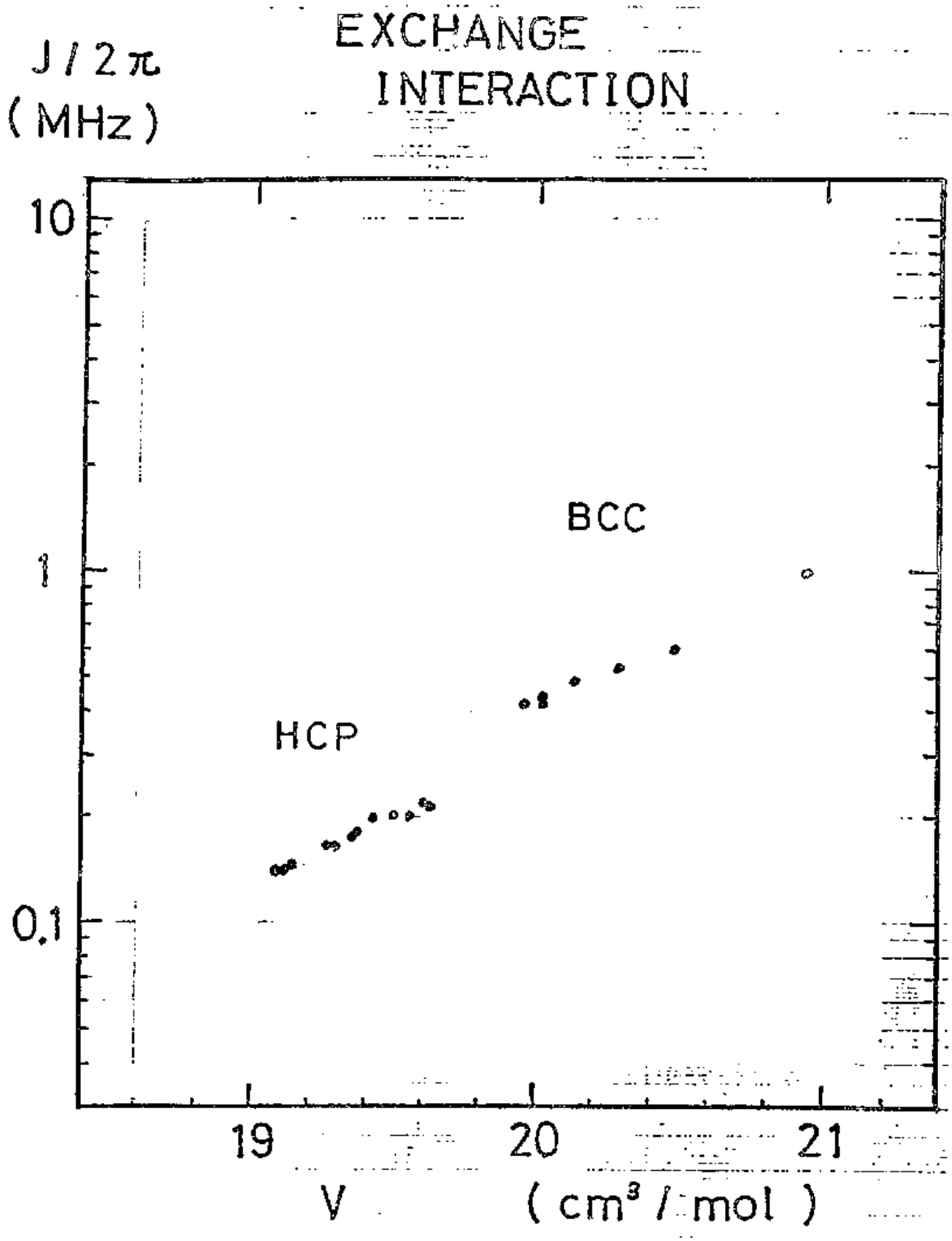

Fig. 35

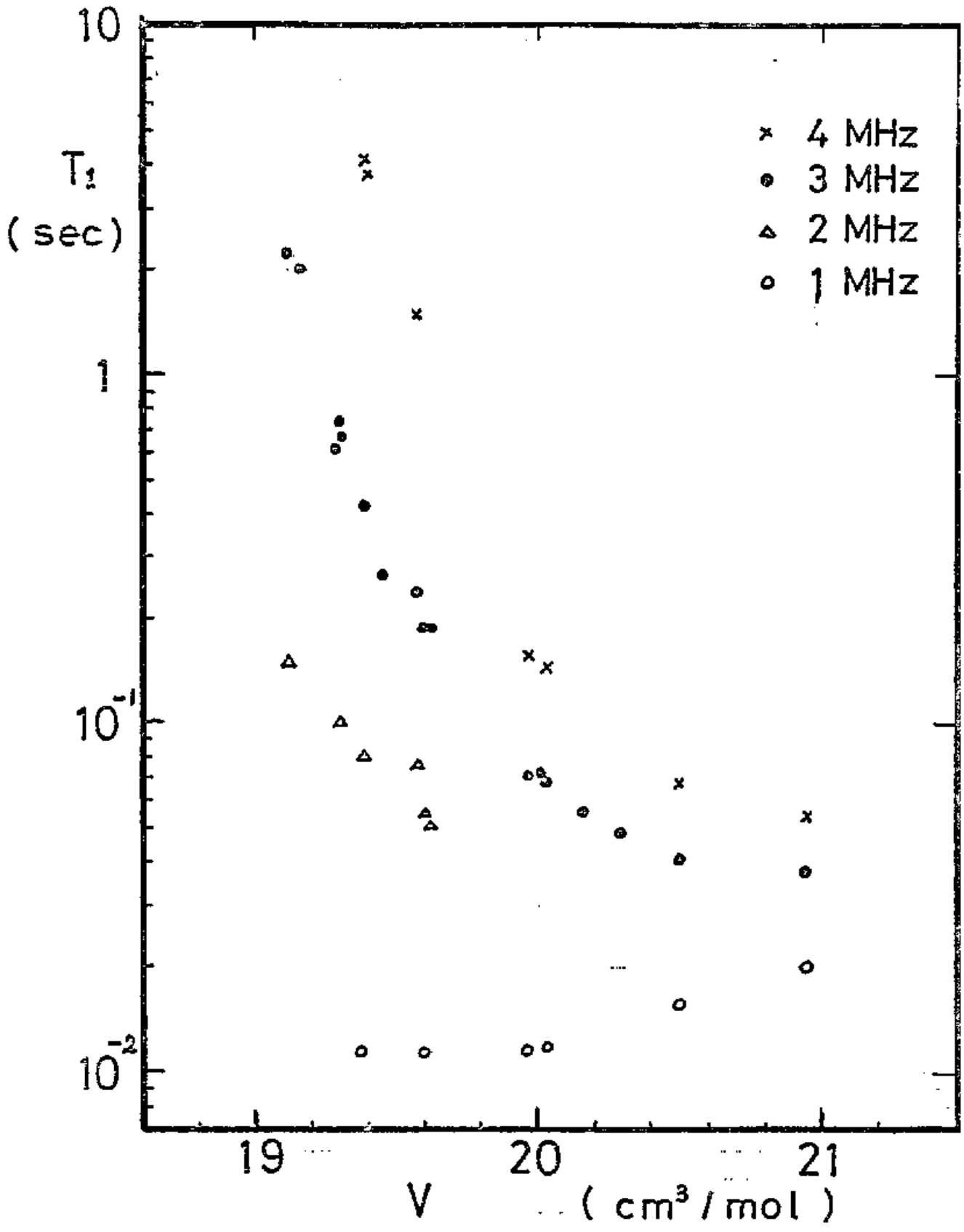

CHAPTER V

ANALYSIS AND DISCUSSION

We have shown the experimental results in hcp and bcc solids with various amount of ^{4}He impurities and they have been well analyzed phenomenologically by the four bath model. In this chapter we will discuss these baths and the relaxation mechanisms between them. In § 1 the relaxation time from the X bath to the L bath which is independent of ^{4}He impurities are analyzed. In § 2 the relaxation time from the X bath to the L bath which is influenced by ^{4}He impurities are discussed for hcp samples. The energy constants of the baths are also analyzed. For bcc samples they are discussed in §3. In § 4 we will discuss the relaxation mechanism between the X bath and the Y bath.

§ 1 Relaxation Time in the Pure Limit

In region II for purer samples both in hcp and bcc phases, the relaxation mechanism which did not depend on the ^{4}He concentration were observed.

In the exchange plateau region, the route of energy relaxation is Zeeman → exchange → vacancy → phonon, and the bottleneck in the route is the Zeeman-exchange coupling, which is temperature independent, But when temperature is lowered, the exchange-vacancy coupling becomes a new bottleneck in the energy flow. This relaxation process is caused by the vacancy motion and thus is not influenced by ^{4}He impurities. This relaxation time is the pure limit relaxation time which has been observed in our experiments.

According to the relaxation topology mentioned above, the relaxation processes which are observed are Zeeman → Exchange and Exchange → Vacancy. The intrinsic relaxation time corresponding to the Zeeman-exchange process is clearly identical with the relaxation time in the exchange plateau region,

$$T_{ZT} = T_I \qquad (5\text{-}1)$$

The observed relaxation times T_{II-1} and T_{II-2} in the pure limit are expected to be

$$T_{II-1} = \frac{k_T}{k_Z + k_T} T_{ZT} \qquad (5-2)$$

$$T_{II-2} = \frac{k_Z + k_T}{k_T} T_{TV} \quad , \qquad (5-3)$$

where T_{TV} is given by Eq. (2-61). While the experimental results of the pure limit relaxation times could be expressed as

$$T_{II-2} = 3.2 \times 10^{-9} \exp(24/T) \qquad (5-4)$$

for V = 19.4 cm^3/mol (hcp solid) and

$$T_{II-2} = 6.3 \times 10^{-11} \exp(12/T) \qquad (5-5)$$

for V = 20.5 cm^3/mol (bcc solid). Thus we get the vacancy formation energy as ϕ = 24($\pm$ 1)K for 19.4 cm^3/mol and ϕ = 12($\pm$ 1)K for 20.5 cm^3/mol. These values are in good agreement with the values deduced from the relaxation time in the vacancy region at high temperature. For the purer samples, the ratios of energy constant at 3 MHz are k_T/k_Z = 0.065 for V = 19.4 cm^3/mol (hcp) and k_T/k_Z = 0.65 for V = 20.5 cm^3/mol (bcc). Using these

experimental values, we obtain the results that the values of $2(z-1)\omega_V$ are 5.2×10^9 sec^{-1} and 4.0×10^{10} sec^{-1} for hcp and bcc solid respectively. These values are also of reasonable order, compared with the values in the vacancy region[22].

It should be noted that the relaxation mechanism due to the exchange moduration was not observed. The relaxation time of this mechanism is insensitive to the ^4He impurity and is proportional to T^{-7} as mentioned in chapter II, 5-2. Till now, this relaxation mechanism has not been observed in solid ^3He.

§ 2 Relaxation in HCP Phase

From the fact that in hcp phase the impurity sensitive relaxation time from the X bath to the phonon bath is proportional to T^{-7}, we analyze the data by the enhanced exchange modulation model mentioned in 5-3 of chapter II. While the experimental result shows that the energy constants of the X bath and the Y bath for samples with higher concentrations are both proportional to x^2. This result suggests that the ^{4}He - ^{4}He strain field interaction bath contributes to the X bath and the Y bath. Thus the energy constants are expected as follows.

$$\frac{k_X}{k_Z} = \frac{k_N + k_E + k_{44,X}}{k_Z} = \frac{18 J_N^2 + 72 J_E^2 x + 28.88 C_X V_0^2 x^2}{\omega_0^2} \qquad (5\text{-}6)$$

$$\frac{k_S}{k_Z} = \frac{k_Z + k_N + k_E + k_{44,X} + k_{44,Y}}{k_Z} = \frac{\omega_0^2 + 18 J_N^2 + 72 J_E^2 x + 28.88 C_X V_0^2 x^2 + 28.88 C_Y V_0^2 x^2}{\omega_0^2} \qquad (5\text{-}7)$$

where $k_{44,X} = C_X k_{44}$ and $k_{44,Y} = C_Y k_{44}$ with $C_X + C_Y = 1$. C_X represents the ratio of energy constant which contributes to k_X to k_{44}. The relaxation times T_{II-2} and T_{III-3} are expressed by T_1 of eq. (2-87) as

$$1/T_{II-2} = \frac{k_N + k_E}{k_Z + k_N + k_E + k_{44,X}} \frac{1}{T_1}$$

$$= \frac{2.49 \times 10^{-35}}{\omega_0^2 + 18 J_N^2 + 72 J_E^2 x + 28.88 C_X V_0^2 x^2} \times \left(\frac{T^7}{\theta^{10}}\right) \frac{B}{N} \qquad (5\text{-}8)$$

$$1/T_{III-3} = \frac{k_N + k_E}{k_Z + k_N + k_E + k_{44,X} + k_{44,Y}} \frac{1}{T_1}$$

$$= \frac{2.49 \times 10^{-35}}{\omega_0^2 + 18 J_N^2 + 72 J_E^2 x + 28.88 C_X V_0^2 x^2 + 28.88 C_Y V_0^2 x^2} \times \left(\frac{T^7}{\theta^{10}}\right) \frac{B}{N} \qquad (5\text{-}9)$$

where B is defined by eq. (2-86).

First we attempt to obtain the interaction constants, comparing the experimental results with the above formulas. In Fig. 24 we have shown the ^{4}He concentration dependence of the energy constant for the samples of V = 19.4 cm^3/mol at $\omega_0/2\pi$ = 3 MHz. For lower concentrations, k_X/k_Z is about 0.065, and for higher concentrations we have $k_X/k_Z = 8.6 \times 10^4\ x^2$ and $k_Y/k_Z \simeq k_S/k_Z = 2.7 \times 10^6\ x^2$. Comparing these experimental values with eq. (5-6) and eq. (5-7), we get $J_N/2\pi$ = 0.18 MHz, $V_0/2\pi$ = 930 MHz, C_X = 0.03 and $C_Y \simeq 0.97$. It is found that the value of J_N is in good agreement with the ^{3}He - ^{3}He exchange constant

obtained from the exchange plateau region. The value of V_0 seems also to be of the reasonable order of magnitude, compared with the values of V_0 estimated from ^{3}He NMR in dilute ^{3}He - ^{4}He mixtures ($V_0/2\pi$ = 2500 MHz)[24], the analysis of the phase separation temperature ($V_0/2\pi$ = 2000 MHz)[10] and the theoretical value ($V_0/2\pi$ = 1500 MHz)[16]. From the fact that both the X bath and the Y bath are thought to be the strain field interaction bath, it might be the case that the strain field interaction bath can not reach thermal equilibrium quickly within itself. This seems to be closely related to the experimental fact that the relaxation behavior between the X bath and the Y bath is nonexponential. These things will be discussed again in chapter V, § 4.

As shown in Fig. 24, comparing our result for V = 19.4 cm^3/mol with that for V = 19.0 cm^3/mol obtained by Richards et al.[6] and that for V = 20.5 cm^3/mol by Bernier et al.[11], it is found that the magnitude of the strain field interaction seems to be insensitive to the molar volume and the solid phase.

Next we discuss the relaxation times. The formulas of T_{II-2} and T_{III-3} involve the unknown parameters of J_E, J_E'' and J_N''. When we describe the exchange constant as a function of the interatomic distance Δ as $J \propto \Delta^m$,

the second derivatives are expressed by $J_N'' = (m_N/\Delta)^2 J_N$ and $J_E'' = (m_E/\Delta)^2 J_E$. When we substitute these relations into eq. (5-8), assuming that $m_E = m_N$ for simplicity and that the Debye temperature is described as $\theta \propto \Delta^{-1}$, T_{II-2} is expected to be proportional to $\Delta^{-(4m+6)}$. Using the data of the molar volume dependence of T_{II-2} for samples of $x = 2.8 \times 10^{-4}$ shown in Fig. 26, we obtain $m = 42 \pm 4$. If we estimate J_E from the value of T_{II-2}, using $\theta = 38\ k$[54] and the parameters obtained above, the value of $J_E/2\pi$ is 4.7 MHz. Such a large J_E should give some contribution to k_X proportional to x, which should be barely appreciable around $x \simeq 1 \times 10^{-3}$. But it is difficult to judge the existance of the contribution because of the peculiar relaxation behaviors around this concentration mentioned in chapter IV, § 4.

In order to show the ^{4}He concentration dependence of T_{II-2} and T_{III-3}, in Fig. 31 we plot the experimental values of them at T = 0.5 K against the ^{4}He concentrations. The solid lines in the figure represent the calculated values on the basis of the four bath model, which are in good agreement with the experimental results.

Fig. 31

Figure Caption

^{4}He Concentration Dependence of T_{II-2} and T_{III-3} at T = 0.500 K in HCP Phase

- ● : V = 19.4 cm^3/mol, $\omega_0/2\pi$ = 3.0 MHz.
- △ : V = 19.41 cm^3/mol, $\omega_0/2\pi$ = 2.19 MHz, from ref 10).
- ▽ : V = 19.25 cm^3/mol, $\omega_0/2\pi$ = 2.19 MHz, from ref 10).
- □ : V = 19.32 cm^3/mol, $\omega_0/2\pi$ = 2.1 MHz, from ref 12).

The solid lines represent the calculated values of T_{XL}, T_{II-2} and T_{III-3} for V = 19.4 cm^3/mol at 3.0 MHz, estimated from the following equations;

$$T_{II-2} = \frac{k_Z + k_X}{k_X} T_{XL}$$

$$T_{III-3} = \frac{k_Z + k_X + k_Y}{k_X} T_{XL} \quad ,$$

where k_X, k_Y and T_{XL} are the emperical formulas obtained from our experimental results, described by

$$T_{XL} = \frac{1 + 1.3 \times 10^6 \, x^2}{3.5 \times 10^4 \, x}$$

$$k_X/k_Z = 0.065 + 8.6 \times 10^4 \, x^2$$

$$k_Y/k_Z = 2.7 \times 10^6 \, x^2 \quad .$$

Fig. 31

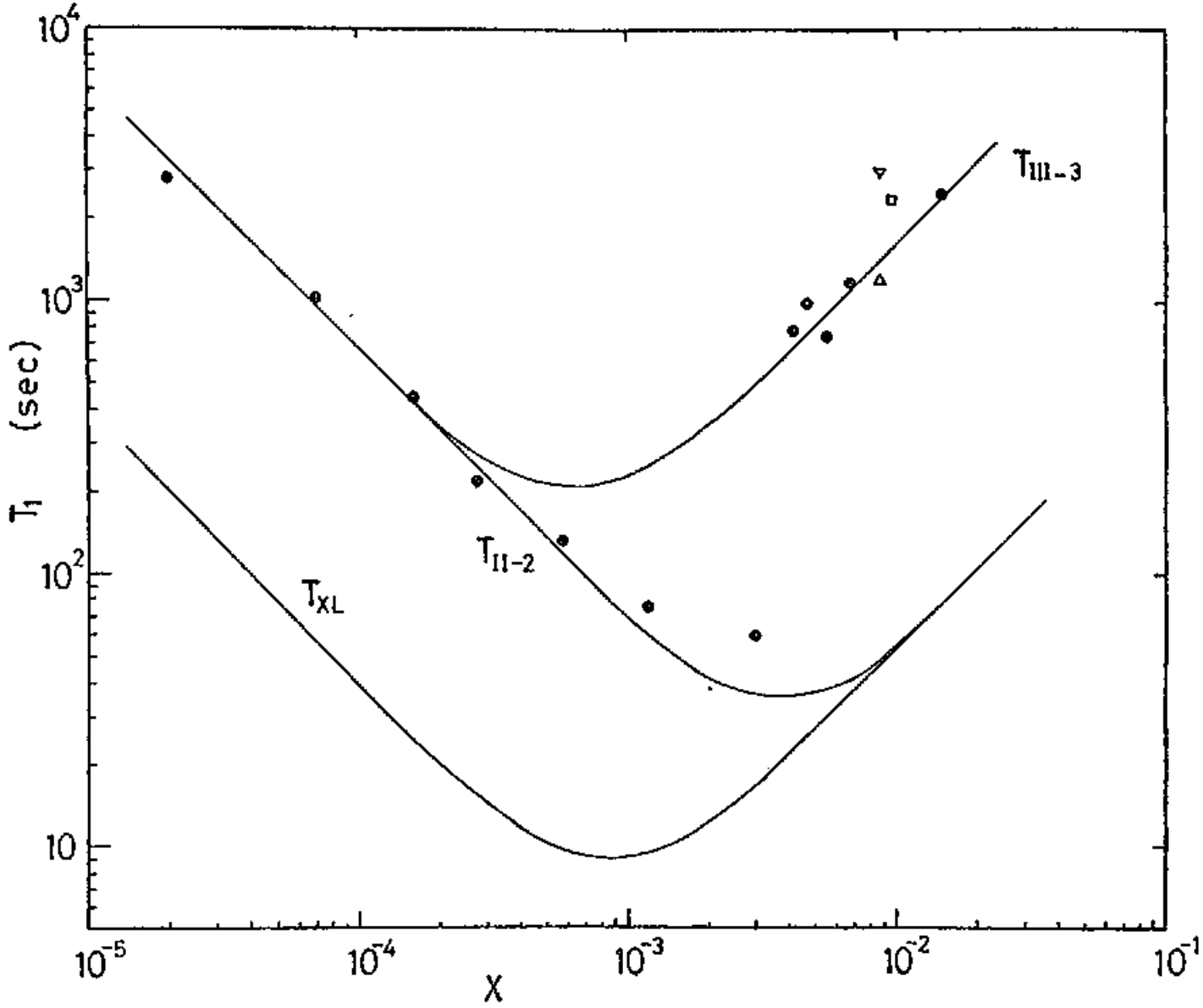

§ 3 Relaxation in BCC Phase

For bcc solid ^{3}He the relaxation mechanism due to the enhanced exchange madulation is considered to be less dominant because of the difference of the crystal structure between the bcc phase and the hcp phase, as mentioned in chapter II, 5-3. It is now usually accepted for bcc solid ^{3}He that the impurity sensitive T_{XL} is due to the phonon scattering by ^{4}He impurities and the relaxation time T_{XL} has a temperature dependence of T^{-9}, as mentioned in chapter II, 5-4. We will analyze our experimental results with this theory.

$$k_X/k_Z = (k_T + k_{34} + k_{44})/k_Z$$

$$= \frac{12J^2 + 32{J_{34}}^2 x + 24.4{V_{OX}}^2 x^2}{\omega_0^2} \qquad (5\text{-}10)$$

T_{II-2} is expressed by T_1 of eq.(2-108) as

$$\frac{1}{T_{II-2}} = \frac{k_{34}}{k_Z + k_T + k_{33} + k_X} \frac{1}{T_1}$$

$$= \frac{4.82 \times 10^{18}}{\omega_0^2 + 12\,J^2 + 32x{J_{34}}^2 + 24.4x^2{V_{OX}}^2}$$

$$\times {J_{34}}^2 x \left(\frac{T}{\Theta}\right)^8 T \qquad (5\text{-}11)$$

We now compare these theoretical formulas with the x dependence of our bcc data of $V = 20.5$ cm^3/mol at

$\omega_0/2\pi$ = 3 MHz. First we analyze the energy constant. Using the value of the ^{3}He - ^{3}He exchange interaction $J/2\pi$ = 0.7 MHz, and if we choose the magnitude of the strain field interaction as $V_{0X}/2\pi$ = 220 MHz, we can fit the eq. (5-10) well to our data shown in Fig. 29. The theoretical curve is shown in the figure. It is found that in the concentration range where $x < 10^{-3}$ the X bath is considered to consist only of the ^{3}He - ^{3}He exchange bath and its energy constant is determined from the ^{3}He - ^{3}He exchange interaction J. With the increase of the ^{4}He impurities the ^{4}He - ^{4}He strain field interaction bath becomes to be effective.

Next we discuss the relaxation time T_{II-2}. In Fig. 32 we show the experimental results of the ^{4}He concentration dependence of T_{II-2} at T = 0.435 K. On the other hand, if we use $J_{34}/2\pi = J/2\pi$ = 0.7 MHz, θ = 28 K [54] and $V_{0X}/2\pi$ = 220 MHz which is determined above, the theoretical formula is expressed from eq. (5-11) as

$$1/T_{II-2})_{theo} = \frac{2.33 \times 10^2 x}{1 + 1.05x + 7.94 \times 10^4 x^2} \qquad (5\text{-}12)$$

at T = 0.435 K. Comparing it with our experimental results, the x dependence is agreeable but the absolute value of $T_{II-2})_{theo}$ is about 7.2 times larger than our data.

One of the reasons of this discrepancy is considered as follows. The thermal conductivity measurement in solid ^{3}He with ^{4}He impurities gives the coupling constant S between the phonon and ^{4}He impurity[55),56)]. If the phonon scattering is due to only the mass difference, the square of the coupling constant S^2 is expressed by $(\Delta m/m_3)^2$. But the measurement suggests that S^2 is about 24 times larger than the value $(\Delta m/m_3)^2$ estimated from the mass difference. This effect has been thought to be caused by the distortion around the impurity. Thus when this effect is considered in the relaxation theory mentioned above, the theoretical value of the relaxation time becomes smaller.

Fig. 32

^{4}He concentration dependence of the relaxation time T_{II-2} at T = 0.435 K.

Figure Caption

BCC, V = 20.5 cm^3/mol, $\omega_0/2\pi$ = 3 MHz.

The solid line represents the values obtained from

$$\frac{1}{T_{II-2}} = \frac{4.82 \times 10^{18}}{\omega_0^2 + 12J^2 + 32xV_{34}^2 + 24.4V_{0X}^2x^2} \times J_{34}^2 \times \left(\frac{T}{\theta}\right)^8 T \times 7.2$$

where $J_{34}/2\pi = J/2\pi = 0.7$ MHz and $V_{0X}/2\pi = 220$ MHz .

Fig. 32

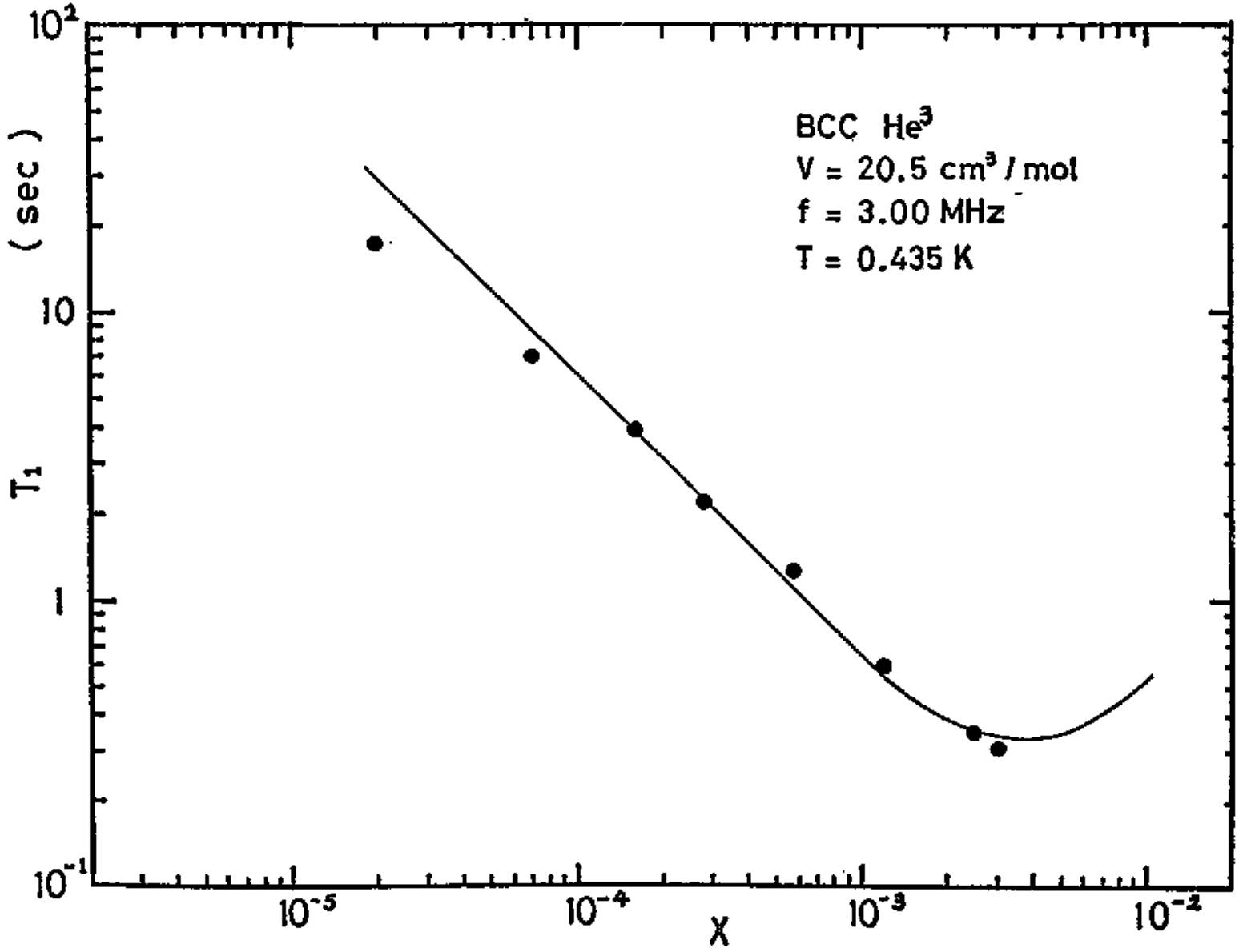
BCC He³
V = 20.5 cm³ / mol
f = 3.00 MHz
T = 0.435 K
T₁ (sec)
10²
10
1
10⁻¹
10⁻⁵
10⁻⁴
10⁻³
10⁻²
X

§ 4 Nonexponential Recovery

We discuss the nonexponential recovery of the magnetization corresponding to the process of T_{III-2}. The nonexponential recovery suggests that the mechanism of this process is not governed by the simple rate equation. For bcc solid ^{3}He with ^{4}He impurities of $1.4 \times 10^{-3} \leq x \leq 5.4 \times 10^{-3}$, this relaxation behavior has been observed below about 0.4 K[11]. The nonexponential relaxation behavior appears not only for the samples with a lot of ^{4}He impurities but also for the purer ^{3}He samples[9),57),58)]. These relaxation times whose feature is nonexponential are shown in Fig. 33. For $x > 10^{-3}$ the concentration dependence of the relaxation time is expressed as $T_1 \propto x^{-n}$ with $n = 3 \sim 4$, but for purer samples ($x < 5 \times 10^{-4}$) the relaxation time is not so influenced by ^{4}He impurities.

For the latter case the relaxation time is affected by the sample volume and the history of the sample such as annealing. Giffard et al.[9),58)] proposed that the mechanism might be the diffusion in the spin system to crystalline faults within the sample. They tried to explain the mechanism by one-dimensional diffusion equation. This diffusion hypothesis was successfully confirmed for the samples formed in the sintered glass with a few microns pores, but could not for the bulk

samples[58].

On the other hand for the samples with a lot of ^4He impurities, $x > 10^{-3}$, it seems to be difficult to explain the experimental results by the one-dimentional diffusion to the surface. We attempted to extend the model to the three-dimensional diffusion. But we find that this trial fails to account for the observation: We first show the three-dimensional diffusion model and their difficulties for the application, and then propose another idea.

4-1 Diffusion Model

We suppose the local magnetization in the solid obeys the diffusion equation;

$$\frac{\partial m(r,t)}{\partial t} = D \nabla^2 m(r,t) \quad , \tag{5-13}$$

where D is the energy diffusion coefficient in solid ^{3}He [19]. Solving this equation under the proper boundary conditions and initial condition, the time evolution of the magnetization which is observed in the NMR experiment is described by

$$M(t) = \int_v m(r,t)\, dV \quad . \tag{5-14}$$

If the space is spherical symmetry, the solution of eq. (5-13) can be separated to the special part and the time part;

$$m(r,t) = R(r)\, F(t) \quad , \tag{5-15}$$

where

$$\begin{cases} F(t) = c \exp(-a^2 Dt) & (5\text{-}16) \\ R(r) = \dfrac{U(r)}{r} & (5\text{-}17) \end{cases}$$

U(r) follows the differential equation;

$$\frac{d^2}{dr^2} U(r) + a^2 U(r) = 0 \quad . \tag{5-18}$$

a and c are the parameter which are determined by the boundary conditions and initial condition.

Let us consider the following case. Suppose that the space is divided by the spherical surface whose radius is R and the energy in the sphere relaxes to the surface. The temperature of the surface is fixed at all times. In this case the boundary condition is $m(R, t) = m_o$ and the initial condition is $m(r,0) = 0$. We have a solution;

$$m(r,t) = m_o + 2 m_o \sum_{n=1}^{\infty} (-1)^n \frac{\sin(\pi nr/R)}{nr/R} \times \exp\left(- \frac{n^2 \pi^2 D}{R^2} t \right) \quad . \tag{5-19}$$

Integrating eq. (5-19) over the sphere, we have a time evolution of the magnetization observed in the experiments, that is

$$\frac{M(\infty) - M(t)}{M(\infty)} \simeq \exp\left(-\sqrt{\frac{t}{T_{1D}}} \right) \quad , \tag{5-20}$$

where

$$T_{1D} = \frac{\pi R^2}{36D} \quad . \tag{5-21}$$

The behavior of the magnetization recovery is in agreement with the observation. We estimate the radius R from our data for $x = 4.2 \times 10^{-3}$. Since $T_{1D} = T_{III-2} \simeq 10$ sec and $D \simeq 10^{-9}$ cm^2/sec[2], we have $R \simeq 3\mu$. The surfaces could be stacking faults or small-angle grain boundary. While from the results of direct studies of the crystal structure using X-ray[59], the crystal size of solid ^3He has been found to be of the order of 1mm, which is in agreement with the results of thermal conductivity measurements[56]. Moreover it is difficult to relate the surface in the model to the surface boundary which remains unchanged by annealing, and to explain the strong ^4He concentration dependence of T_{III-2} and k_Y.

Next we consider the model that there is a core in the sphere whose radius is R. The core whose radius is r_o is at the constant temperature and the energy in the sphere relaxes to the core by diffusion. The boundary conditions are described as

$$\begin{cases} m(r_o,\ t) = m_o \\ \left.\dfrac{\partial m(r,t)}{\partial t}\right|_{r=R} = 0 \end{cases}$$

and the initial condition is

$$m(r,\ 0) = 0$$

for $r_o < r \leq R$.

Under these conditions we solve the diffusion equation (5-13) and have a solution for $r > r_o$ as

$$m(r,t) = m_o - m_o \sum_{n=0}^{\infty} \frac{2r_o}{a_n\{R \sin^2 a_n (R - r_o) - r_o\}} \times \frac{\sin a_n (r - r_o)}{r} \exp(-Da_n^2 t) \quad . \tag{5-22}$$

Then integrating over the sphere, the time evolution of the magnetization is expressed as

$$\frac{M(\infty) - M(t)}{M(\infty)} = \frac{6r_o^2}{R^3 - r_o^3} \sum_{n=0}^{\infty} \frac{1}{a_n^2\{R \sin^2 a_n (R - r_o) - r_o\}} \times \exp(-Da_n^2 t) \quad . \tag{5-23}$$

On this model it seems that the magnetization recovery is not a simple exponential function of time.

in eq. (5-23) is determined from the following equations;

$$\begin{cases} \tan a_n(R - r_o) = a_n R \\ a_n > 0 \end{cases} \qquad (5\text{-}24)$$

When we regard the core to be a ^{4}He atom, and the radius R of the sphere to be the mean distance of ^{4}He atoms, we have $r_o/R \ll 1$ and obtain

$$\begin{cases} a_o \simeq \frac{1}{R}\left(\frac{3r_o}{R}\right)^{\frac{1}{2}} \\ a_n \simeq \frac{(2n+1)\pi}{2}\,\frac{1}{R - r_o} \qquad (n \geq 1) \end{cases} \qquad (5\text{-}25)$$

The term of $n = 0$ is dominant in the summation of eq. (5-23), when $r_o/R \ll 1$. Thus Eq. (5-23) gives

$$\frac{M(\infty) - M(t)}{M(\infty)} = \exp(-Da_o^2 t) \qquad (5\text{-}26)$$

and the magnetization recovery is expressed by a single exponential function of time, which is inconsistent with our observation. The relaxation time is expressed as

$$T_{1D} = \frac{1}{Da_o^2} = \frac{R^3}{3Dr_o} \qquad (5\text{-}27)$$

For reference, when we attempt to estimate R, assuming that $T_{1D} \simeq T_{III-2} \simeq 10$ sec, $D \simeq 10^{-9}$ cm^2/sec and $r_o \simeq 4$ Å, we get $R \simeq 500$ Å. In order to explain the ^{4}He concentration dependence of T_{III-2}, if the core is assumed to be a cluster of three impurity atoms, the mean distance between these clusters are $R \simeq 200$ Å. But there is no reason to consider the cluster specially containing three atoms as a heat reservoir. If we assume the core radius to be sufficiently large, the magnetization recovery would be nonexponential, since a_n terms where $n \geq 1$ becomes effective. But such cores would not be expected to exist in solid ^{3}He. Moreover it is probably difficult that these clusters have such a large energy constant as k_Y observed in our experiment.

Under these considerations we find that the diffusion models fail to account for the nonexponential recovery of the magnetization in solid ^{3}He containing a lot of ^{4}He impurities.

4-2 Problem of Internal Thermal Equilibrium

We have regarded the Y bath and the some part of the X bath as the ^{4}He - ^{4}He strain field interaction bath, from the facts that their energy constants are proportional to x^2 and have reasonable magnitude. The mechanism which couples the ^{3}He - ^{3}He exchange bath and the ^{4}He - ^{4}He strain field interaction system is ^{3}He - ^{4}He exchange motions. When ^{3}He and ^{4}He atoms exchange their positions in solid, the process gives rise to the change of the energy in the ^{3}He - ^{3}He exchange bath due to the change of the ^{3}He spin configuration. The magnitude of the energy change is of order of $\sqrt{z}\, J_{33}$. Simultaneously the jump of the ^{4}He atom accompanies the change of the ^{4}He configuration, and thus varies the energy in the strain field interaction system. Its magnitude is of order of $\boldsymbol{\Delta}\cdot\nabla V(r)$, where $\boldsymbol{\Delta}$ is the nearest neighbor distance and $V(r)$ is the strain field interaction. Accordingly the energy is transferred between these two systems and they gradually come to thermal equilibrium with each other.

Then it is supposed that the ^{3}He - ^{4}He exchange can take place where the condition, $\boldsymbol{\Delta}\cdot\nabla V(r) \sim \sqrt{z}\, J_{33}$, is satisfied according to the energy conservation law. The ^{4}He atom which does not satisfy the above condition can not exchange its position with the neighboring ^{3}He atom,

but owing to the change of surrounding ^{4}He configurations, the ^{4}He atom may be able to have a chance to satisfy the condition and to jump. That is to say, the position of the ^{4}He atoms which can satisfy the condition is different in space and the surroundings change in time. The motions of the ^{4}He atoms will probably take place co-operatively.

While the mechanism which leads the ^{4}He - ^{4}He strain field interaction system to the thermal equilibrium is also the ^{3}He - ^{4}He exchange motion. The strain field interaction system come to thermal equilibrium by changing the ^{4}He configuration due to the ^{3}He - ^{4}He exchange. Therefore the characteristic time in which the strain field interaction system attains its internal thermal equilibrium is thought to be the same order as the relaxation time of the energy flow between the exchange system and the strain field interaction system.

In general if each of two systems comes to thermal equilibrium within itself in a time sufficiently shorter than the coupling time between them, and thus the concept of their own temperature is established, the usual bath model is appliable. In the case, the relaxation between them should be described by the rate equation and the relaxation process is expected to be described by a single exponential function of time. But if not, the process must not be described by a single exponential function.

Consequently in our case the magnetization recovery is thought to behave as a nonexponential one and may appear to have the form of $\exp(- (t/T_1)^{\frac{1}{2}})$.

On this idea the temperature in the ^4He - ^4He strain field interaction system can not be defined during the relaxation process. So we hesitate to consider the Y system to be a bath, but we have introduced the Y bath phenomenologically for convenience.

The mean energy change in the exchange system is of the order of $\sqrt{z}\, J_{33}$ and that in the strain field interaction system is estimated as $\Delta \cdot \Delta V(r) \sim \Delta \frac{\partial}{\partial r} V_0 (\frac{\Delta}{r})^4 \sim V_0 x^{4/3}$. Using $J_{33}/2\pi \sim 0.2$ MHz and $V_0/2\pi \sim 1000$ MHz, we find that the energy changes are the same order when $x \sim 4 \times 10^{-3}$. That is, the distribution functions of the energy changes in the two systems will have the same widths at this concentration.

Since the relaxation rate which is observed in the experiment may be related to the co-operative motions of ^4He atoms and the temperature of the system can not be defined, the conventional methods for the calculation of the relaxation time can not be used.

Fig. 33

^{4}He Concentration Dependence of the relaxation time T_{III-2}

Figure Caption

The relaxation times which characterize the nonexponential recovery of the magnetization observed by Bernier and Deville[11] and Giffard, Truscott and Hatton[9] are also shown.

- ● : HCP, $V = 19.4\ cm^3/mol$, $\omega_0/2\pi = 3.0$ MHz.
- △ : BCC, $V = 20\ cm^3/mol$, $\omega_0/2\pi = 1.5$ MHz [11].
- ⊗ : BCC, $V = 20.5\ cm^3/mol$, $\omega_0/2\pi = 1.5$ MHz [11].
- \+ : BCC, $V = 21\ cm^3/mol$, $\omega_0/2\pi = 1.5$ MHz [11].
- □ : BCC, $V = 20\ cm^3/mol$, $\omega_0/2\pi = 3.2$ MHz [9].

Fig. 33

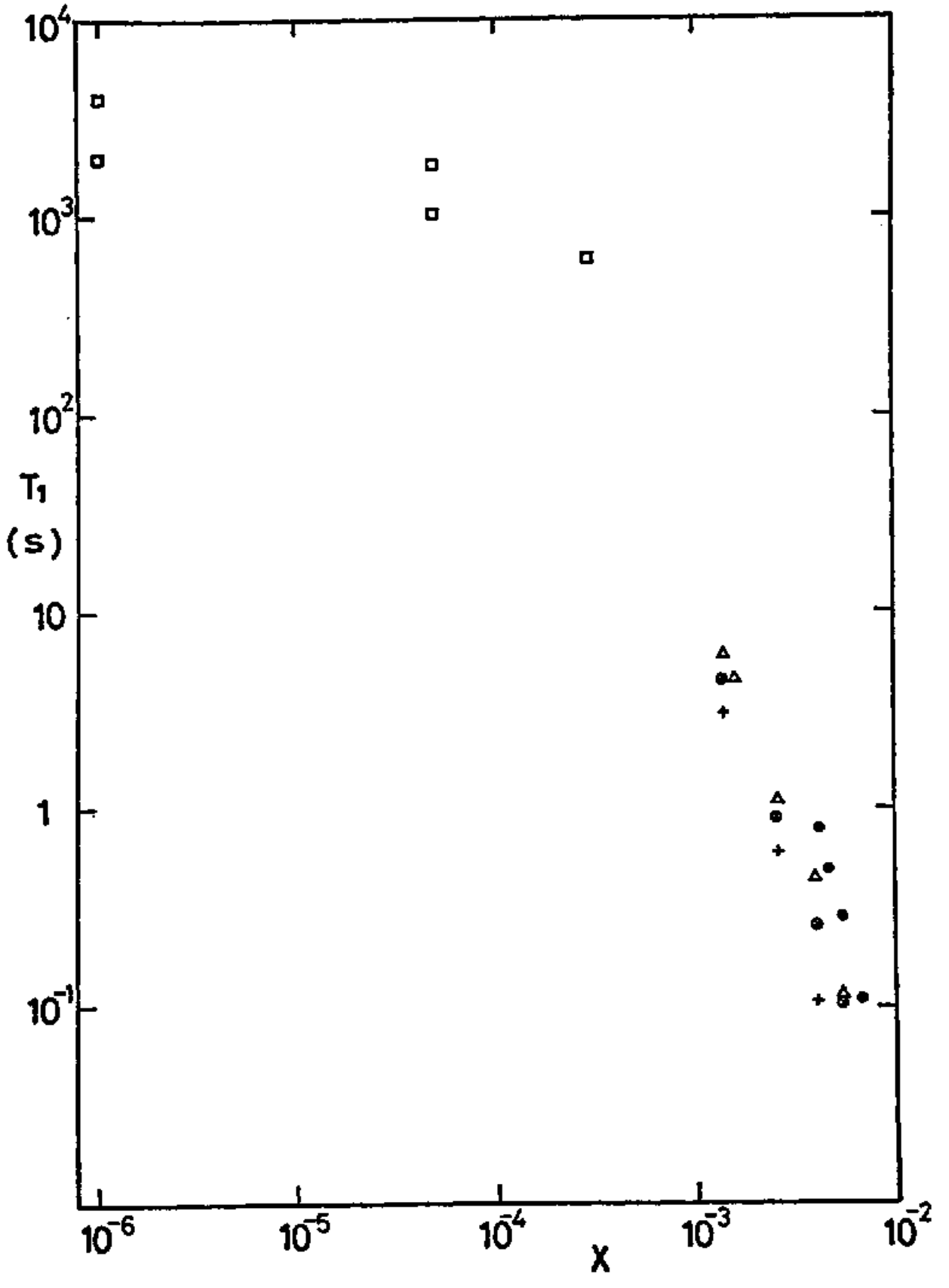

VI CONCLUSION

We have studied extensively the spin relaxation times in solid ^{3}He with various concentrations of ^{4}He impurities. Below about 1.2 K, various kinds of relaxation times were observed and some of them depended on the temperature and ^{4}He concentrations. To explain the experimental results, we have introduced the four bath model phenomenologically. The baths are the Zeeman bath, the X bath, the Y bath and the phonon bath. The X bath consists of the exchange bath and some part of the ^{4}He - ^{4}He strain field interaction bath. The main part of the ^{4}He - ^{4}He strain field interaction bath was observed as the Y bath. The energy constants of the ^{4}He - ^{4}He strain field interaction bath is proportional to x^2. The magnitude of the ^{4}He - ^{4}He strain field interaction deduced from our experiment was found to be about 1000 MHz.

The relaxation mechanism between the Zeeman bath and the X bath is due to the modulation of the dipole interaction between the nuclear magnetic moments caused by the ^{3}He - ^{3}He exchange motions. The relaxation time of this process is independent of the temperature and ^{4}He concentration, but is strongly dependent of the NMR frequency and the molar volume.

The magnetization recovery which corresponds to the process between the X bath and the Y bath is nonexponential function of time. The relaxation time was obtained by fitting the magnetization recovery to the equation of $\exp(-(t/T_1)^{\frac{1}{2}})$. This relaxation time was strongly affected by ^{4}He impurities. This relaxation mechanism seems to be related to the process of the internal thermal equilibrium process in the ^{4}He - ^{4}He strain field interaction bath. The elementary process may take place by the ^{3}He - ^{4}He exchange motion but the relaxation rate observed in the experiments is considered to be related to the time of the co-operative motions of the ^{4}He atoms.

The relaxation from the exchange bath to phonon bath is caused by the vacancy motions in the solid for the very pure solid ^{3}He. This relaxation time is proportional to $\exp(\varepsilon /k_B T)$ and is independent of ^{4}He impurities. For the impure samples the relaxation time in hcp solid ^{3}He was proportional to T^{-7}. The relaxation mechanism is tried to explain by the enhanced exchange modulation near the ^{4}He atoms. While for the bcc solid ^{3}He the relaxation time was proportional to T^{-n} with $7 \leq n \leq 9$. The inelastic phonon scattering by ^{4}He impurities accompanying the ^{3}He - ^{4}He exchange process is thought to be dominant in the bcc solid. The difference between the relaxation mechanisms in two

phases is considered to be caused by the difference of the crystal structures.

In the course of this study we have revealed the excitation systems and their interactions in solid ^{3}He with ^{4}He impurities, and it is found that the small amount of ^{4}He impurities play important roles in the spin lattice relaxation mechanism.

ACKNOWLEDGEMENTS

The author would like to express his sincere gratitude to Professor A. Hirai for his valuable suggestions and friutful discussions in the course of this work. He also would like to thank Dr. T. Mizusaki for his continual aid in the experiments, stimulating discussions and hearty encouragements. He is indebted to Dr. Y. Hirayoshi and Mr. T. Kusumoto for their devoted help in the experiments and discussions. He wish to thank Professor T. Tsuneto and Dr. Y. Yamashita for their continual interests and useful discussions. He thanks members of Hirai Unit for the informative and pleasant discussions and for providing various convenience in carrying out the experiments. He is indebted to Professor K. Asada of the faculty of technology, Kyoto University, for the use of the mass spectrometer and also to Mr. H. Nishishita and Mr. N. Kasugai for supplying a lot of liquid helium.

REFERENCES

1) N. Bloemberg and S. Wang; Phys. Rev. 93, 72 (1954)

2) H. A. Reich; Phys. Rev. 129, 630 (1963)

3) R. L. Garwin and A. Landesman; Phys. Rev. 133, A1503 (1964)

4) B. T. Beal, R. P. Giffard, J. Hatton, M. G. Richards and P. M. Richards; Phys. Rev. Lett. 12, 393 (1964)

5) R. C. Richardson, E. Hunt and H. Meyer; Phys. Rev. 138, A1326 (1965)

6) M. G. Richards, J. Hatton and R. P. Giffard; Phys. Rev. 139, A91 (1965)

7) R. P. Giffard and J. Hatton; Phys. Rev. Lett. 18, 1106 (1967)

8) M. Bernier; J. Low Temp. Phys. 3, 29 (1970)

9) R. P. Giffard, W. S. Truscott and J. Hatton; J. Low Temp. Phys. 4, 153 (1971)

10) M. Bernier; The Proc. of the 13th International Conference on Low Temp. Phys. (Colorado) P79 (1972)

11) M. Bernier and G. Deville; J. Low Temp. Phys. 16, 349 (1974)

12) R. L. Garwin and H. A. Reich; Phys. Rev. Lett. 12, 354 (1964)

13) W. N. Yu and H. A. Reich; Solid State Comm. 7, 1521 (1969)

14) R. A. Guyer and L. I. Zane; Phys. Rev. Lett. 24, 660 (1970)

15) M. Bernier and A. Landesman; J. Phys. 32, C5a-213 (1971)

16) K. Nakajima, T. Tsuneto and Y. Yamashita; J.Phy. Soc. Japan; 37; 1291 (1974)

17) A. Hirai and T. Mizusaki; BUTSURI 30, 540 (1975)

18) N. R. Werthamer; Amer. J. Phys. 37, 763 (1969)

19) R. A. Guyer; Solid State Phys.

20) A. F. Andreev and I. M. Lifshitz; JETP. 29, 1107 (1969)

21) R. A. Guyer; J. Low Temp. Phys. 8, 427 (1972)

22) R. A. Guyer, R. C. Richardson and L. I. Zane; Rev. Mod. Phys. 43, 532 (1971)

23) W. Huang, H. A. Goldberg and R. A. Guyer; Phys. Rev. B11, 3374 (1975)

24) Y. Hirayoshi, T. Mizusaki, S. Maegawa and A. Hirai; J. Low Temp. Phys. 30, 137 (1978)

25) A. S. Greenberg, W. C. Thomlinson and R. C. Richardson; J. Low Temp Phys. 8, 3 (1972)

26) M. C. Richards, J. Pope, A. Window; Phys. Rev. Lett. 29, 708 (1972)

27) V. N. Grigor'ev, B. N. Esel'son and V. A. Mikheev; JETP. 39, 153 (1974)

28) A. F. Andreev; Sov. Phys. Usp. 19, 137 (1976)

29) J. D. Eshelby; Solid State Phys., ed. F. Seitz and D. Turnbull (Academic Press, New York, 1956) vol. 3, p. 121

30) R. A. Guyer; Phys. Rev. A5, 2541 (1972)

31) N. Bloembergen, E. M. Purcell, R. V. Pound; Phys. Rev. 73, 679 (1948)

32) P. W. Anderson and P. R. Weiss; Rev. Mod. Phys. 25, 269 (1953)

33) R. C. Richardson, A. Landesman, E. Hunt and H. Meyer; Phys. Rev. 146, 244 (1966)

34) A. C. Anderson, W. Reese and J. C. Wheatley; Phys. Rev. 127, 671 (1962)

35) B. Pipes and W. M. Fairbank; Phys. Rev. Lett. 23, 520 (1969)

36) J. Sites, D. Osheroff, R. C. Richardson and D. M. Lee; Phys. Rev. Lett. 23, 835 (1969)

37) W. P. Kirk, E. B. Osgood and M. C. Garber; Phys. Rev. Lett. 23, 833 (1969)

38) M. F. Panczyk, R. A. Seribner, G. C. Straty and E. D. Adams; Phys. Rev. Lett. 19, 1102 (1969)

39) M. F. Panczyk and E. D. Adams; Phys. Rev. 187, 321 (1969)

40) R. B. Griffiths; Phys. Rev. 124, 1023 (1961)

41) M. Bernier and A. Landesman; Solid State Commu. 7, 529 (1969)

42) H. R. Glyde; Phys. Rev. 177, 262 (1969)

43) P. N. Henriksen, M. F. Panczyk and E. M. Adams; Solid State Commu. 8, 735 (1970)

44) A. Abragam; The principles of Nuclear Magnetism, Oxford U. P. Oxford, England

45) P. M. Richards; Phys. Rev. A137, 1327 (1965)

46) G. C. Straty and E. D. Adams; Rev. of Scie. Inst. 40, 1393 (1969)

47) R. P. Giffard, R. B. Harrison, J. Hatton and W. S. Truscott; Cryogenics 179 (1967)

48) R. P. Giffard; thesis, Oxford (1968)

49) E. R. Grilly and R. L. Mills; Ann. of Phys. 8, 1 (1959)

50) G. C. Straty and E. D. Adams; Phys. Rev. 150, 123 (1966)

51) E. R. Grilly; J. Low Temp. Phys. 4, 615 (1971)

52) BMDP Biomedical Computer Programs, W. J. Dixon, Univ. of California Press (1975), Nonlinear Regression Program P3R, a least squares fit to a non-linear function by means of Gauss-Newton iterations

53) C. Boghosian, H. Meyer and J. E. Rivers; Phys. Rev. 146, 110 (1966)

54) H. H. Sample and C. A. Swenson; Phys. Rev. 158, 188 (1967)

55) B. K. Agrawal; Phys. Rev. 162, 731 (1967)

56) B. Bertman, H. A. Fairbank, R. A. Guyer and C. W. White; Phys. Rev. 142, 79 (1966)

57) E. R. Hunt, R. C. Richardson, J. R. Thompson, R. Guyer and H. Meyer; Phys. Rev. 163, 181 (1967)

58) R. P. Giffard, J. P. Stagg, W. S. Truscott and J. Hatton; J. Low Temp Phys. 31, 817, (1978)

59) A, F. Schuch and R. L. Mills; Phys. Rev. Lett. 8, 469 (1962)

60) M. G. Richards and J. M. Homer; Phys. Rev. 182, 318 (1969)

LISTS OF FIGURES AND TABLES

参考論文 1

Volume 50A, number 3 PHYSICS LETTERS 2 December 1974

^{3}He NUCLEAR MAGNETIC RELAXATION IN SOLID HELIUM NEAR ITS MELTING TEMPERATURE

T. MIZUSAKI, Y. HIRAYOSHI, S. MAEKAWA and A. HIRAI
Department of Physics, Faculty of Science, Kyoto University, Kyoto, Japan

Received 10 October 1974

From the NMR measurement, the correlation time of the motion of a ^{3}He spin via vacancies was found to be a constant along the solid-liquid coexistence curve. This implies that the ratio of the formation energy of a vacancy to the melting temperature is a constant within 1%, whose absolute value was 10.8 ± 1.0.

During the past decade, ^{3}He NMR studies on solid helium have been the subject of intense experimental and theoretical investigations [1]. Spin relaxation mechanisms in various temperature ranges seem to have become almost clear, except at very low temperatures. At the highest temperature range, just below the melting temperature, the dominant relaxation mechanism is known to be due to the modulation of the dipole-dipole interaction between ^{3}He spins via the vacancy wave excitation. Now we have undertaken a study on the properties of thermal vacancies and the melting phenomena by using solid helium. It is suitable for such studies, because it is possible to make very pure samples and the molar volume or the melting temperature can be easily changed by applying moderate pressure. This note is a report of preliminary results of this study.

The ^{3}He spin relaxation times T_1, T_2 and $T_{1\rho}$ (a spin relaxation time in a rotating reference frame) were measured in the hcp phase of a solid mixture of ^{3}He and ^{4}He with 4.8% ^{3}He. The temperature range was between 4.2 K and 1.4 K and the operating frequencies were 10 MHz and 3 MHz. The experimental procedures were essentially the same as those of Miyoshi et al. [2]. Since the measurements were carried out near the melting temperature, great care was taken in annealing the sample. It was annealed just above the melting temperature for about one hour, until the data were reproducible during cooling down and warming up the sample. The measurements were also carried out along the solid-liquid coexistence curve. There, we have carefully separated the NMR signal in the solid phase from that in the liquid.

In the present case, according to the BPP model [3], relaxation times are given by the following expressions, with conventional notations [1, 4].

$$1/T_1 = \tfrac{2}{3}M_2\left\{\frac{\tau_c}{1+(\omega_0\tau_c)^2}+\frac{4\tau_c}{1+4(\omega_0\tau_c)^2}\right\}$$

$$1/T_2 = \tfrac{2}{3}M_2\left\{\tfrac{3}{2}\tau_c+\tfrac{5}{2}\frac{\tau_c}{1+(\omega_0\tau_c)^2}+\frac{\tau_c}{1+4(\omega_0\tau_c)^2}\right\}$$

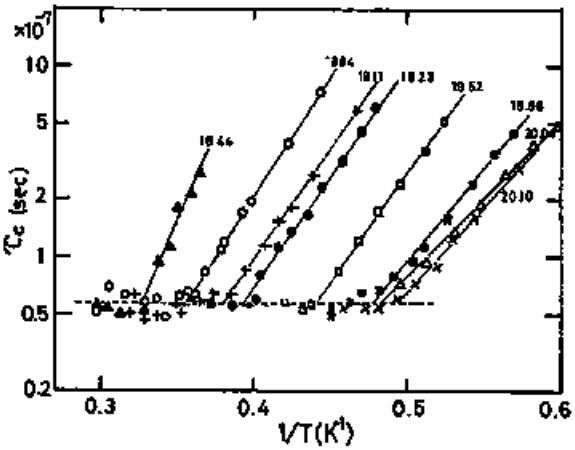

Fig. 1. Temperature dependence of the correlation time (τ_c) of the motion of a ^{3}He spin in a 4.8% ^{3}He–^{4}He mixture, obtained from the analysis of ^{3}He NMR relaxation data. The solid lines are the results of the least square fitting for the data in the solid phase. The dotted line is that for the data along the liquid-solid coexistence curve, in which the molar volume of the solid is continuously changing. The values of the molar volumes for the solid phase are included in the figure.